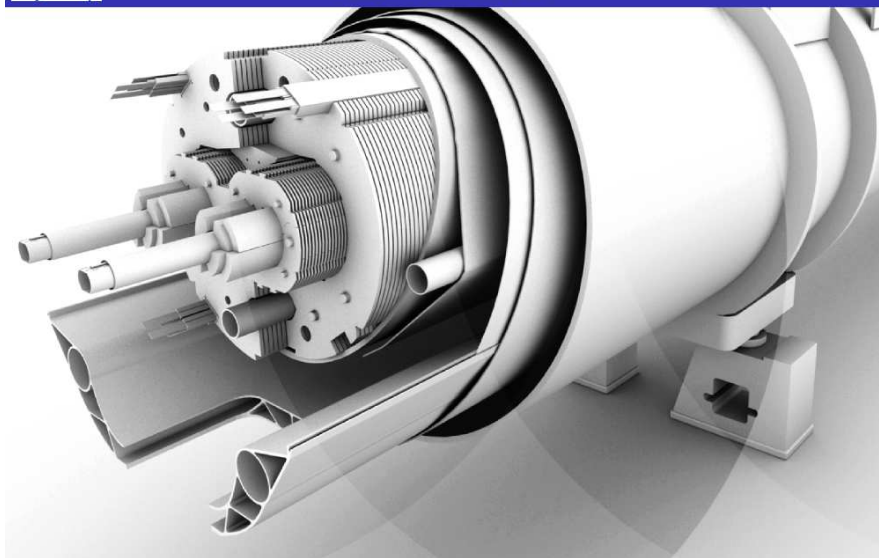




# Accelerator Physics and the LHC

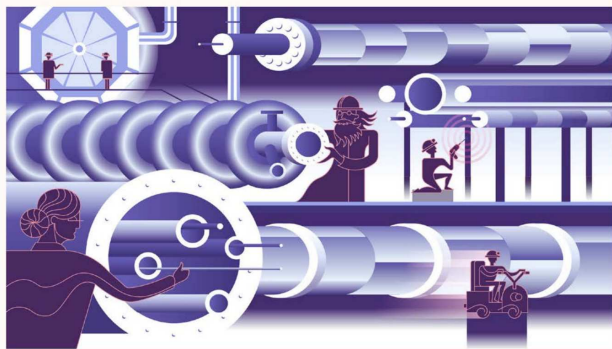
Ewen .H. Maclean



symmetry

topics

follow +



Artwork by Sandbox Studio, Chicago with Ana Kova

## The hottest job in physics?

04/26/16 | By Troy Rummler

Accelerator scientists are in demand at labs and beyond.

While the supply of accelerator physicists in the United States has grown modestly over the last decade, it hasn't been able to catch up with demand fueled by industry interest in medical particle accelerators and growing collaborations at the national labs.

**~35,000  
particle  
accelerators  
world-wide**



# Medicine



Sign in

News

Sport

Weather

Shop

Reel

Travel

## NEWS

Home

Video

World

UK

Business

Tech

Science

Stories

Entertainment & Arts

Wales

Wales Politics

Wales Business

North West

North East

Mid

South West

physicsworld



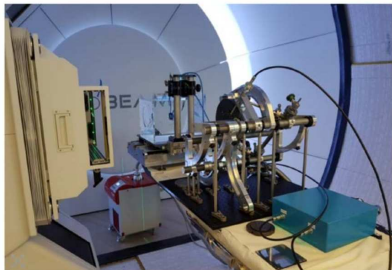
Magazine | Latest | People | Impact

particle therapy

PARTICLE THERAPY | ANALYSIS

### Proton therapy on an upward trajectory

16 Feb 2019



Setting the standard: NPL's portable calorimeter provides a more accurate reference point for proton beam dosimetry. (Courtesy: NPL)

## Wales cancer patients to get proton beam therapy on NHS

12 December 2018



Share



The centre in Newport will be the second in the UK to offer proton beam therapy on the NHS

# Industry & energy



UK Research  
and Innovation

Funding Research Innovation Skills Public engagement News, events and publications About

## News, Events & Publications

Home / News / STFC launches VELA – bringing a new imaging capability for UK industry

## STFC launches VELA – bringing a new imaging capability for UK industry

13 March 2015



CERN COURIER | Reporting on international high-energy physics

Physics ▾ Technology ▾ Community ▾ In focus Magazine



NEWS

## GUINEVERE: towards cleaner nuclear energy

27 March 2012

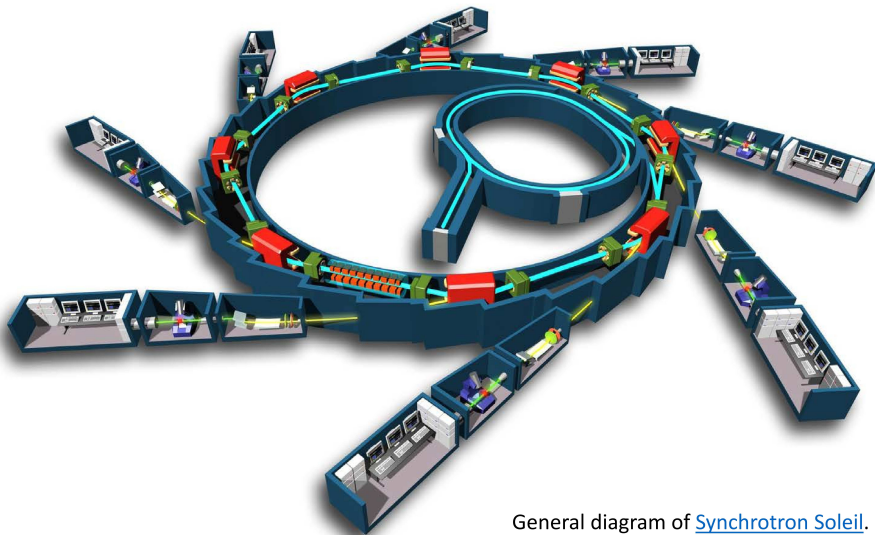


The accelerator used to produce fast neutrons.  
Image credit: SCK•CEN. Used by permission.

A particle accelerator has been successfully coupled to a nuclear reactor for the first time at the Belgian Nuclear Research Centre (SCK•CEN). The demonstration model GUINEVERE is now in operation, showing the feasibility of an accelerator-driven system (ADS) for nuclear energy ([Mumbai engages ADS for nuclear energy](#)). By using an ADS, the accelerator can be turned off to stop the reactor immediately. This system, known as subcritical, is safer than standard nuclear reactors.

GUINEVERE is a test installation of limited power to fine-tune the operation and control of future subcritical reactors. Unlike conventional reactor systems, it produces fast neutrons that can be used for the transmutation of high-level radioactive waste into less-toxic products with shorter life spans, helping to improve their geological disposal.

# ■ Light Sources

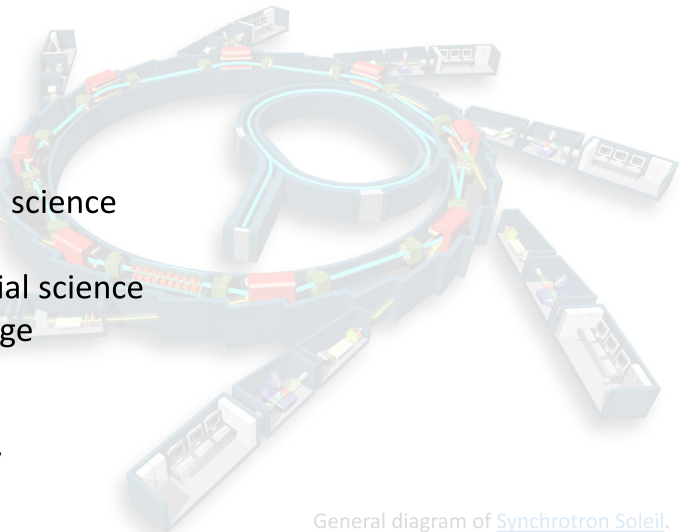


General diagram of [Synchrotron Soleil](https://www.soleil.fr/).

# ■ Light Sources

Facilitate many types of research:

- Life science
- Chemistry
- Engineering
- Earth science
- Environmental science
- Life science
- Physics/material science
- Cultural heritage
- Forensics
- Food science
- Oceanography
- ...



General diagram of [Synchrotron Soleil](#).

# Light Sources

## Facilitate many types of research:

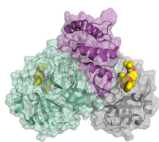
### Life science

[https://www.helmholtz-berlin.de/forschung/unsere-forschung/photonenforschung/corona-forschung\\_en.html](https://www.helmholtz-berlin.de/forschung/unsere-forschung/photonenforschung/corona-forschung_en.html)

#### Research on SARS-CoV-2 at BESSY II

At synchrotron light sources like BESSY II, research is currently gaining crucial insights into combating the SARS-CoV-2 virus. The results are helping to contain the spread and fight the disease more effectively.

For corona research, BESSY II has provided access via a fast-track method even during the strictest lockdown phases. Immediately after the genome of the novel coronavirus SARS-CoV-2 was sequenced in early 2020, the first measurements of viral proteins started at BESSY II.



Schematic picture of the coronavirus protease.  
(© H. Taberner / HZB)

- **A first major success at the beginning of 2020** was the decoding of the three-dimensional structure of the main protease of the SARS-CoV-2 virus, which was already achieved at BESSY II in February 2020. This protein is elementary in the life cycle of the coronavirus because it is involved in the reproduction of the viruses. Knowledge of its 3D structure helps in the search for suitable active substances that dock onto the protein and hinder its function. Because without information about the target protein, the search for an active agent is like looking for a needle in a haystack. Structure-based drug discovery\* helps to identify the best candidates for active substances from the multitude of possible substances. [Read more here \(news piece\)](#)
- **The BMBF is currently funding the two projects "CTS-COV-2" and "STOP CORONA"** at the two light sources PETRA III and BESSY II. In both projects, the main protease of the virus, which was decoded at BESSY II, was selected as the target for a drug.
- In the STOP-CORONA project, which began as a collaboration between the Helmholtz-Zentrum Berlin (HZB), the University of Lübeck and the University of Würzburg, the aim is to use small-organic substances, so-called fragments, to identify active surfaces of the main viral protease. For this fragment screening, the HZB has two libraries available FZK-Entry with 96 substances and FZK-Universal with 1103 substances. In a first step, crystals of the main protease were tested against the FZK-Entry library. From the binders obtained, a more strongly binding subsequent substance could be identified by optimisation. This substance is currently in binding studies and will be further optimised. These results provide important insights for drug discovery against SARS-CoV-2, as drugs are still urgently needed to get COVID-19 under control. However, Corona research at synchrotrons is not limited to X-ray structure analysis.

#### RESEARCH

##### CORONAVIRUS

### Crystal structure of SARS-CoV-2 main protease provides a basis for design of improved $\alpha$ -ketoamide inhibitors

Lián Zhang<sup>1</sup>, Daming Luo<sup>1</sup>, Xiaoyang Dong<sup>1</sup>, Ute Corts<sup>1</sup>, Christian Brühl<sup>2</sup>, Lucie Sauerbrey<sup>1</sup>, Stephan Beckert<sup>1</sup>, Katharina Roth<sup>1</sup>, Ralf Hilgenberg<sup>1</sup>\*

The coronavirus disease 2019 (COVID-19) pandemic caused by severe acute respiratory syndrome-coronavirus 2 (SARS-CoV-2) is a global health emergency. An attractive drug target among coronaviruses is the main protease (M<sup>pro</sup>), also called 3CL<sup>pro</sup>, because of its essential role in processing the polyproteins that are translated from the viral RNA. We report the X-ray structure of the unglycosylated SARS-CoV-2 M<sup>pro</sup> and its complex with an  $\alpha$ -ketoamide inhibitor. This was derived from a previously designed inhibitor but with the N192F amino bond incorporated into a pyridone ring to enhance the half-life of the compound in plasma. On the basis of the unglycosylated structure, we developed the lead compound with a potent inhibitor of the SARS-CoV-2 M<sup>pro</sup>. The pharmacokinetic characterization of the optimized inhibitor reveals a pronounced long t<sub>1/2</sub> and suitability for administration by the intranasal route.

In December 2019, a new coronavirus caused an outbreak of pulmonary disease in the city of Wuhan, the capital of China (1). The virus has since spread globally (2, 3). The virus has been named severe acute respiratory syndrome-coronavirus 2 (SARS-CoV-2) (4) because the RNA genome is about 80% identical to that of the SARS coronavirus (SARS-CoV), both viruses being by order of the genus *Coronaviridae* (5, 6). The disease caused by SARS-CoV-2 is called coronavirus disease 2019 (COVID-19). Following the beginning of the outbreak, cases were connected to the Wuhan seafood and animal market (7). While, efficient virus-to-human transmission has not been reported, given the rate of cases (8, 9) (March 2020), the World Health Organization (WHO) declared the outbreak a pandemic. As of 9 April, there were >3,000,000 registered cases globally, with a >5% case fatality rate.

One of the best-characterized drug targets among coronaviruses is the main protease (M<sup>pro</sup>), also called 3CL<sup>pro</sup> (10). Along with the papain-like protease(s), this enzyme is essential for processing the polyproteins that are

translated from the viral RNA (11). The M<sup>pro</sup> enzyme is not known to change affinity to the viral polyprotein 1a (proteinase 1b, ~700 kDa), the major cleavage site at most sites in the 1a-2a linker. This 2a-192F marks the cleavage site, hindering the activity of ribonuclease L, which binds viral replication, because no human proteins with a similar cleavage specificity are known, such inhibitors are unable to be used. Previously, we designed and synthesized polyproteins, when used as long-acting inhibitors of the main protease of beta-coronavirus and alpha-coronavirus as well as the 3C-like protease (12a). We showed that half-maximal effective concentration (EC<sub>50</sub>) of 0.01 and optimal 10-fold EC<sub>50</sub> respiratory syn-

drovirus (MS2-CoV) by 12aF7 with an IC<sub>50</sub> of 0.001  $\mu$ M, values against SARS-CoV and a wide range of enteroviruses in various cell lines, although the antiviral activity seemed to depend to a great extent on the cell type used in the experiments (6). To improve the half-life of the compound in plasma, we modified M<sup>pro</sup> by adding the 29-32 amino acid residue in a pyridone ring (Fig. 1, green circle) in the expectation that this might prevent cellular proteases from accessing this bond and cleaving it. Further, to increase the solubility of the compound in plasma and to reduce its binding to plasma proteins, we replaced the hydrophobic 2-ethylamino group by the more polar 2-aminoethylamino group (Fig. 1, red circle) to give K16 (see below for details). To examine whether the intranasal pyridone ring is compatible with the three-dimensional structure of the target, we determined the crystal structure at 1.9 Å resolution of the M<sup>pro</sup> of SARS-CoV-2 (Fig. 2). The three-dimensional structure is highly similar to that of the SARS-CoV M<sup>pro</sup>, as reported from the 9th sequence identity (see Fig. 2B) and most sequence conservation between the two enzymes structure in M<sup>pro</sup> 1-148 (13) for all 60 positions (conservation between SARS-CoV-2 M<sup>pro</sup> structure and SARS-CoV M<sup>pro</sup> PDB entry 3W02) (14). The pyridone-like and 2-aminoethylamino group in the domain I and II residues 10 to 36 and 200 to 185, respectively, are six-stranded antiparallel  $\beta$ -sheets that together the helix-loop-sheet structure between them. Domain III (residues 196 to 316) is also a globular cluster of  $\beta$ -sheets, involved in regulating the dimerization of the M<sup>pro</sup>, mainly through a side-chain interaction between Cys197 of one protease and Arg197 of the other (15). The tight cluster formed

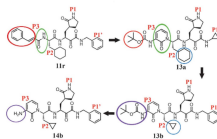


Fig. 1. Chemical structures of  $\alpha$ -ketoamide inhibitors 11a, 12a, 13a, and 14b. Colored circles and arrows highlight the modifications from one development step to the next (see text).

# Art and History



Downloaded via  
Shanghai

*Anal. Chem.* 2008, 80, 6436–6442

## Visualization of a Lost Painting by Vincent van Gogh Using Synchrotron Radiation Based X-ray Fluorescence Elemental Mapping

Joris Dik,<sup>\*,1</sup> Koen Janssens,<sup>2</sup> Geert Van Der Snickt,<sup>1</sup> Luuk van der Loeff,<sup>1</sup> Karen Rickers,<sup>3</sup> and Marine Cotte<sup>1,4</sup>

*Department of Materials Science, Delft University of Technology, Mekelweg 2, 2628CD Delft, The Netherlands, Centre for Micro- and Trace Analysis, Department of Chemistry, Universiteit Antwerpen, Universiteitsplein 1, 2610 Antwerp, Belgium, Kröller-Müller Museum, Houtkampweg 6, P.O. Box 1, 6730 AA Otterlo, The Netherlands, Deutsches Elektronen-Synchrotron (DESY), Notkestrasse 85, 22603 Hamburg, Germany, Centre for Research and Restoration of the French Museums, UMR-171-CNRS, Palais du Louvre, Porte des Lions, 14 quai François Mitterrand, 75001 Paris, France, and European Synchrotron Radiation Facility BP220, 38043 Grenoble Cedex, France*

Vincent van Gogh (1853–1890), one of the founding fathers of modern painting, is best known for his vivid colors, his vibrant painting style, and his short but highly productive career. His productivity is even higher than generally realized, as many of his known paintings cover a previous composition. This is thought to be the case in one-third of his early period paintings. Van Gogh would often reuse the canvas of an abandoned painting and paint a new or modified composition on top. These hidden paintings offer a unique and intimate insight into the genesis of his works. Yet, current museum-based imaging tools are unable to properly visualize many of these hidden images. We present the first-time use of synchrotron radiation based X-ray fluorescence mapping, applied to *Grass by Van Gogh*. We recorded decimeter-scale, X-ray fluorescence intensity maps, reflecting the distribution of specific elements in the paint layers. In doing so we succeeded in visualizing the hidden face with unprecedented detail. In particular, the distribution of Hg and Sn in the red and light tones, respectively, enabled an approximate color reconstruction of the flesh tones. This reconstruction proved to be the missing link for the comparison of the hidden face with Van Gogh's known paintings. Our approach literally opens up new vistas in the nondestructive study of hidden paint layers, which applies to the oeuvre of Van Gogh in particular and to old master paintings in general.

Vincent van Gogh is generally recognized as one of the founding fathers of modern painting.<sup>1</sup> In recent decades his work has undergone extensive art historical and technical study. One

striking feature that emerged is Van Gogh's frequent reuse of paintings in order to recycle the canvas.<sup>2,3</sup> The artist would simply paint a new composition on top of an existing work. This is usually attributed to the artist's lifelong economic hardship and the rapid, energetic evolution of his artistic ideas. Visualizing such hidden paintings is of interest to both specialists in the field of Van Gogh and the public alike. Covered paintings in general provide an insight into the making of artworks and the underlying conceptual changes. In the case of Van Gogh, they also present a touchstone for comparison with preparatory drawings and the abundant literary record. The extensive correspondence with his brother Theo van Gogh, an art dealer based in Paris, is full of remarks by Vincent on his work.

Nondestructive imaging of such hidden paint layers is usually realized by means of tube-based X-ray radiation transmission radiography (XRR). The absorption contrast in these images is mostly caused by the heavy metal components of pigments employed, such as lead in lead white or mercury in vermilion. Conventional XRR, however, has a number of important limitations. First of all, the observed X-ray absorbance is a summation of all element-specific absorbances. This implies that the contribution to the overall image contrast due to (low quantities of) weakly absorbing elements will frequently be obscured by heavier elements that are present in higher concentrations. Second, prior to the application of the paint layer, a canvas is usually primed with a homogeneous layer of lead white. This raises the overall background of the absorption image derived from the paint layers. Finally, the polychromatic character of an X-ray tube further reduces the contrast in radiographic images. As a result, conventional XRR imaging of paintings frequently provides only a fragmentary view of their substructure, which can severely hamper the readability of hidden compositions.<sup>4</sup>

\* Corresponding author. Phone: +31 15 2789571. E-mail: j.dik@tudelft.nl

<sup>1</sup> Delft University of Technology

<sup>2</sup> Universiteit Antwerpen

<sup>3</sup> Kröller-Müller Museum

<sup>4</sup> Deutsches Elektronen-Synchrotron (DESY)

<sup>5</sup> Palais du Louvre

<sup>6</sup> European Synchrotron Radiation Facility

(1) Blikker, J. *The New Condition: Van Gogh's Paintings, Drawings, Sketches*. John Benjamins: Philadelphia, PA, 1996.

(2) Van Houten, S. *Van Gogh Museum*, J. 1995, 63–65.

(3) Hendriks, E. *Van Gogh's Working Practice: A Technical Study. In New Views on Van Gogh's Jewellery in Antwerp on Paris: An Integrated Art Historical and Technical Study of His Paintings in the Van Gogh Museum*; Hendriks, E., Van Tilburg, L., Eds.; University of Amsterdam, Amsterdam, The Netherlands, 2006; pp 211–245.

(4) King, K. D.K.; Des Louches, M.; Wilson, A.; Turner, I.; Ginn, P.; Venoc, C.; Benoit, A. *AMM: Proc. A Mater. Sci. Process.* 2006, 83, 247–51.

# Art and History



Downloaded via  
Shanghai

*Anal. Chem.* 2008, 80, 6436–6442

## Visualization of a Lost Painting by Vincent van Gogh Using Synchrotron Radiation Based X-ray Fluorescence Elemental Mapping

Joris Dik,<sup>1,\*</sup> Koen Janssens,<sup>2</sup> Geert Van Der Snickt,<sup>1</sup> Luuk van der Loeff,<sup>1</sup> Karen Rickers,<sup>3</sup> and Marine Cotte<sup>1,4</sup>

*Department of Materials Science, Delft University of Technology, Mekelweg 2, 2628CD Delft, The Netherlands, Centre for Micro- and Trace Analysis, Department of Chemistry, Universiteit Antwerpen, Universiteitsplein 1, 2610 Antwerp, Belgium, Kröller-Müller Museum, Houlikampweg 6, P.O. Box 1, 6730 AA Otterlo, The Netherlands, Deutsches Elektronen-Synchrotron (DESY), Notkestrasse 85, 22603 Hamburg, Germany, Centre of Research and Restoration of the French Museums, UMR-171-CNRS, Palais du Louvre, Porte des Lions, 14 quai François Mitterrand, 75001 Paris, France, and European Synchrotron Radiation Facility BP220, 38043 Grenoble Cedex, France*

Vincent van Gogh (1853–1890), one of the founding fathers of modern painting, is best known for his vivid colours, his vibrant painting style, and his short but highly productive career. His productivity is even higher than generally realized, as many of his known paintings cover a previous composition. This is thought to be the case in one-third of his early period paintings. Van Gogh would often reuse the canvas of an abandoned painting and paint a new or modified composition on top. These hidden paintings offer a unique and intimate insight into the genesis of his works. Yet, current museum-based imaging tools are unable to properly visualize many of these hidden images. We present the first-time use of synchrotron radiation based X-ray fluorescence mapping, applied to visualize a woman's head hidden under the work *Patch of Grass* by Van Gogh. We recorded decimeter-scale, X-ray fluorescence intensity maps, reflecting the distribution of specific elements in the paint layers. In doing so we succeeded in visualizing the hidden face with unprecedented detail. In particular, the distribution of Hg and Sn in the red and light tones, respectively, enabled an approximate color reconstruction of the flesh tones. This reconstruction proved to be the missing link for the comparison of the hidden face with Van Gogh's known paintings. Our approach literally opens up new vistas in the nondestructive study of hidden paint layers, which applies to the oeuvre of Van Gogh in particular and to old master paintings in general.

Vincent van Gogh is generally recognized as one of the founding fathers of modern painting.<sup>1</sup> In recent decades his work has undergone extensive art historical and technical study. One

striking feature that emerged is Van Gogh's frequent reuse of paintings in order to recycle the canvas.<sup>2,3</sup> The artist would simply paint a new composition on top of an existing work. This is usually attributed to the artist's lifelong economic hardship and the rapid, energetic evolution of his artistic ideas. Visualizing such hidden paintings is of interest to both specialists in the field of Van Gogh and the public alike. Covered paintings in general provide an insight into the making of artworks and the underlying conceptual changes. In the case of Van Gogh, they also present a touchstone for comparison with preparatory drawings and the abundant literary record. The extensive correspondence with his brother Theo van Gogh, an art dealer based in Paris, is full of remarks by Vincent on his work.

Nondestructive imaging of such hidden paint layers is usually realized by means of tube-based X-ray radiation transmission radiography (XRR). The absorption contrast in these images is mostly caused by the heavy metal components of pigments employed, such as lead in lead white or mercury in vermilion. Conventional XRR, however, has a number of important limitations. First of all, the observed X-ray absorbance is a summation of all element-specific absorbances. This implies that the contribution to the overall image contrast due to (low quantities of) weakly absorbing elements will frequently be obscured by heavier elements that are present in higher concentrations. Second, prior to the application of the paint layer, a canvas is usually primed with a homogeneous layer of lead white. This raises the overall background of the absorption image derived from the paint layers. Finally, the polychromatic character of an X-ray tube further reduces the contrast in radiographic images. As a result, conventional XRR imaging of paintings frequently provides only a fragmentary view of their substructure, which can severely hamper the readability of hidden compositions.<sup>4</sup>

\* Corresponding author. Phone: +31 15 2786571. E-mail: j.dik@tudelft.nl

<sup>1</sup> Delft University of Technology

<sup>2</sup> Universiteit Antwerpen

<sup>3</sup> Kröller-Müller Museum

<sup>4</sup> Deutsches Elektronen-Synchrotron (DESY)

<sup>5</sup> Palais du Louvre

<sup>6</sup> European Synchrotron Radiation Facility

(1) Biskker, J. *The New Condition: Van Gogh's Paintings, Drawings, Sketches*. John Benjamins: Philadelphia, PA, 1996.

(2) Van Houten, S. *Van Gogh Museum*, J. 1995, 63–65.

(3) Hendriks, E. *Van Gogh's Working Practice: A Technical Study. In New Views on Van Gogh's Jewellery in Antwerp on Paris: An Integrated Art Historical and Technical Study of His Paintings in the Van Gogh Museum*; Hendriks, E., Van Tilburg, L., Eds.; University of Amsterdam: Amsterdam, The Netherlands, 2006; pp 211–245.

(4) King, K.; Dik, J.; De Lencastre, M.; Wilson, A.; Turtsev, I.; Gasi, P.; Veneco, C.; Boreis, A. *AMM: Phys. & Mater. Sci. Process.* 2006, 83, 247–51.



# Accelerators for HEP

300

*Address of the President, Sir Ernest Rutherford, O.M., at the Anniversary Meeting, November 30, 1927.*

At this Anniversary Meeting we are naturally conscious of the losses suffered by our Society during the year. These include thirteen of our Fellows and three Foreign Members. We have also to record the loss of one of our Fellows under Statute 12, EDWARD CECIL GUINNESS, EARL OF IVEAGH, elected 1906.

Sir WILLIAM AUGUSTUS TILDEN passed away on December 11, 1926, in his 85th year. He was appointed Professor of Chemistry and Metallurgy in the Mason College, Birmingham, in 1880, and in 1894 became Professor of Chemistry in the Royal College of Science. He retained this latter position until his retire-

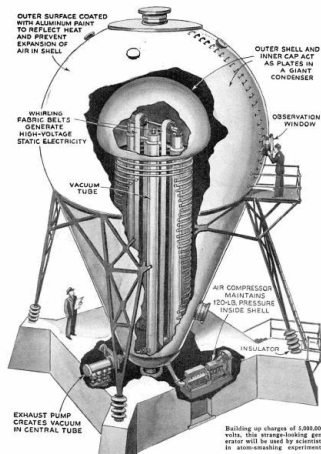
\*\*\*

...the  $\alpha$ -particle has sufficient energy to penetrate deeply into the nucleus and to cause its disintegration manifested by the liberation of swift protons.

It would be of great scientific interest if it were possible in laboratory experiments to have a supply of electrons and atoms of matter in general, of which the individual energy of motion is greater even than that of the  $\alpha$ -particle. This would open up an extraordinarily interesting field of investigation which could not fail to give us information of great value, not only on the constitution and stability of atomic nuclei but in many other directions.

It has long been my ambition to have available for study a copious supply of atoms and electrons which have an individual energy far transcending that of the  $\alpha$  and  $\beta$ -particles from radioactive bodies. I am hopeful that I may yet have my wish fulfilled, but it is obvious that many experimental difficulties will have to be surmounted before this can be realised, even on a laboratory scale.

We shall now consider briefly the present situation with regard to the production of intense magnetic fields. Electro-magnets are ordinarily employed for this purpose and the magnetic fields obtainable are in the main limited



Building up charges of 1,000,000 volts, this strange-looking generator will be used by scientists in atom-smashing experiments

## Westinghouse Atom Smasher, 5MeV 1937 – 1958, Pennsylvania, USA

For historical development of particle accelerators see, e.g.

P.J. Bryant, *A brief history and review of accelerators*,

CERN Accelerator School: 5th General Accelerator Physics Course,  
Jyväskylä, Finland, Sep 1992 <https://cds.cern.ch/record/261062/>

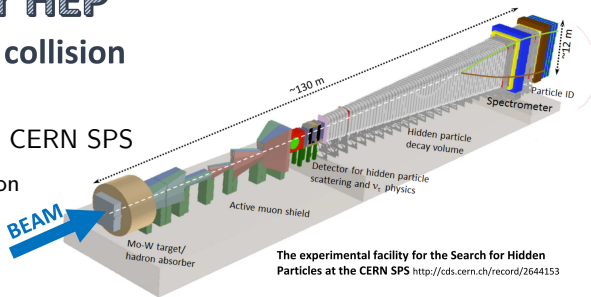


# Accelerators for HEP

## ➔ Different types of collision

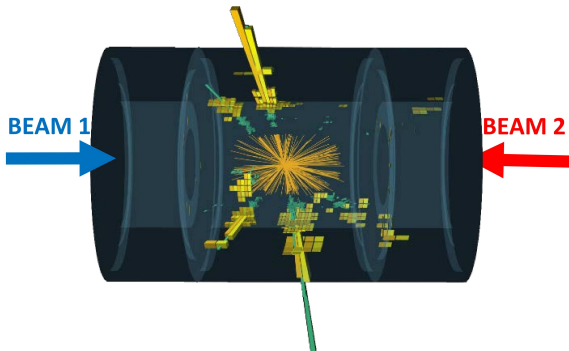
### Fixed target e.g. SHIP @ CERN SPS

- Simpler design/implementation  
→ **cost!**
- Potential for very high intensity beams & large numbers of collisions

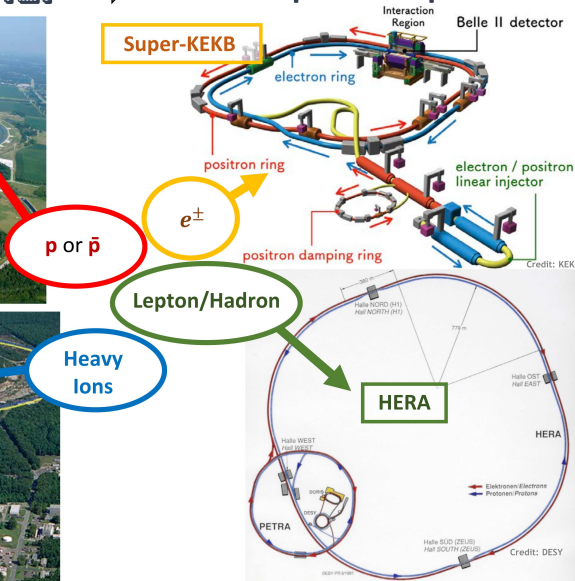
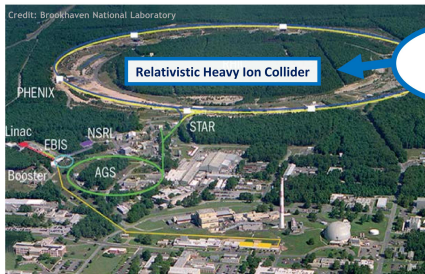
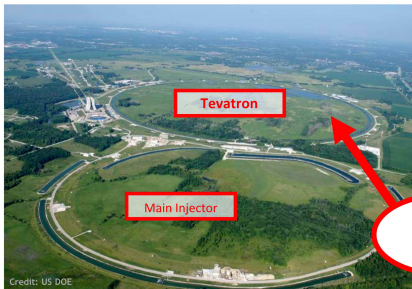


### Collider e.g. LHC @ CERN

- More complex design  
+ many extra challenges
- **LAB frame = CM frame**  
→ maximum energy available for new particle creation



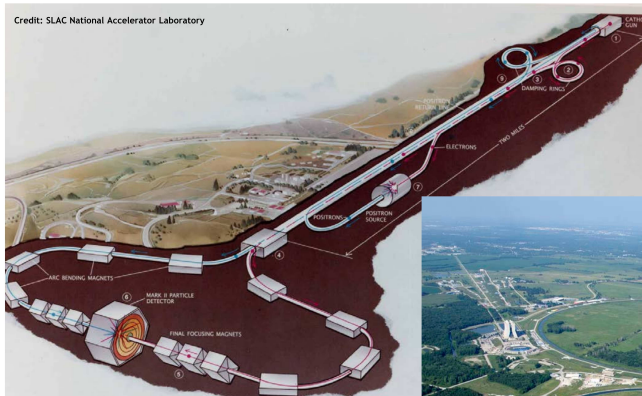
# Accelerators for HEP → Different particle species



For overview of colliders see e.g. : V. Shiltsev and F. Zimmermann *Modern and future colliders* Rev. Mod. Phys. 93, 015006  
<https://journals.aps.org/rmp/abstract/10.1103/RevModPhys.93.015006>

# Accelerators for HEP → various accelerator geometry

Credit: SLAC National Accelerator Laboratory



‘Circular’ collider  
e.g. Tevatron

‘Linear’ collider  
e.g. SLC



Credit: US DOE

# Accelerators for HEP

## Linear Accelerator → 'Linac'

*Colloquially 'Linac' can refer both to a general Linear Accelerator facility or to a specific accelerating structure*

### ■ Single pass accelerator

→ beam goes through once

→ facility not always straight, e.g. SLC

### ■ Energy depends on length

## For HEP 2 main applications:

### ■ Low energy hadrons

### ■ High energy $e^-$ or $e^+$ collider

e.g. Stanford Linear Collider (1987-98, 3 km/0.09TeV)

e.g. next-gen lepton colliders: ILC (50 km / 1TeV)

e.g. next-gen lepton colliders: CLIC (50 km / 3TeV)



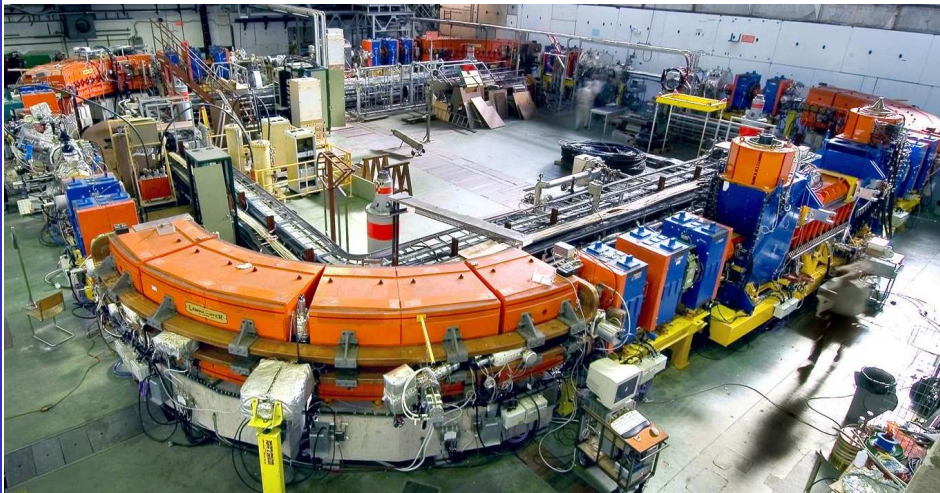
**CERN Linac2  
1978 - 2019**

# Synchrotron

→ e.g. LHC, LEP, Tevatron, RHIC, HERA, SPS, PS...

→ 'circular accelerator', 'collider ring'  
(doesn't actually need to be a circle)

- Repeated passage around the accelerator ring → great for HEP!  
→ re-use accelerating structures & repeatedly collide same beams
- During acceleration guiding fields increase to keep the beam on ( $\sim$ ) same orbit



## Key Points

### ■ Accelerators aren't just for HEP

- $\approx 1/5$  of *Physics Nobel Prizes* directly used an accelerator!
- *Further 20 Nobel Prizes across Physics/Chemistry/Medicine* have been awarded for research using X-rays!
- <https://www.epfl.ch/labs/lpap/wp-content/uploads/2018/10/AcceleratorsNobelPrizes.pdf>

### ■ Accelerators for HEP come in a wide variety of flavours

- specific design will depend on the HEP motivation

## Acceleration

$$\vec{F} = q(\vec{E} + \vec{v} \times \vec{B})$$

$$\Delta W = \int_{s_1}^{s_2} \vec{F} \cdot d\vec{s} = \int_{s_1}^{s_2} q\vec{E} \cdot d\vec{s}$$

- To accelerate charged particle do work via Lorentz force
- Magnetic field does no work  
 $\vec{s} \cdot \left(\frac{d\vec{s}}{dt} \times \vec{B}\right) = 0$

$$\vec{E} = -\nabla\phi - \frac{\partial\vec{A}}{\partial t}$$

### Electrostatic accelerators

- Acceleration via high DC voltage

### RF

- Acceleration via time-varying fields
- 'radiofrequency technology'



## Electrostatic accelerators

e.g. Cockcroft-Walton (left), Van-de-Graff, ...

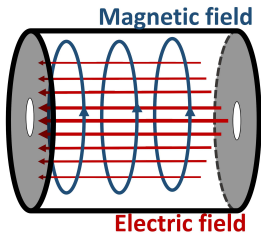
- Limited by DC-breakdown voltage
- Can't be used for repeated acceleration around a closed loop (e.g. in a synchrotron)

$$\oint \nabla \phi \cdot d\vec{s} = 0$$

- Critical element in the design of particle sources

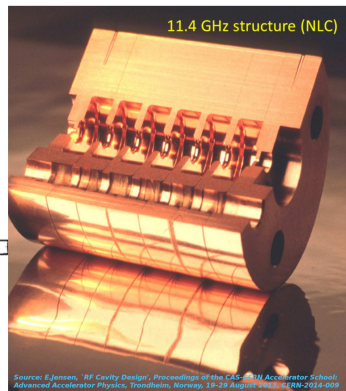
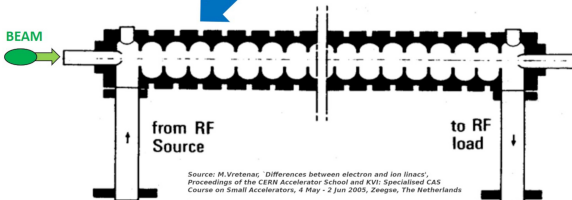
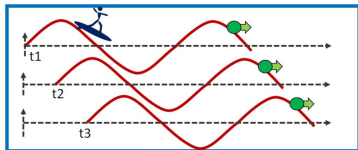


## RF Cavities

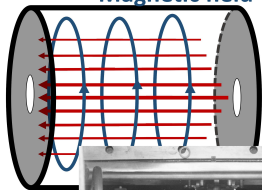


- Basis of all modern high-energy accelerators
- Conducting cavity or waveguide enforces boundary conditions which have solution with an accelerating mode

There are many varieties of RF-cavity:  
e.g. travelling wave structures

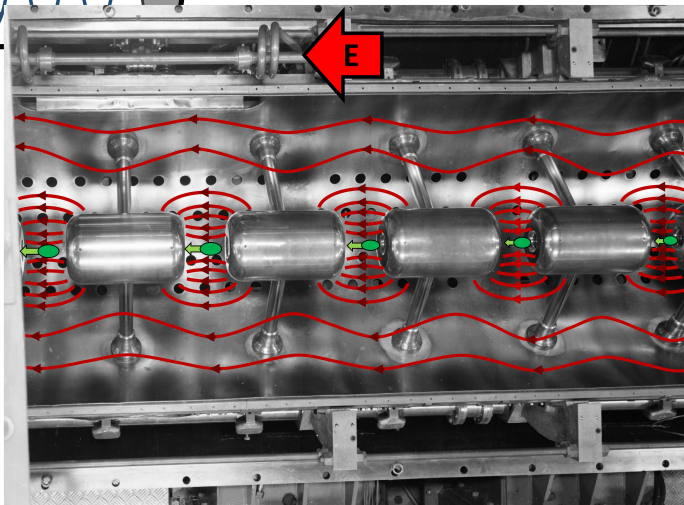


Magnetic field

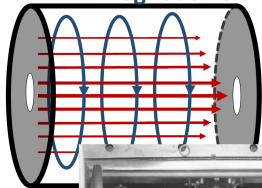


## RF Cavities

There are many varieties of RF-cavity:  
e.g. standing wave drift tube Alvarez structure

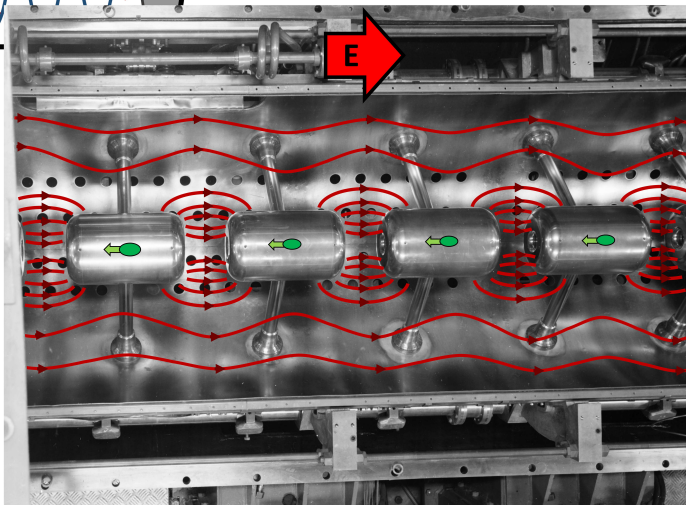


Magnetic field



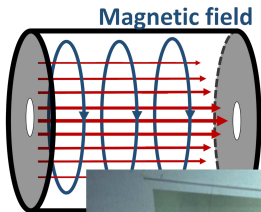
## RF Cavities

There are many varieties of RF-cavity:  
e.g. standing wave drift tube Alvarez structure



## RF Cavities

There are many varieties of RF-cavity:  
e.g. superconducting elliptical cavities (LEP)

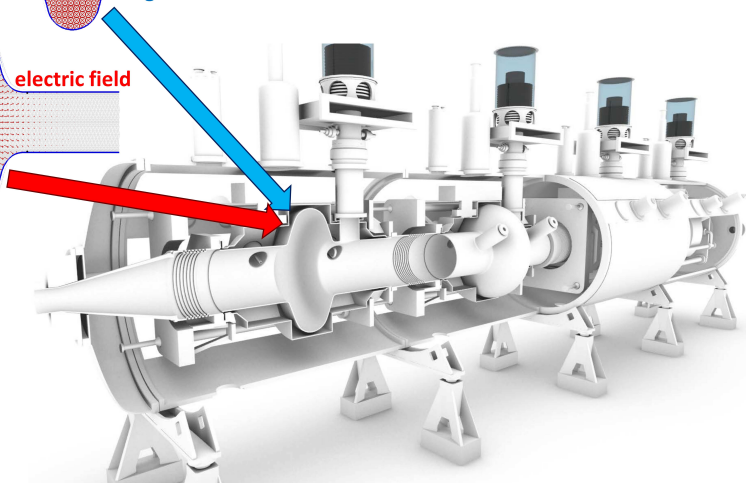
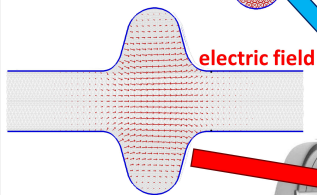
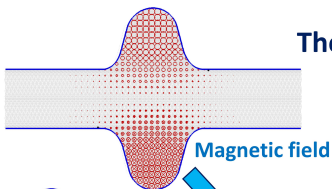


## RF Cavities

There are many varieties of RF-cavity:

e.g. superconducting elliptical cavity (LHC)

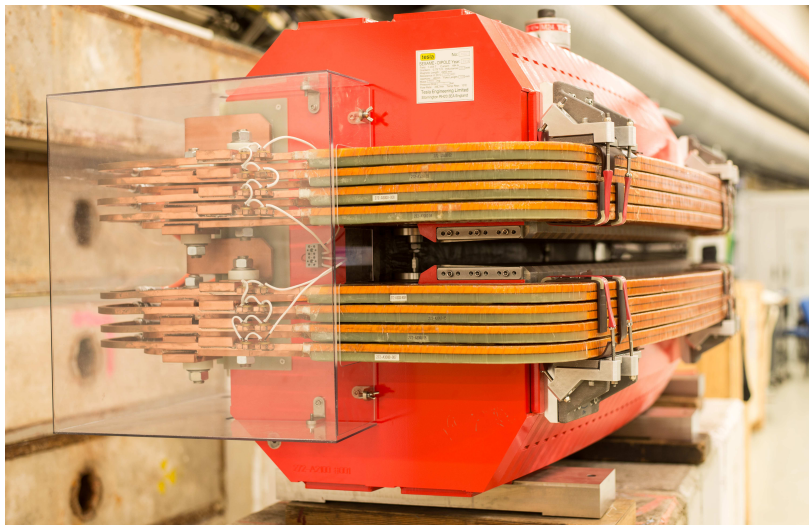
- RF frequency is harmonic of revolution frequency



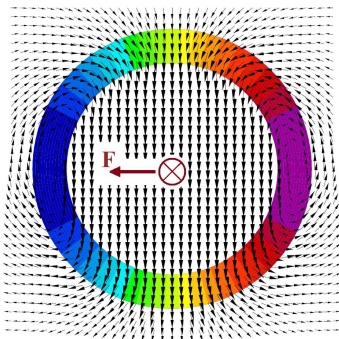
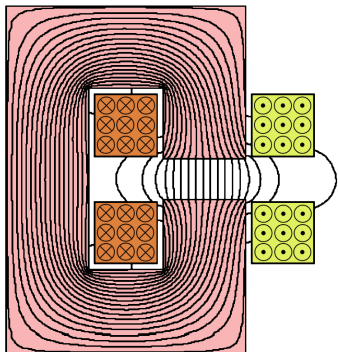
## Bending

$$\vec{F} = q(\vec{E} + \vec{v} \times \vec{B})$$

- Use Lorentz force from **dipole magnets** to bend bunches around the synchrotron ring

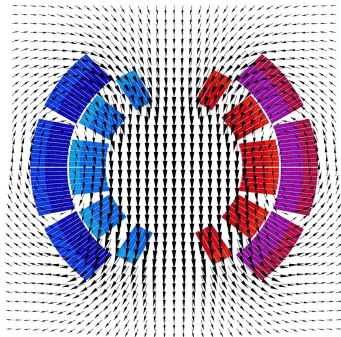
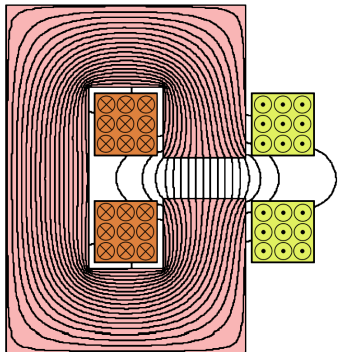


- conventional dipole field defined by core
- Conventional dipoles limited to  $\sim 2\text{ T}$  by saturation of core
- $> 2\text{ T}$  need very large current  $\rightarrow$  **superconductors!!!!**
- Field defined by coil geometry  $\rightarrow I \propto \cos \Theta$



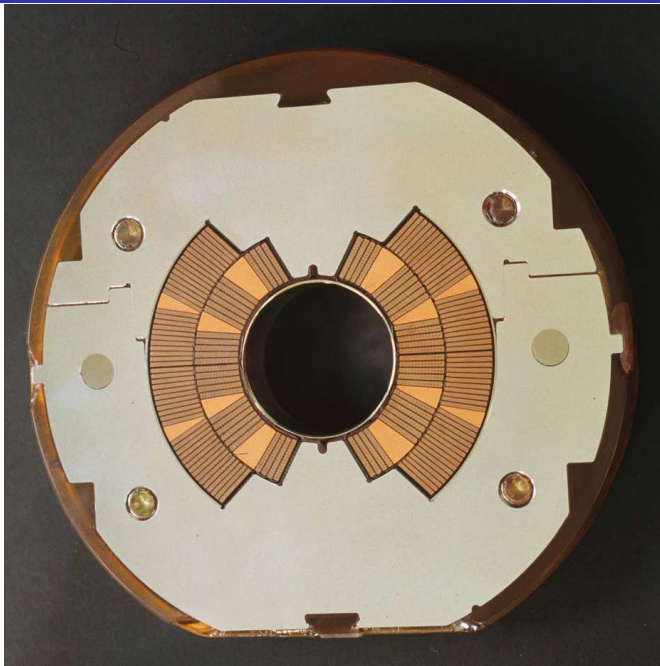
For discussion of magnet design: S.Russenschuck, Design of accelerator magnets, CAS, Loutraki 2000 <https://cds.cern.ch/record/865932> and T.Zickler, Normal Conducting & Permanent Magnets, CAS, Zurich 2018, <https://indico.cern.ch/event/643268/contributions/2610551/>

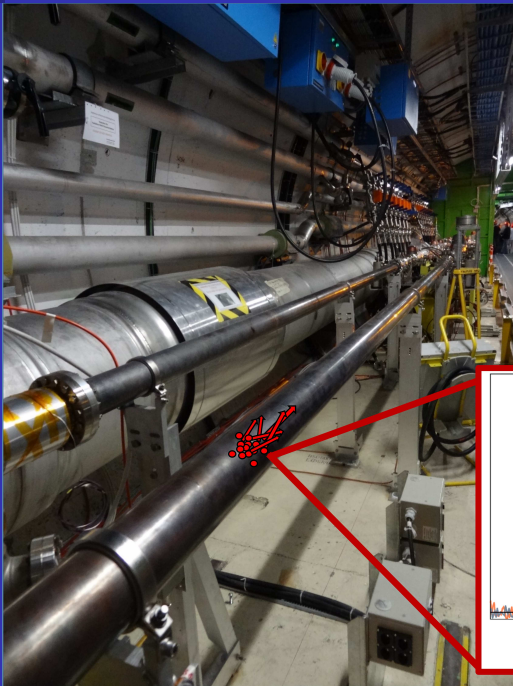
- Conventional dipole field defined by core
- Conventional dipoles limited to  $\sim 2\text{ T}$  by saturation of core
- $> 2\text{ T}$  need very large current  $\rightarrow$  **superconductors!!!!**
- Field defined by coil geometry  $\rightarrow I \propto \cos \Theta$



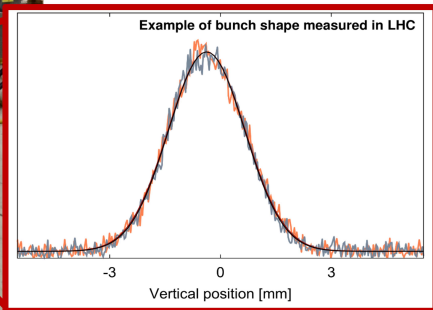
For discussion of magnet design: S.Russenschuck, Design of accelerator magnets, CAS, Loutraki 2000 <https://cds.cern.ch/record/865932> and T.Zickler, Normal Conducting & Permanent Magnets, CAS, Zurich 2018, <https://indico.cern.ch/event/643268/contributions/2610551/>







- Beams typically contained inside `beam-pipe' at high vacuum
- Particle bunches have finite size and angular divergence
- Individual particles follow slightly different trajectories around the synchrotron
- To contain the particles in the synchrotron also need to **focus** particles back towards the center of the beam pipe

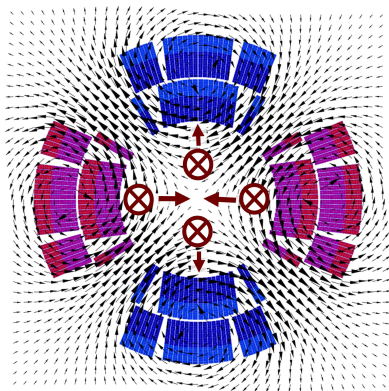
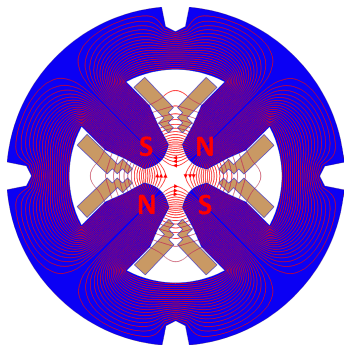


## Focusing

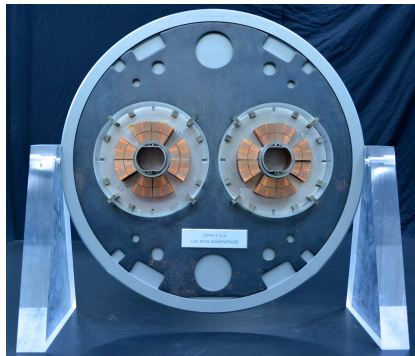
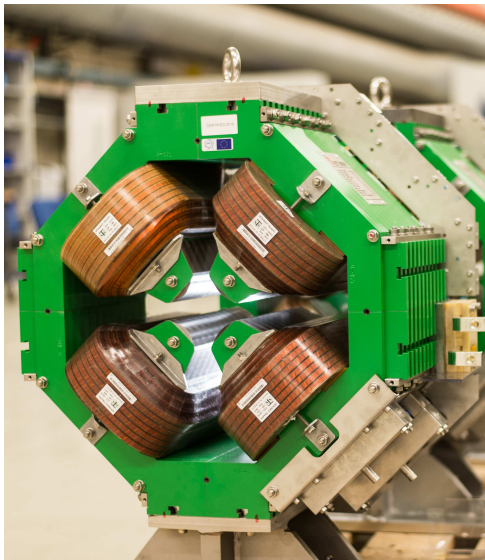
### ■ Use quadrupole fields to focus particle beams

→  $F \propto$  displacement from center

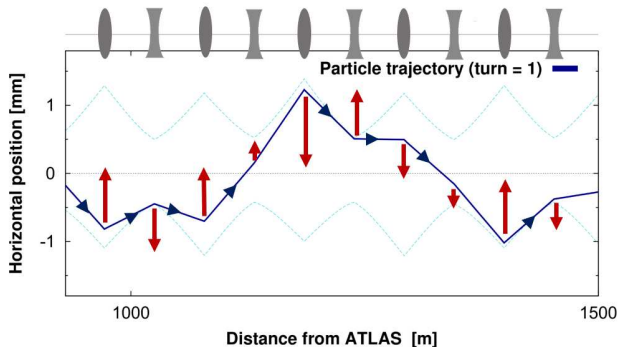
→  $I \propto \cos 2\Theta$



For discussion of magnet design: S.Russenschuck, Design of accelerator magnets, CERN accelerator school, Loutraki, Greece, Oct' 2000 <https://cds.cern.ch/record/865932>

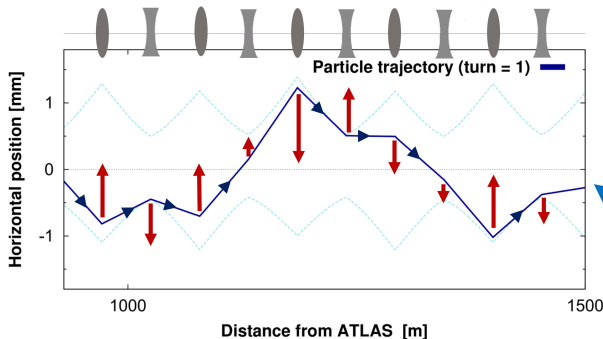


- Single quadrupole can focus in either H or V. Not both.
- Use alternating lattice of focusing/defocusing quads



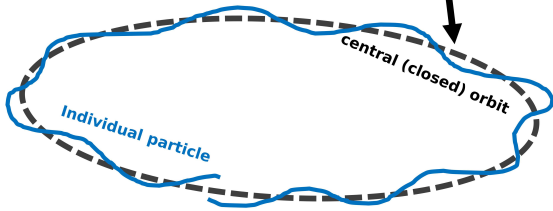
- Particle will oscillate around central orbit, within an envelope defined by the  $\beta$  function

$$x = \sqrt{2J_x\beta_x(s)} \cos(\phi_x(s) + \phi_0) \quad (1)$$



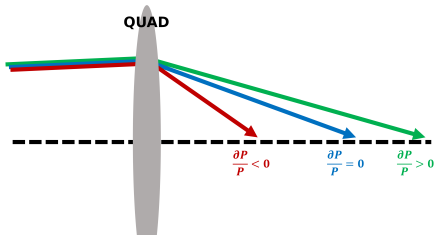
central (closed) orbit defined by dipole magnets

Individual particles oscillate about central (closed) orbit according to quadrupole placement and strength



- Number of times a particle oscillates about the closed orbit in 1 turn is the **TUNE** ( $Q_{x,y}$ ) of the accelerator
- One of the most important properties of any accelerator
- In the LHC  $Q_{x,y} \approx (62.31, 60.32)$

Accelerators can also use a variety of higher-order **multipole** magnets to control various aspects of linear & nonlinear beam dynamics



- Quadrupoles focus **low** & **high** momentum particles differently
- **CHROMATICITY**:  $Q' = \partial Q / \partial (\frac{\delta P}{P_0})$
- Momentum dependent focusing causes **tune-spread** within the bunch

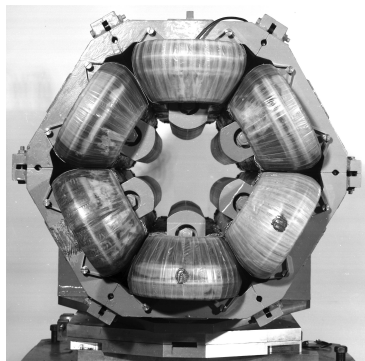
■ Chromaticity controlled with **SEXTUPOLES** →

■  $2n$ -pole field defined by complex potential:

$$\Psi_n = \left( \frac{\partial^{n-1} B_x}{\partial y^{n-1}} + i \frac{\partial^{n-1} B_y}{\partial x^{n-1}} \right) \frac{(x+iy)^n}{n!}$$

$$\Psi_n = (B_n + iA_n) \frac{(x+iy)^n}{n}$$

■ **octupoles**, **decapoles**, **dodecapoles** have all been used in particle accelerators



## Key Points

- What is a synchrotron?
- What is the Tune ( $Q_{x,y}$ )?
- How do we accelerate?  
→ Particles come in bunches
- Dipoles and quadrupoles to bend/focus
- Nonlinear multipole magnets can also be used, e.g. sextupoles for chromaticity correction

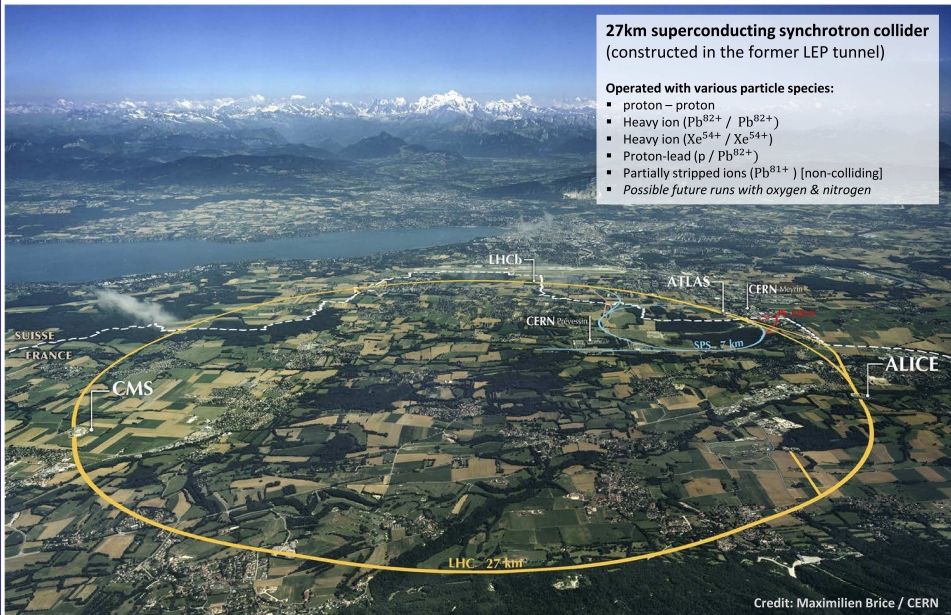


# Accelerators for HEP → Large Hadron Collider (LHC) is the highest energy accelerator in operation today

**27km superconducting synchrotron collider**  
(constructed in the former LEP tunnel)

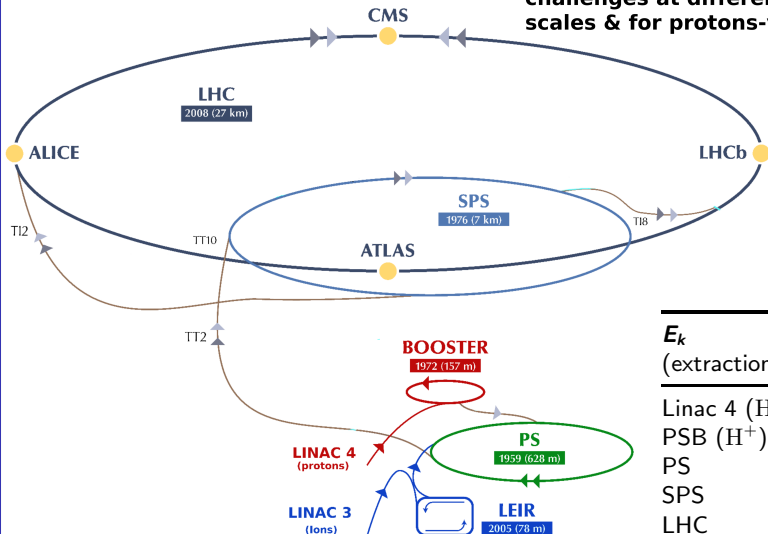
**Operated with various particle species:**

- proton – proton
- Heavy ion ( $\text{Pb}^{82+}$  /  $\text{Pb}^{82+}$ )
- Heavy ion ( $\text{Xe}^{54+}$  /  $\text{Xe}^{54+}$ )
- Proton-lead ( $p$  /  $\text{Pb}^{82+}$ )
- Partially stripped ions ( $\text{Pb}^{81+}$ ) [non-colliding]
- Possible future runs with oxygen & nitrogen



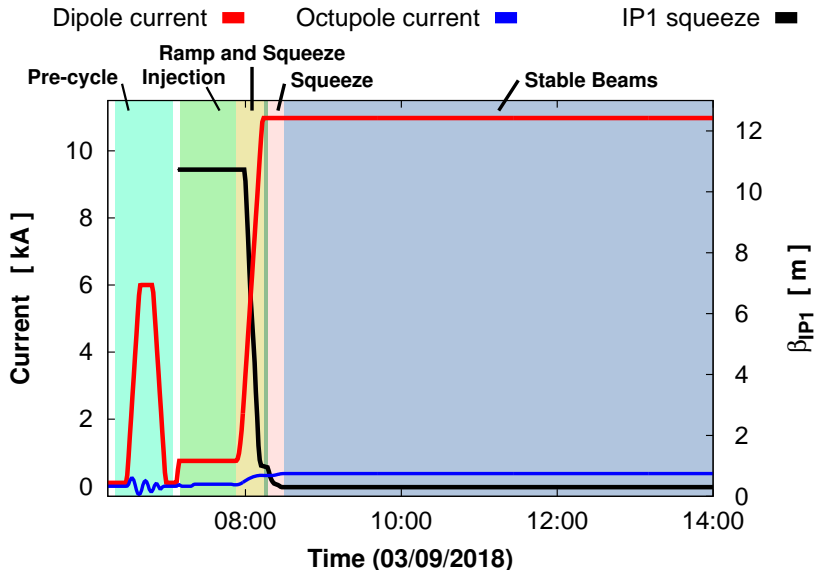
# Accelerators for HEP

- LHC has 2 injector chains
- Optimized to tackle different challenges at different energy scales & for protons-vs-heavy ions



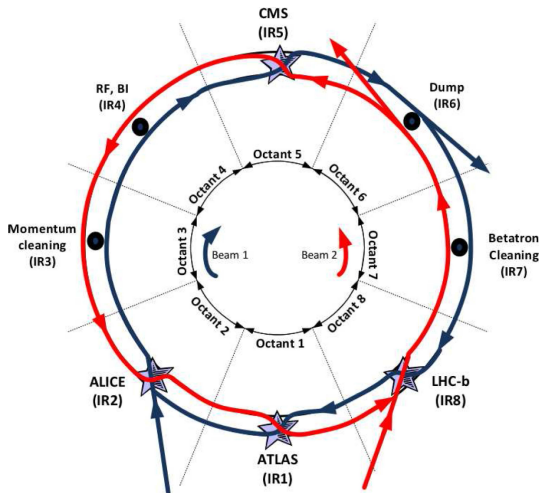
$E_k$ (extraction)	post-LIU ( $\geq 2020$ )
Linac 4 ( $H^-$ )	160 MeV
PSB ( $H^+$ )	2.0 GeV
PS	25 GeV
SPS	449 GeV
LHC	$\geq 6.8$ TeV

## The LHC cycle (2018)



# The Large Hadron Collider (LHC)

- 2 counter-rotating beams in a twin-ring synchrotron
- 8 straight insertion regions (IRs) & 8 bending Arcs 'A12 → A81'



- IR2: LHC B1 injection + HEP (ALICE)
- IR8: LHC B2 injection + HEP (LHCb)

---

- IR1: HEP (ATLAS)
- IR5: HEP (CMS)

---

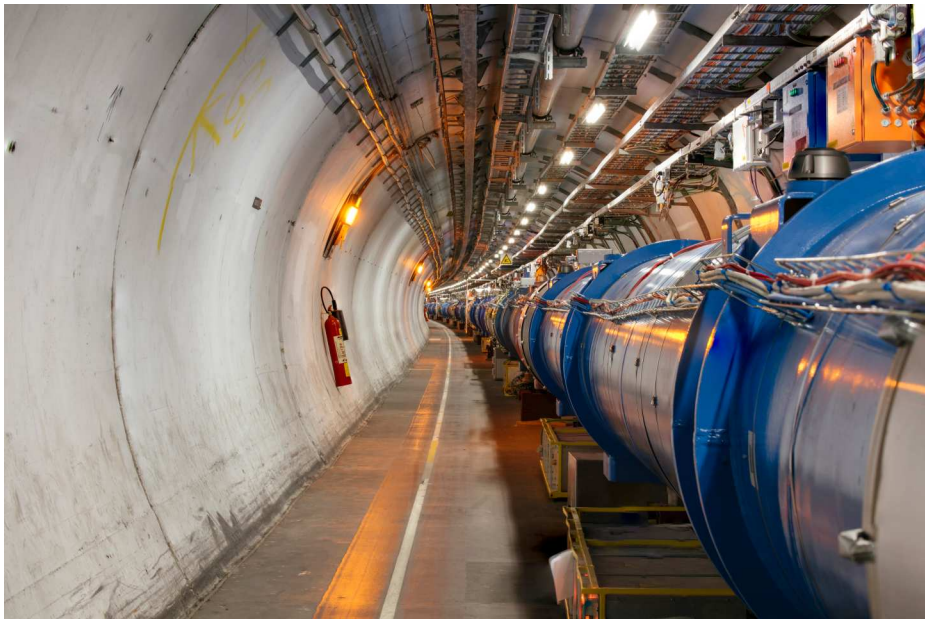
- IR3: COLLIMATION (momentum)
- IR7: COLLIMATION (transverse)

---

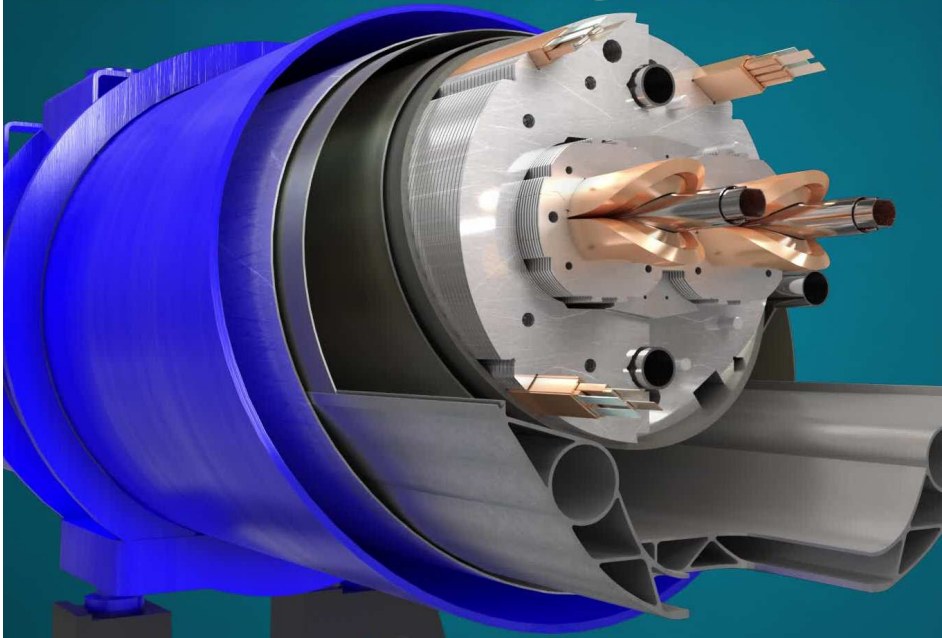
- IR4: Acceleration + instrumentation

---

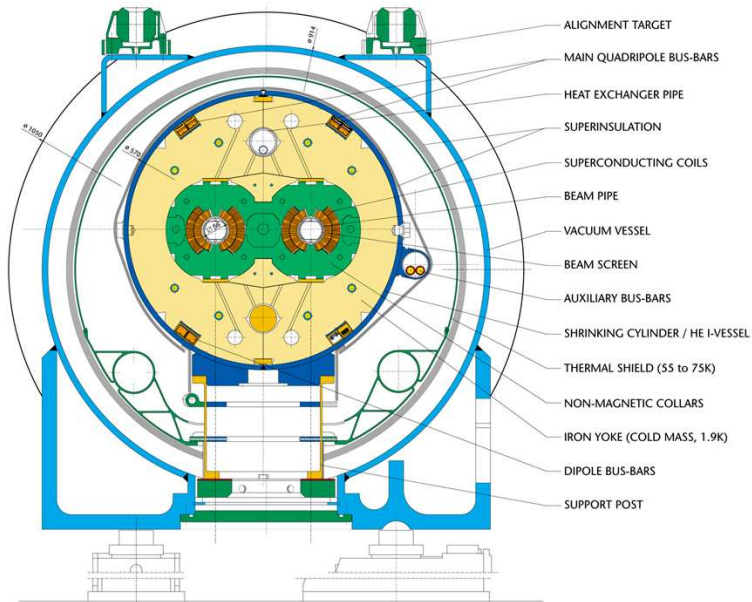
- IR6: LHC B1+B2 BEAM DUMP



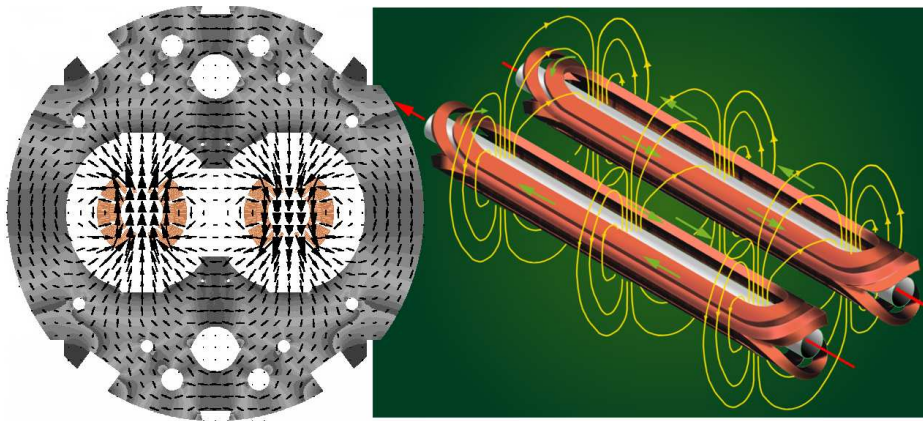
# LHC arcs use $\approx 8\text{T}$ superconducting dual bore dipoles



# Arcs utilize superconducting $\approx 8\text{ T}$ dual bore dipoles



## Arcs utilize superconducting $\approx 8$ T dual bore dipoles

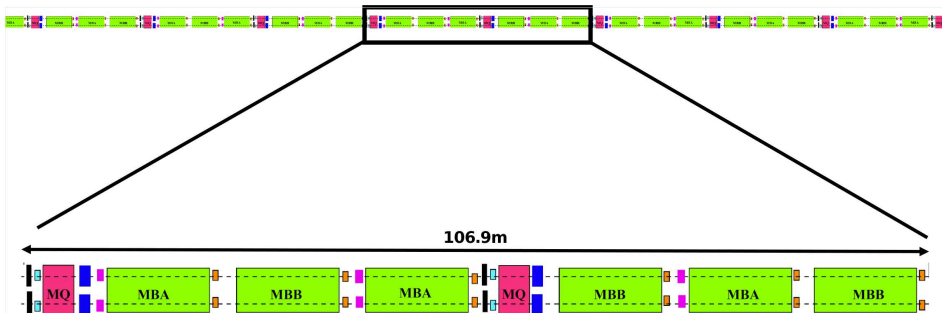




# Arcs have repeating pattern ('lattice') of magnets

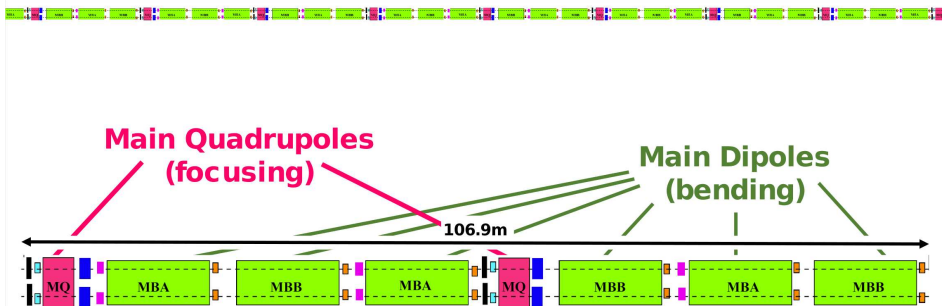


## 23 repeating 'cells' per Arc



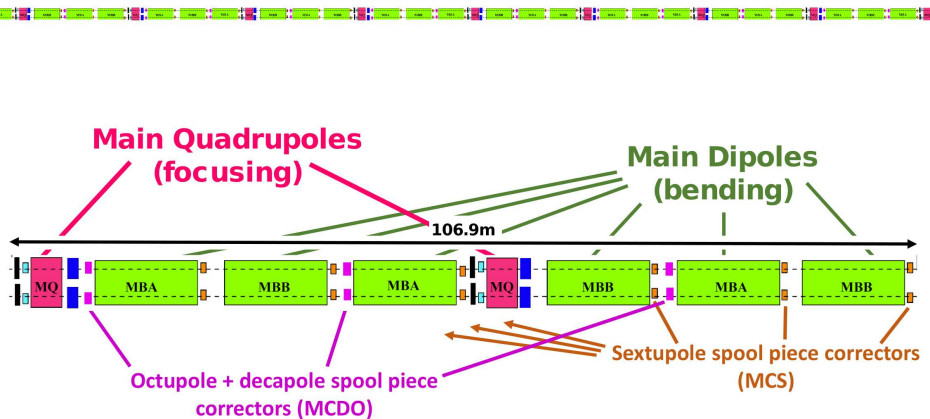
Magnets powered in series (arc-by-arc or families)

## 23 repeating 'cells' per Arc



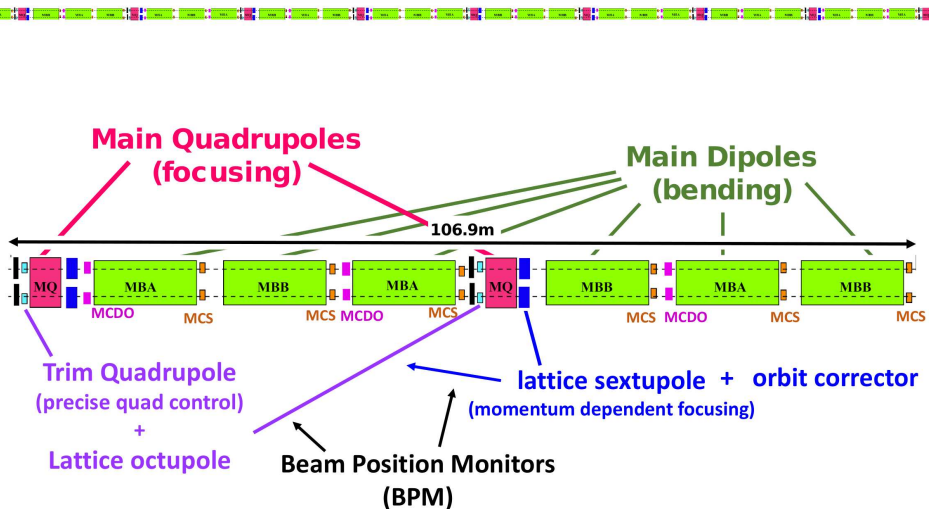
Most space occupied by dipoles and main quadrupoles

## 23 repeating 'cells' per Arc



Higher order magnets correct field imperfections in main dipoles

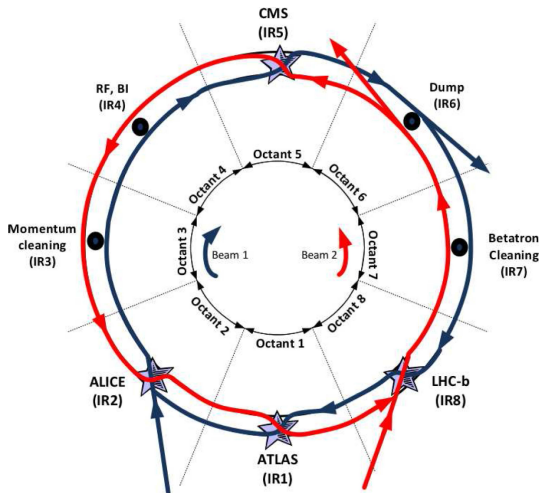
## 23 repeating 'cells' per Arc



Need room for beam instrumentation & magnet connections

# The Large Hadron Collider (LHC)

- 2 counter-rotating beams in a twin-ring synchrotron
- 8 straight insertion regions (IRs) & 8 bending Arcs 'A12 → A81'



- IR2: LHC B1 injection + HEP (ALICE)
- IR8: LHC B2 injection + HEP (LHCb)

---

- IR1: HEP (ATLAS)
- IR5: HEP (CMS)

---

- IR3: COLLIMATION (momentum)
- IR7: COLLIMATION (transverse)

---

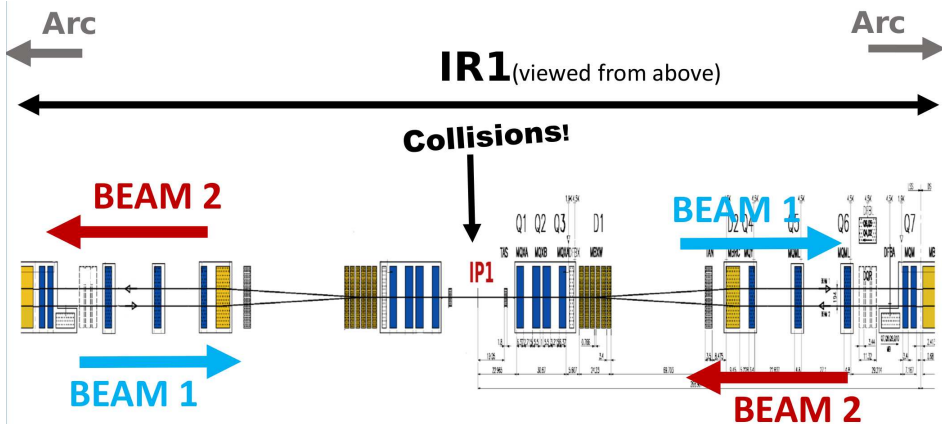
- IR4: Acceleration + instrumentation

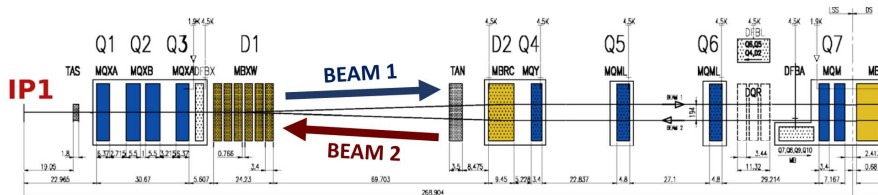
---

- IR6: LHC B1+B2 BEAM DUMP

## Structure of a HEP insertion:

- e.g. **Insertion Region 1 (IR1)** hosting the ATLAS experiment
- Beams collide at the **Interaction Point (IP1)**



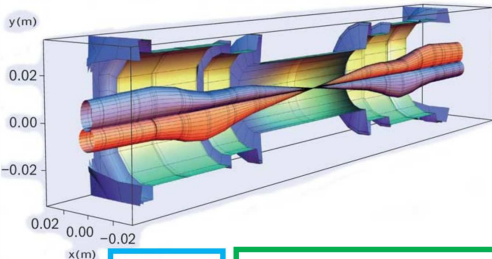


**Right side of IR1, viewed from above**



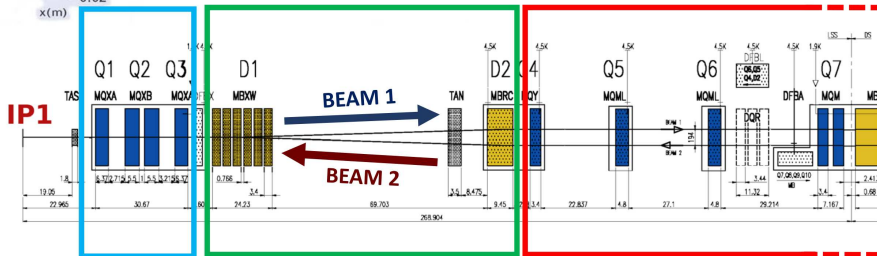






## Separation dipoles

(bring beams together in common aperture)



## Quadrupole triplets

Squeeze beam from  $\sim 1\text{mm}$  in Arc to  $\sim 10\mu\text{m}$  at IP

## Also corrector magnets

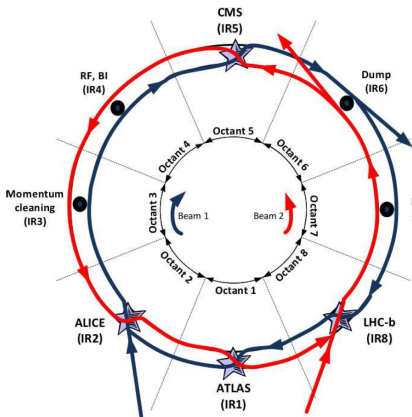
(coupling, sextupole, octupole, dodecapole)

## Matching section

(individually powered quads control transition from arc)

## Insertions have variety of functions in LHC, e.g.

→ All RF cavities in the LHC are located at IR4



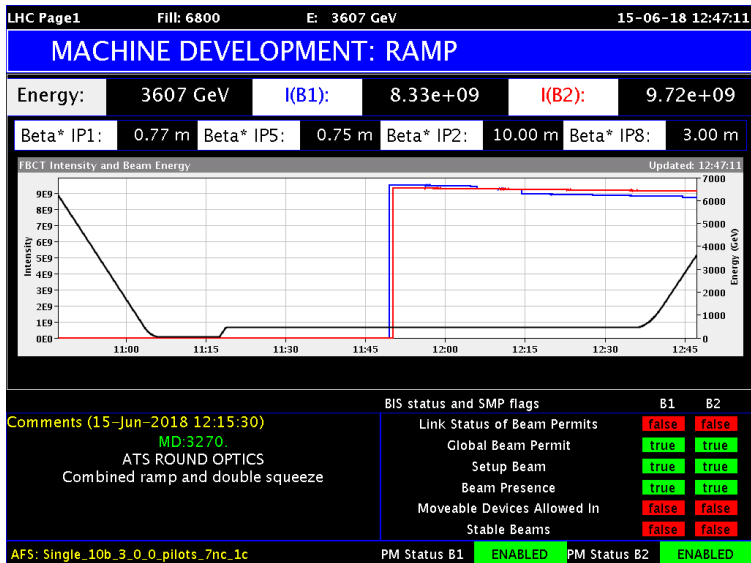


## Day to day operation of the CERN accelerators handled by the operations group, from the CERN Control Center (CCC)

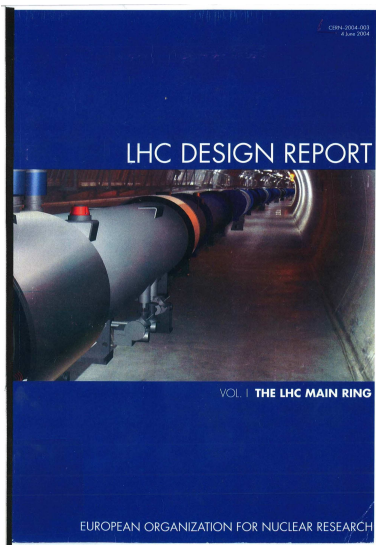


# LHC page 1: machine status & OP comments

<https://op-webtools.web.cern.ch/vistar/vistars.php>



## For general questions about LHC one commonly used resource is the LHC Design Report



LHC Design Report, v.1 : the LHC Main Ring

<http://cds.cern.ch/record/782076/>

LHC Design Report, v.2 : the LHC Infrastructure and General Services

<http://cds.cern.ch/record/815187>

LHC Design Report, v.3 : the LHC Injector Chain <http://cds.cern.ch/record/823808>

**BE CAREFUL: some parameters may be out of date**

→ **LHC has already exceeded its design performance in many ways!**



## Key Points

### ■ Overall structure of LHC

- 8 Arcs - this is where the beams are bent around the ring
- 8 IRs - various functions

### ■ Repeating lattice in the arcs → the LHC arc cell

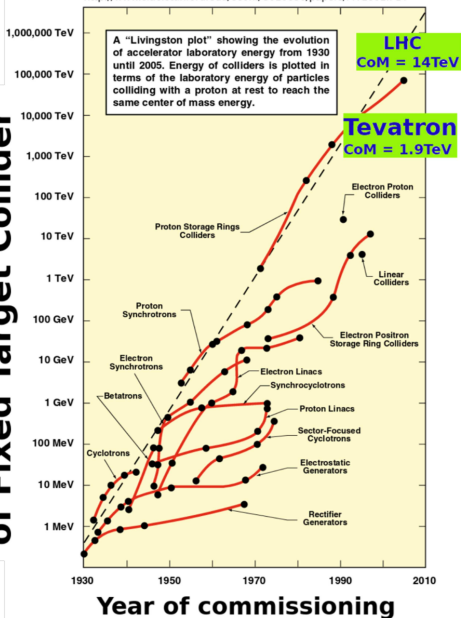
- can't fill the arc completely with dipoles!
- also quadrupoles for focusing, sextupoles for momentum-dependent focussing & chromaticity, nonlinear magnets for correcting field errors, instrumentation...

### ■ Typical layout of an insertion region

### ■ LHC injector Chain and operational Cycle

# Equivalent Beam Energy of Fixed Target Collider

From 2001 Snowmass AQccelerator R&D report,  
Part I : Executive Summaries, eConf C010630, SLAC-R-599  
<http://www.slac.stanford.edu/econf/C010630/papers/MT1001.PDF>



Beam-beam collider is essential for operation at energy frontier

Fixed target CoM energy:

$$E_{CM} \approx \sqrt{2m_t E_b}$$

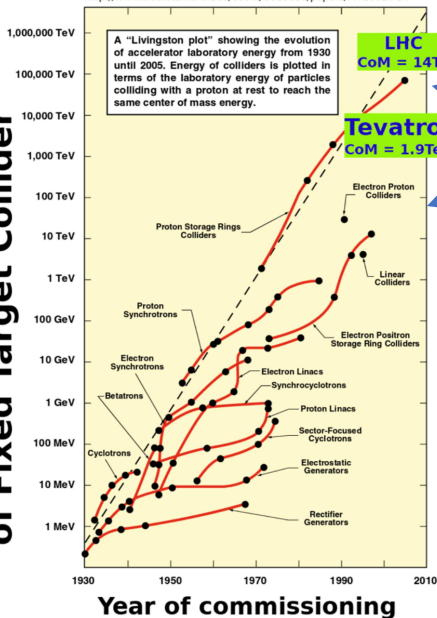
Collider CoM energy:

(head-on, equal mass)

$$E_{CM} = 2E_b$$

From 2001 Snowmass AQccelerator R&D report,  
 Part I : Executive Summaries, eConf C010630, SLAC-R-599  
<http://www.slac.stanford.edu/econf/C010630/papers/MT1001.PDF>

A "Livingston plot" showing the evolution of accelerator laboratory energy from 1930 until 2005. Energy of colliders is plotted in terms of the laboratory energy of particles colliding with a proton at rest to reach the same center of mass energy.

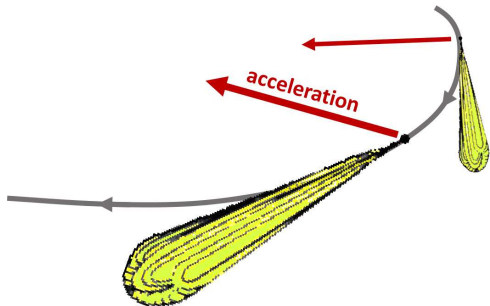


Clear distinction between energies achieved with  $e^{\pm}$  vs hadron colliders

## Limiting factor for circular $e^+$ / $e^-$ accelerators:

→ particles emit **synchrotron radiation** as they are bent around ring

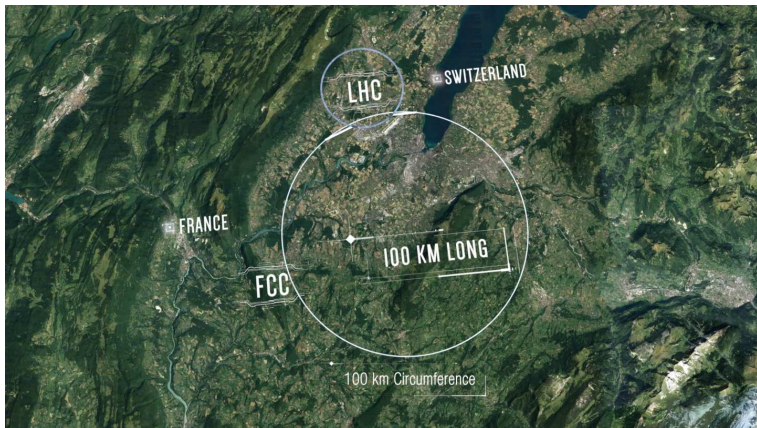
$$\Delta E/\text{turn} \propto \frac{(\beta_{\text{rel}}\gamma_{\text{rel}})^4}{\rho}$$



- LEP (e) energy loss:  $\sim 3 \text{ GeV/turn}$  (@ 101 GeV)
- LHC (p) energy loss:  $\sim 5 \text{ keV/turn}$  (@ 6.5 TeV)

To achieve higher energy-scales with  $e^{\pm}$  need to significantly increase the bending radius and circumference!

- FCC-ee: 100km, 88 – 365 GeV  $e^+/e^-$  collider )
- similar CEPC project in proposed in China

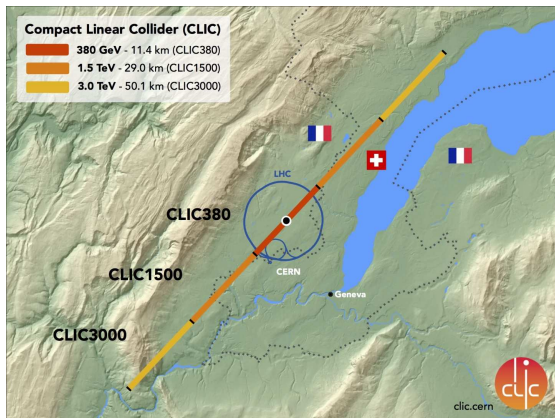


Even at 100km energy-loss/turn 3-4 $\times$  more than LEP!

→ design challenging as beam-energy changes around the ring!

## Several proposals for next-generation linear colliders!

- Not limited by synchrotron radiation
- Energy limited by collider length and accelerating gradient!

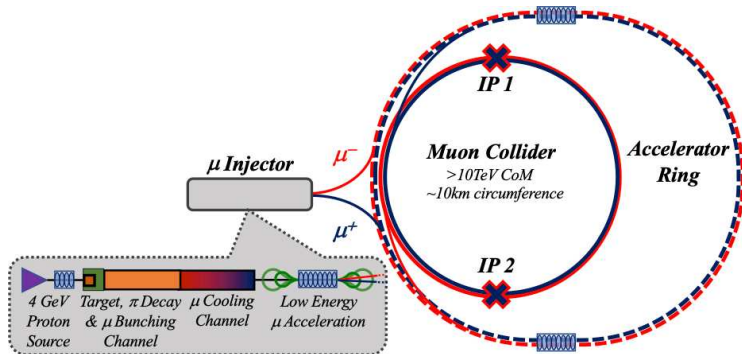


- CLIC: 11km/380GeV
- CLIC: up to 50km/3TeV )
- similar ILC project proposed in Japan



## Collide heavier particles to limit energy loss via SR

- Conventionally means progressing to hadron collider e.g. LEP → LHC!
- Active R/D into possibility of muon collider
  - challenging due to short muon lifetime





## Limiting factor for circular hadron (or muon) collider:

$$\vec{F} = q(\vec{E} + \vec{v} \times \vec{B})$$

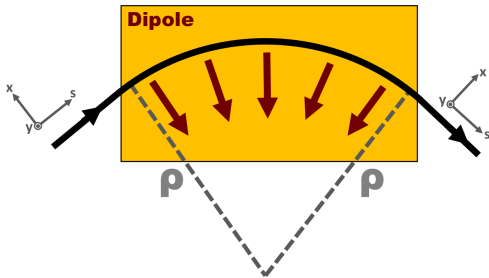
- Use Lorentz force to deflect beams around the synchrotron ring

Must create strong enough magnetic field to bend beams around whatever radius is defined by the tunnel geometry

$$F_{\text{Lorentz}} = F_{\text{centrip}}$$

$$qvB = \frac{\gamma m_{\text{rest}} v^2}{\rho} = \frac{pv}{\rho}$$

$$B\rho = \frac{p}{q}$$

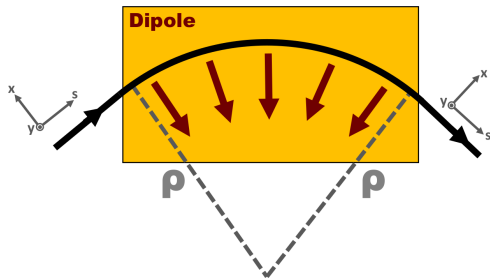


## Limiting factor for circular hadron collider:

→ need sufficient magnet strength to bend beams around the ring

$$B\rho \text{ [Tm]} = \frac{p \text{ [kgms}^{-1}\text{]}}{q \text{ [C]}}$$

$$B\rho \text{ [Tm]} = \frac{10}{2.998} p \text{ [GeV/c]}$$



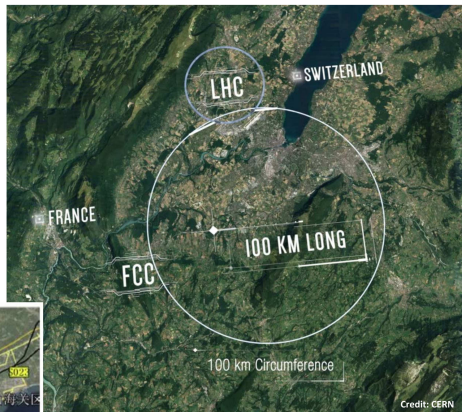
$B\rho$  is '**magnetic rigidity**': defines the maximum energy you can reach for a given dipole field in a given tunnel geometry

## To go to higher-energy scales with $p^\pm$ :

- significant increase to circumference
- significant increases to magnetic field



**Figure 3.3:** Illustration of the CEPC-SPPC ring sited in Qinghuangdao. The small circle is 50 km, and the big one 100 km. Which one will be chosen depends on the funding scenario.



For more details:

***Future Circular Collider Conceptual Design Report Volume 3***

<https://link.springer.com/article/10.1140/epjst/e2019-900087-0>

For more details:

***CEPC-SPPC Preliminary Conceptual Design Report. 2. Accelerator***

<https://inspirehep.net/literature/1395736>

***CEPC Conceptual Design Report: Volume 1 – Accelerator***

<https://arxiv.org/abs/1809.00285>

# But what about the moon?



Credit: NASA/Goddard Space Flight Center/Arizona State University

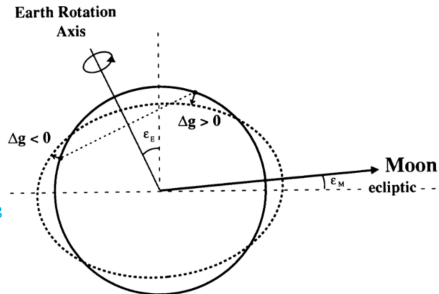
## Tidal deformation of earths crust changes the LHC circumference



If uncorrected this causes a drift in the beam energy

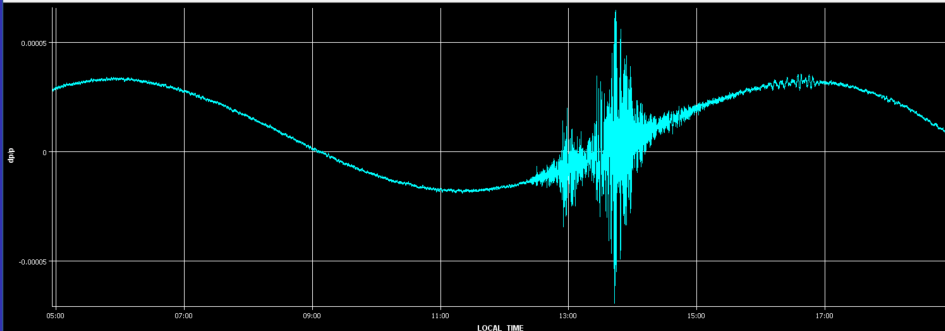
Effect of terrestrial tides on the LEP beam energy

L. Arnaudon et al. CERN SL/94-07 <http://cds.cern.ch/record/260368>



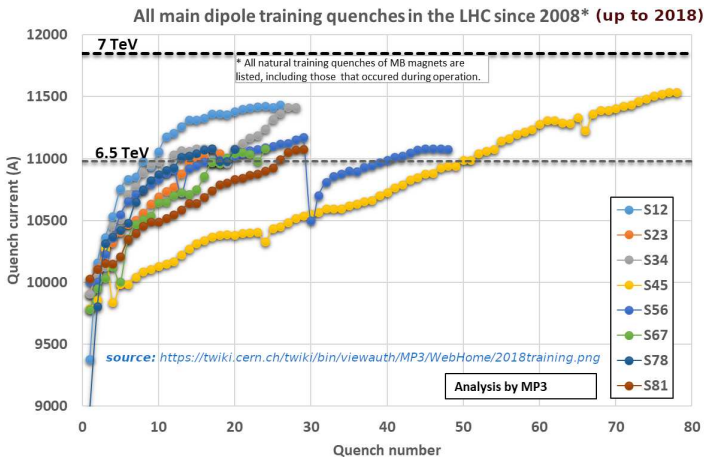
Timeseries Chart between 2016-11-13 04:55:51.338 and 2016-11-13 18:55:51.338 (LOCAL\_TIME)

LHC BOFSU-RADIAL\_LOOP\_ERROR\_B1



## SC-magnets must be trained to reach higher fields/currents

- Time needed for training was a key factor in the choice of LHC energy in Run2 and Run3



## High-energy beams plus extremely high stored energy in magnets poses serious challenges for machine protection

Report of the Task Force on the Incident of 19th September 2008 at the LHC", CERN-LHC-PROJECT-Report-1168:

*"The dipole bus bar at the location of the arc was vaporized, as well as the M3 line bellows around it, thus breaking open the helium enclosure..."*



## High-energy beams plus extremely high stored energy in magnets poses serious challenges for machine protection

Report of the Task Force on the Incident of 19th September 2008 at the LHC", CERN-LHC-PROJECT-Report-1168:

*"The force was applied to the external support jacks, displacing the cryomagnets from them and in some cases, rupturing their ground anchors or the concrete in the tunnel floor."*





## Key Points

- Different limitations on beam-energy for  $e^{\pm}$  and hadron accelerators
- What is magnetic rigidity & where does it come from?
- Various options being explored for next energy frontier accelerator
- Real world effects pose various challenges w.r.t. beam energy!

**WATCH OUT:** HEP normally discuss CoM → ABP may use alternative definition of energy! e.g. individual beam energy, energy per nucleon,...

What do particle physicists care about???

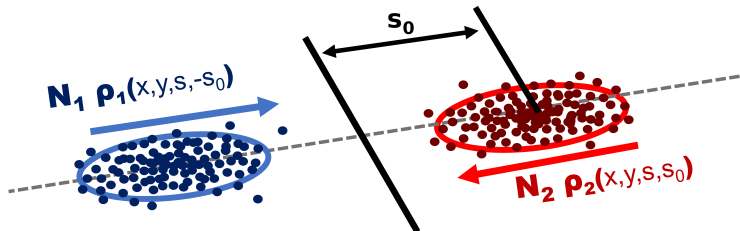
→ How much data (how many collisions) are generated?

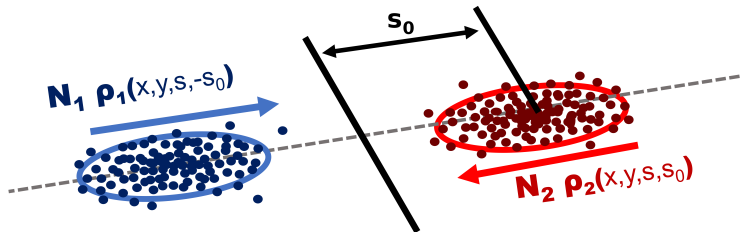
# Luminosity

## Event rate for a HEP interaction:

$$R = L \times \sigma$$

- $R$ : *Event Rate* [ $\text{s}^{-1}$ ]
- $\sigma$ : *Cross Section* [ $\text{barn} = 10^{-24} \text{cm}^2$ ]  
*property of the HEP interaction*
- $L$ : *Luminosity* [ $\text{inverse barn} / \text{s}$ ]  
*property of the collider*





$$L = f \sqrt{(\bar{v}_1 - \bar{v}_2)^2 - (\bar{v}_1 \times \bar{v}_2)^2} / c^2 N_1 N_2 \int_{-\infty}^{+\infty} \int \int \int \rho_1(x, y, s, -s_0) \rho_2(x, y, s, s_0) dx dy ds ds_0$$

For detailed discussion of Luminosity relations:

W.Herr & B.Muratori, *Concept of Luminosity*, CERN Accelerator School, Zeuthen, Germany, 15 - 26 Sep 2003

Toshio Suzuki, *General Formulas of Luminosity for Various Types of Colliding Beam Machines*, KEK-76-3, (1976)

M.A. Furman, *The Møller Luminosity Factor*, LBNL-53553, CBP Note-543, September 24, 2003

C.Møller, *General properties of the characteristic matrix in the theory of elementary particles I*,

K. Danske Vidensk. Selsk. Mat.-Fys. Medd. 23, 1 (1945) <http://gymarkiv.sdu.dk/MFM/kdvs/mfm 2020-29/mfm-23-1.pdf>

with some approximation:

$$L = \frac{(f_{rev} n_{coll}) N_1 N_2}{2\pi \sqrt{(\sigma_{x,1}^2 + \sigma_{x,2}^2)} \sqrt{(\sigma_{y,1}^2 + \sigma_{y,2}^2)}}$$

### Assume:

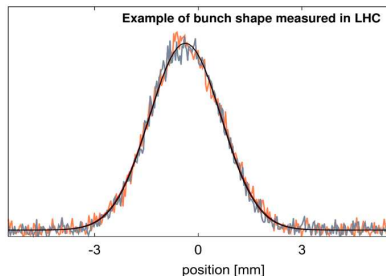
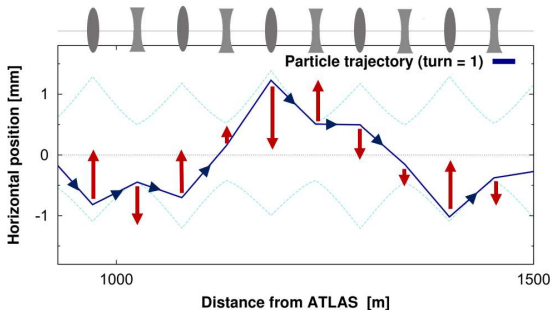
- uncorrelated gaussian bunch profiles in x,y,s
- head-on colinear collision of equal/opposite velocity beams
- equal bunch lengths  $\sigma_{s,1} \approx \sigma_{s,2}$
- revolution frequency of 2 beams are in sync
- $n_{coll}$  colliding bunches are all described by similar  $N_{1,2}, \sigma$

$$L = \frac{(f_{rev} n_{coll}) N_1 N_2}{2\pi \sqrt{(\sigma_{x,1}^2 + \sigma_{x,2}^2)} \sqrt{(\sigma_{y,1}^2 + \sigma_{y,2}^2)}}$$

### Beamsize:

$$\sigma_{x,y} = \sqrt{\beta_{x,y}(s) \epsilon_{x,y}}$$

- $\beta(s)$ : 'beta-function' [m]
  - **Property of the magnetic lattice**
  - **varies around the ring**
- $\epsilon$ : 'emittance' [ $\mu\text{m}$ ]
  - **Property of the particle bunch**
  - **Invariant around the ring**



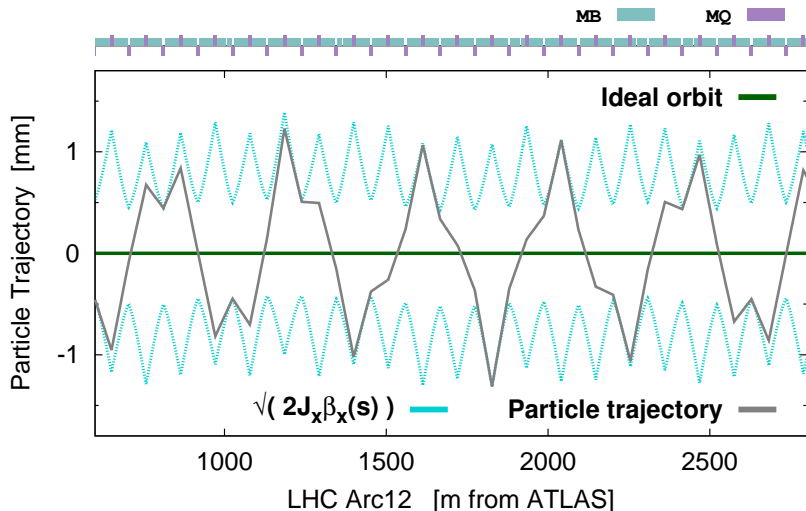
Particle motion about central closed-orbit described by **Hill's equation**:

- linear restoring force from quadrupoles is a function of location around the ring
- restoring force is periodic to at least the accelerator circumference

$$\frac{d^2x}{ds^2} - K(s)x = 0$$

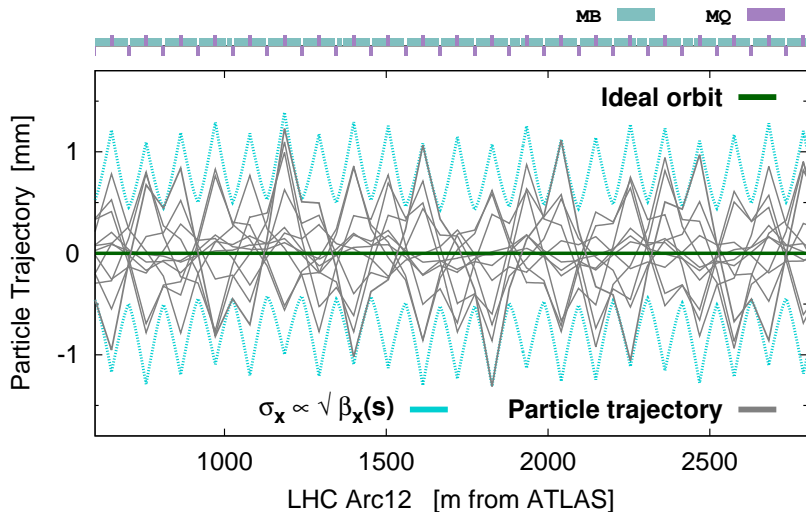
$$x = \sqrt{2J_x\beta_x(s)} \cos(\phi_x(s) + \phi_0)$$

## $\beta$ -function describes envelope of particle oscillations

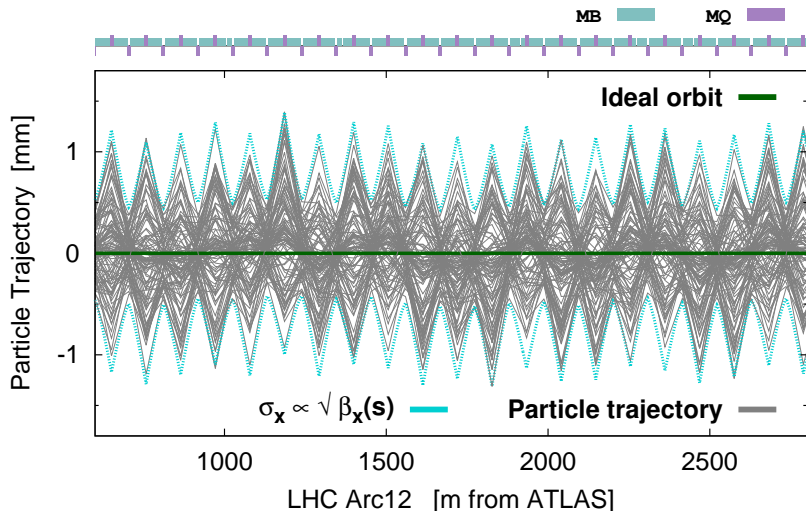




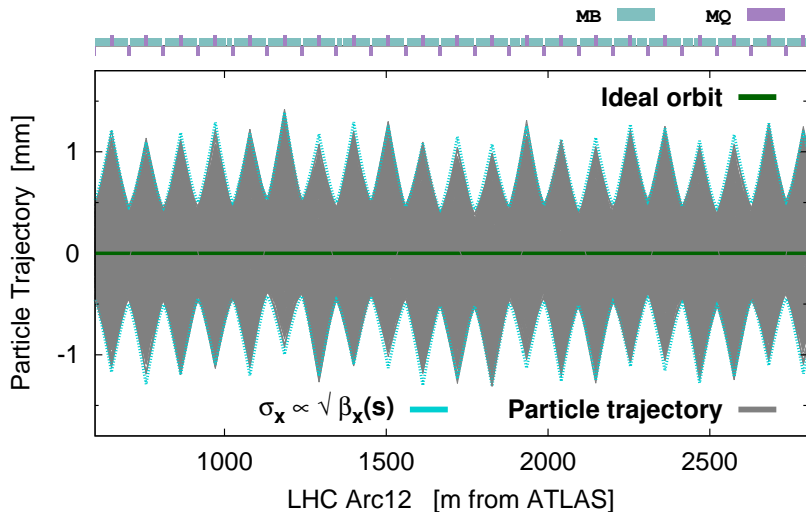
## $\beta$ -function describes envelope of particle oscillations



## $\beta$ -function describes envelope of particle oscillations

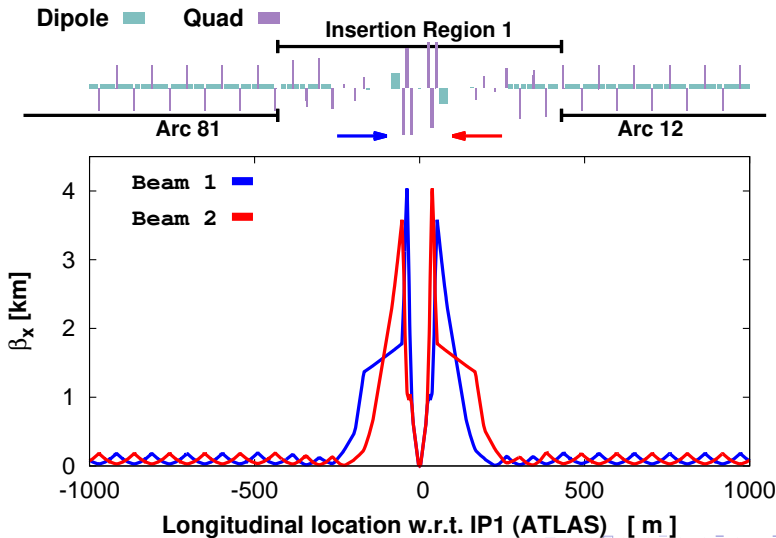


## $\beta$ -function describes envelope of particle oscillations



## Triplet quadrupoles in experimental IRs squeeze $\beta_{x,y}$

→  $\beta^*$  = minimum  $\beta$  in the IR  $\approx 25$  cm

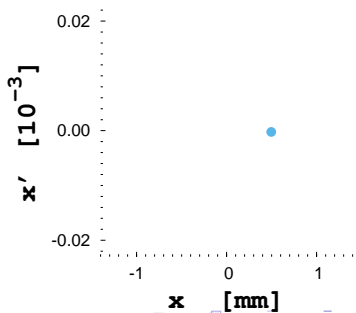
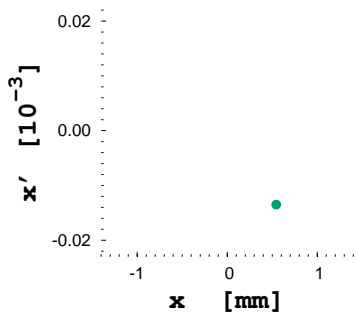
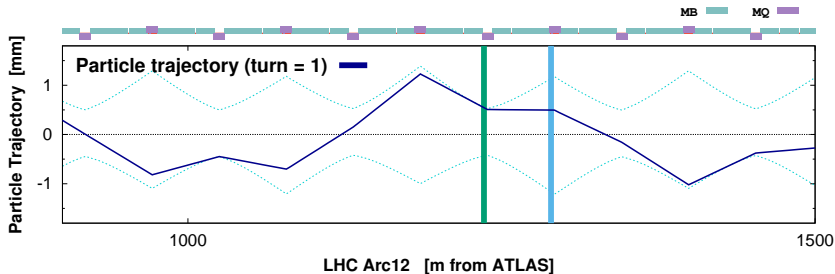


## Around 2026-27 LHC will shut down for major upgrades into the High-Luminosity-LHC

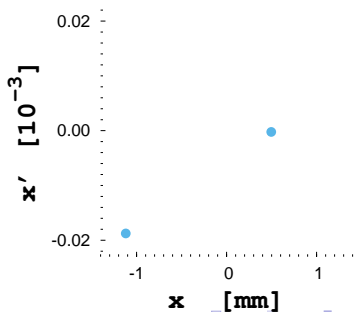
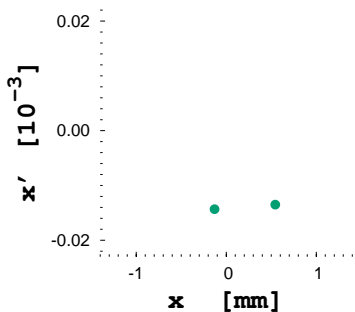
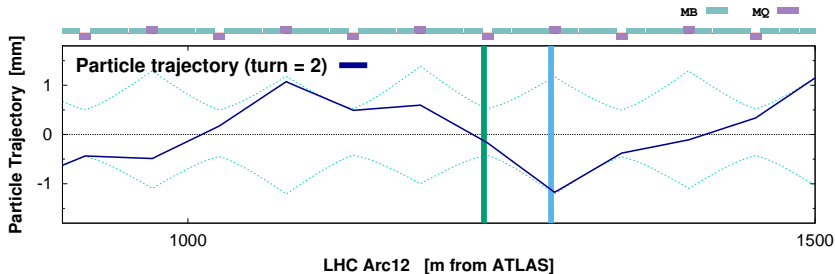
- Installation of new triplet magnets ( $Nb_3Sn$ ) allowing further reduction of  $\beta$
- Testing and construction ongoing!



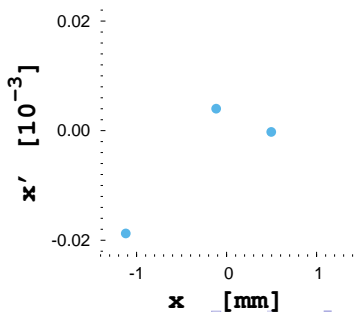
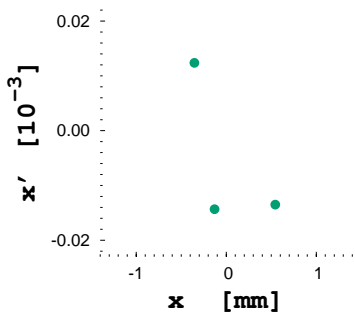
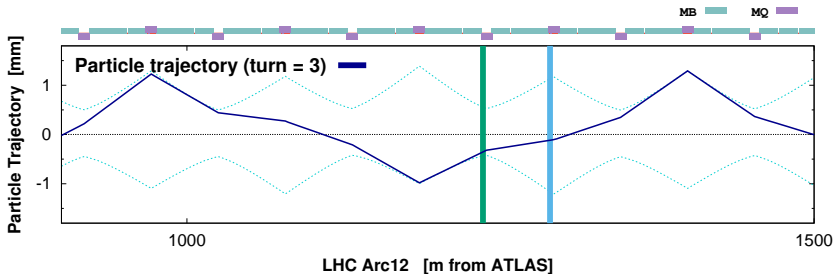
# Characterise particle trajectory by position ( $x$ ) and angle ( $x' = \frac{dx}{ds}$ )



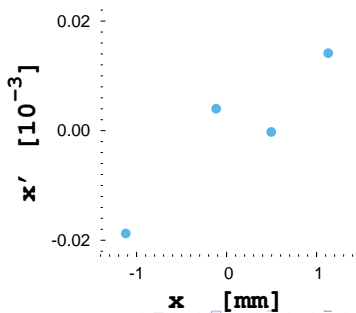
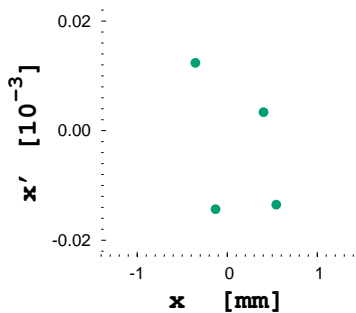
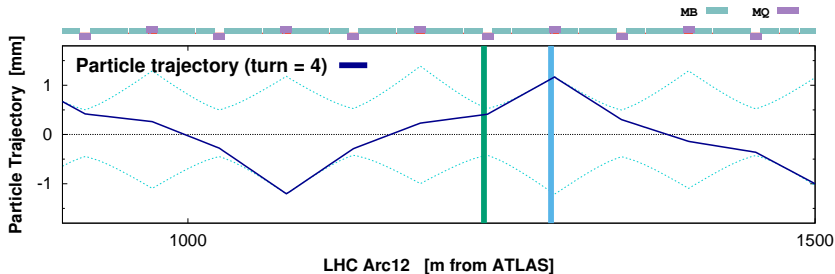
# Characterise particle trajectory by position ( $x$ ) and angle ( $x' = \frac{dx}{ds}$ )



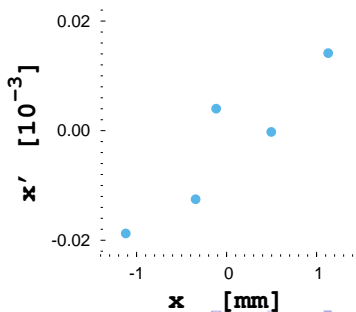
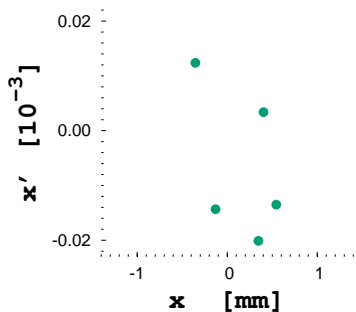
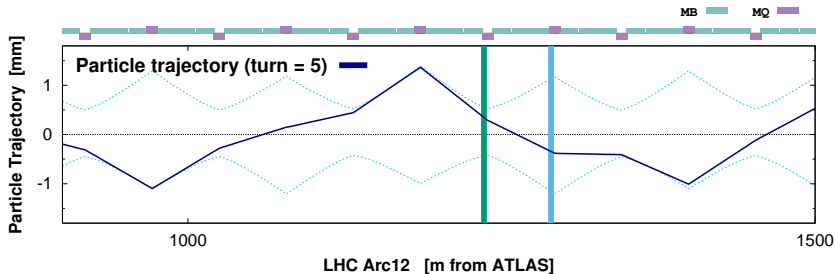
# Characterise particle trajectory by position ( $x$ ) and angle ( $x' = \frac{dx}{ds}$ )



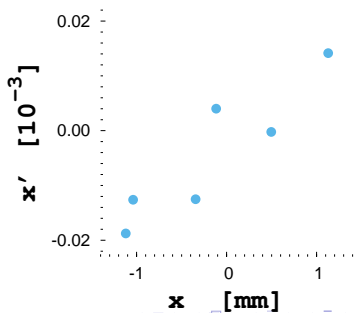
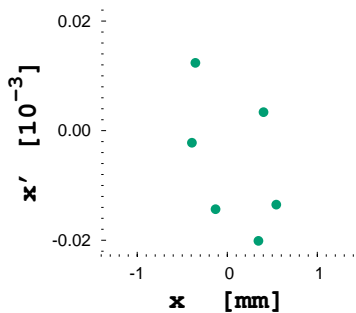
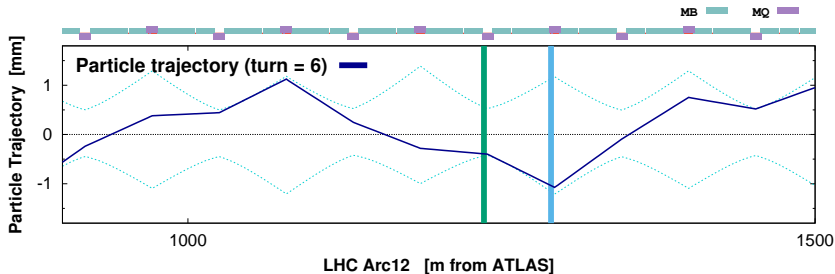


Characterise particle trajectory by position ( $x$ ) and angle ( $x' = \frac{dx}{ds}$ )

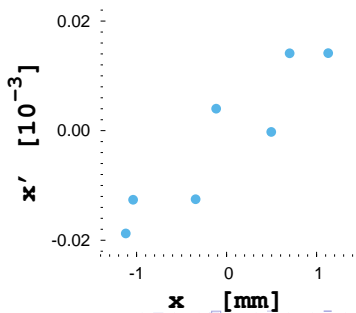
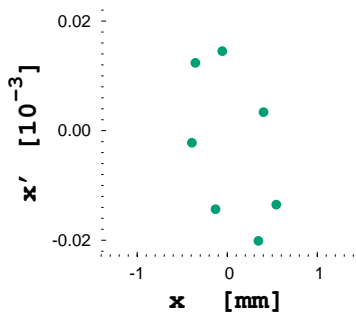
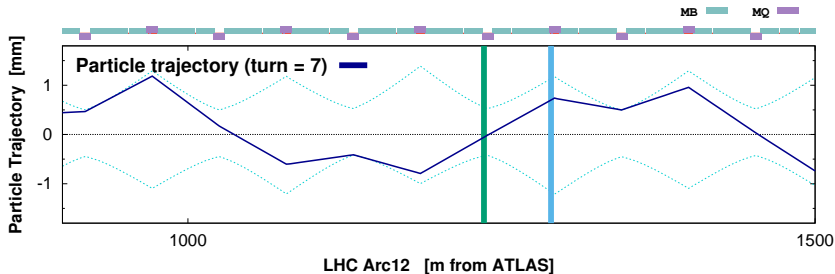
# Characterise particle trajectory by position ( $x$ ) and angle ( $x' = \frac{dx}{ds}$ )

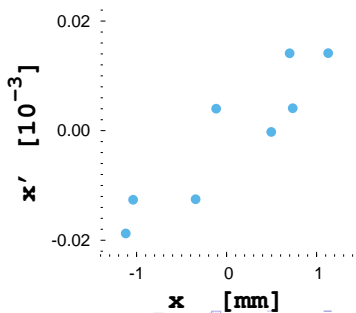
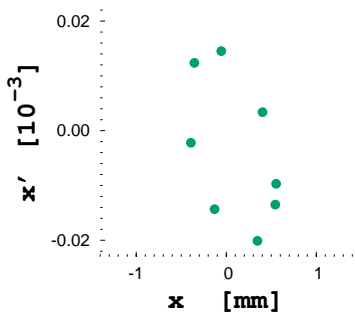
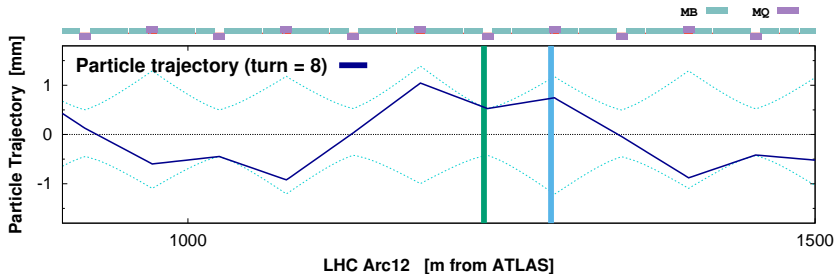


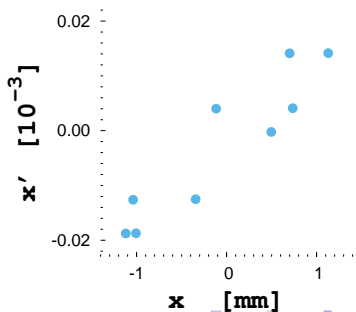
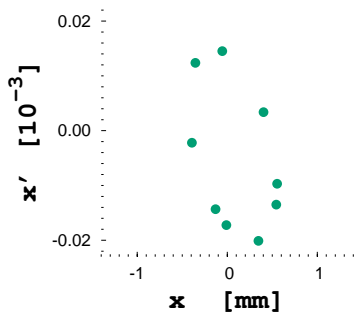
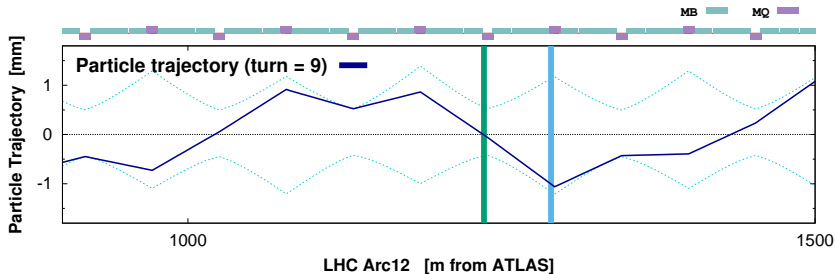
# Characterise particle trajectory by position ( $x$ ) and angle ( $x' = \frac{dx}{ds}$ )

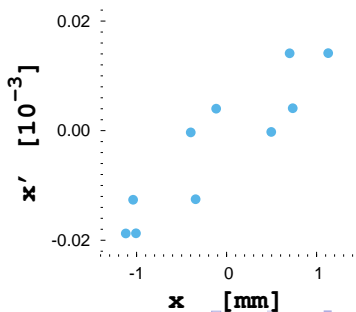
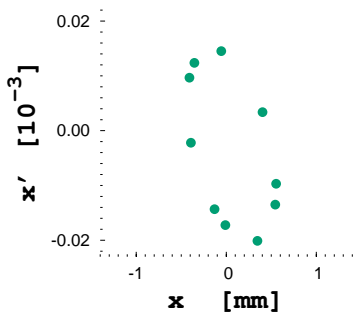
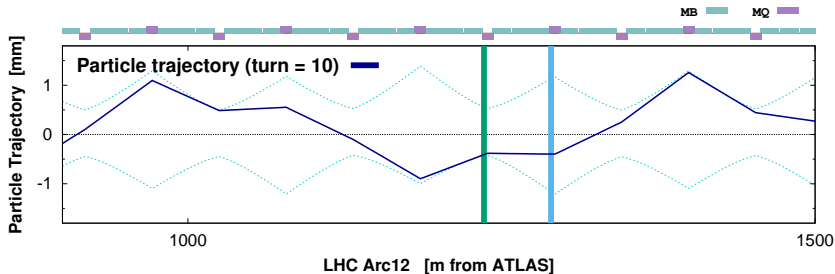


# Characterise particle trajectory by position ( $x$ ) and angle ( $x' = \frac{dx}{ds}$ )



Characterise particle trajectory by position ( $x$ ) and angle ( $x' = \frac{dx}{ds}$ )

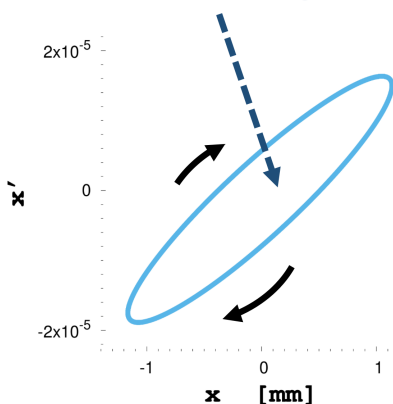
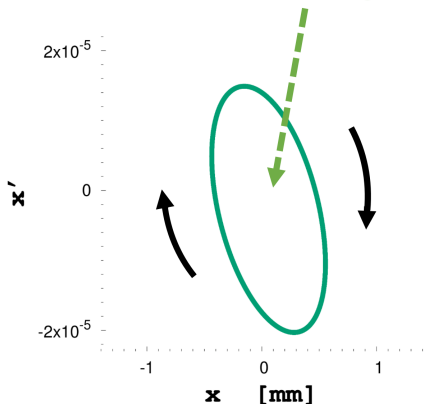
Characterise particle trajectory by position ( $x$ ) and angle ( $x' = \frac{dx}{ds}$ )

Characterise particle trajectory by position ( $x$ ) and angle ( $x' = \frac{dx}{ds}$ )

## Particles trace out elliptical paths in $(x, x')$ phase space

- shape changes around the ring
- **Area of ellipse is invariant** (for constant energy)

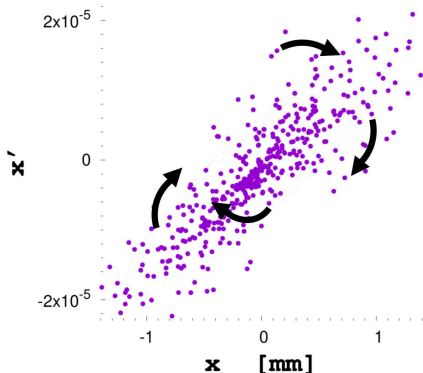
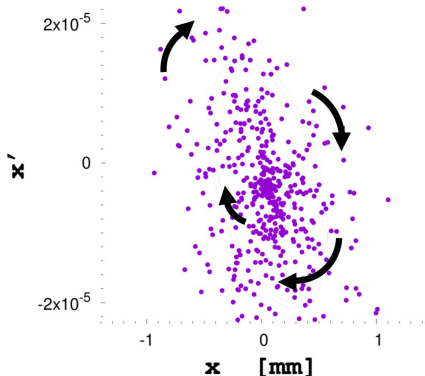
**VOLUME ENCLOSED @  $s$  = VOLUME ENCLOSED @  $s + \Delta s$**





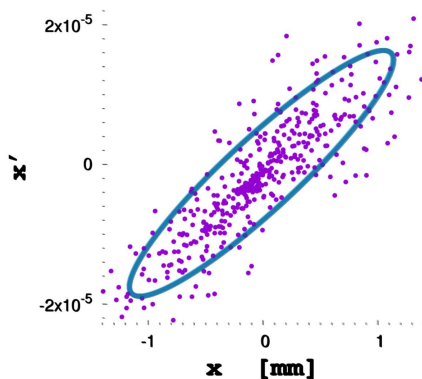
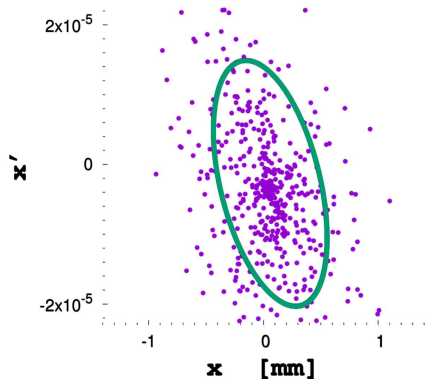
## Particles trace out elliptical paths in $(x, x')$ phase space

- in practice have many particles
- all follow similar elliptical trajectories (linear approximation)



## Particles trace out elliptical paths in $(x,x')$ phase space

- **'beam emittance'** is  $\text{area}/\pi$  of ellipse enclosing  $1\sigma$  of the particles in the bunch



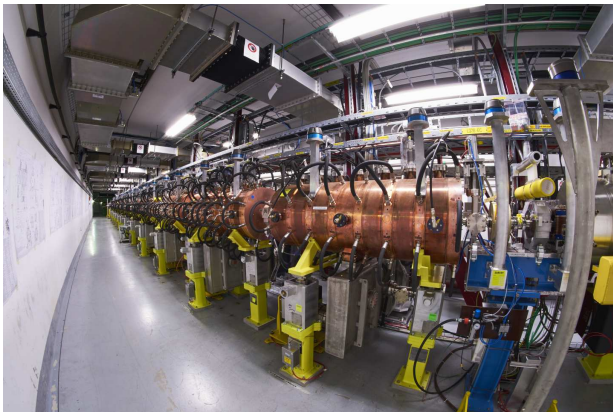
## Around 2026-27 LHC will shut down for major upgrades into the High-Luminosity-LHC

- Key component of HL-LHC project is upgrade of LHC injectors e.g. Linac2 (1978) → Linac4 (2021)



## Around 2026-27 LHC will shut down for major upgrades into the High-Luminosity-LHC

- Key component of HL-LHC project is upgrade of LHC injectors e.g. Linac2 (1978) → Linac4 (2021)



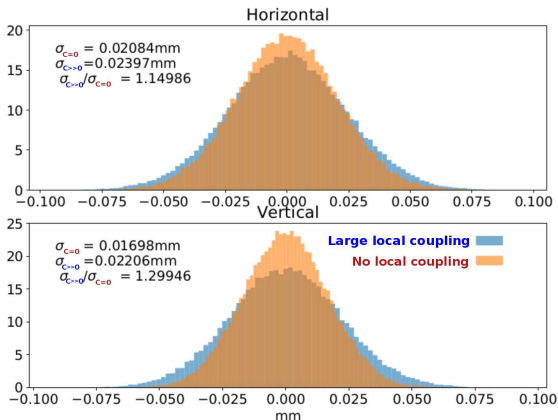
## More accurate beam-size description considers coupled 4D-phase-space

$$\Sigma_x^2 = \beta_{11}\epsilon_1 + \beta_{12}\epsilon_2$$

$$\Sigma_y^2 = \beta_{21}\epsilon_1 + \beta_{22}\epsilon_2$$

Betatron motion with coupling of horizontal and vertical degrees of freedom  
 V.A.Lebedev, S.A.Bogacz  
 FERMILAB-PUB-10-383-AD

Plot courtesy T.H.B. Persson (CERN)



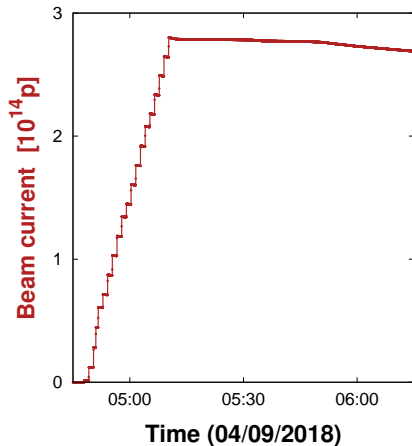
Poor local coupling correction in IR2 during 2018 Pb/Pb run

caused **50 %** reduction to Luminosity delivered to ALICE  
 until diagnosed & corrected

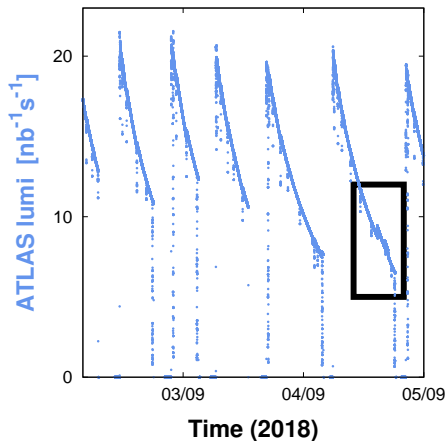
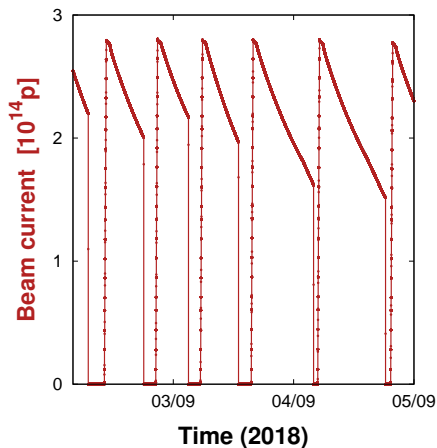
$$L = \frac{(f_{rev} n_{coll}) N_1 N_2}{2\pi \sqrt{(\sigma_{x,1}^2 + \sigma_{x,2}^2)} \sqrt{(\sigma_{y,1}^2 + \sigma_{y,2}^2)}}$$

- $N_{1,2}$ : Number of particles per bunch

- Accumulate bunch trains in the LHC ring at 450GeV
- Accelerate to 6.8TeV
- Bring bunches into collision & store for several hours
- Dump / Repeat

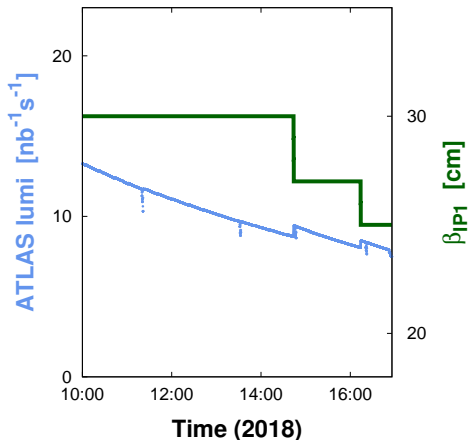
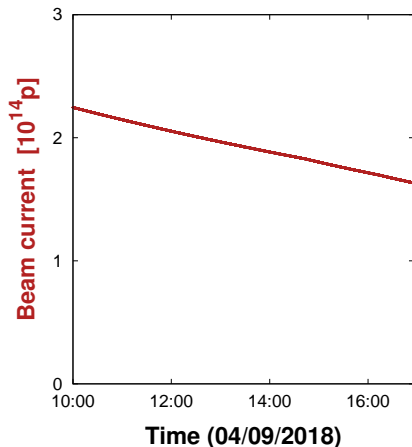


- **Beam intensity decays during a fill**
- Show a corresponding reduction in instantaneous luminosity
- Bulk of decay (LHC ideal conditions) is losses of particles which are colliding at the IPs **'burnoff'**



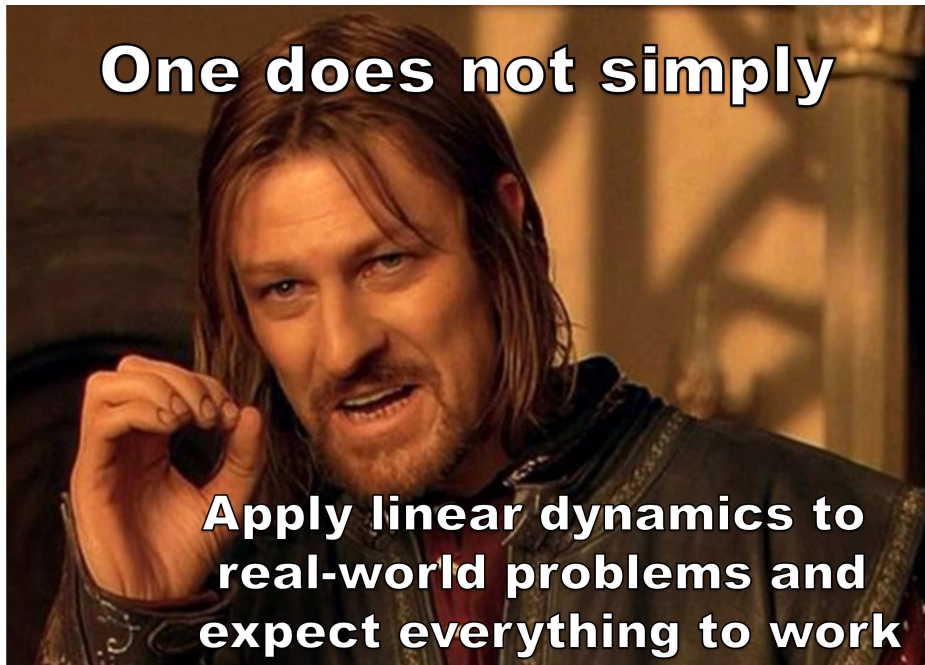


- Can try to maintain luminosity while  $N_{1,2}$  decays by changing other accelerator parameters which influence luminosity
- **‘Luminosity levelling’** → e.g.  $\beta^*$ -levelling

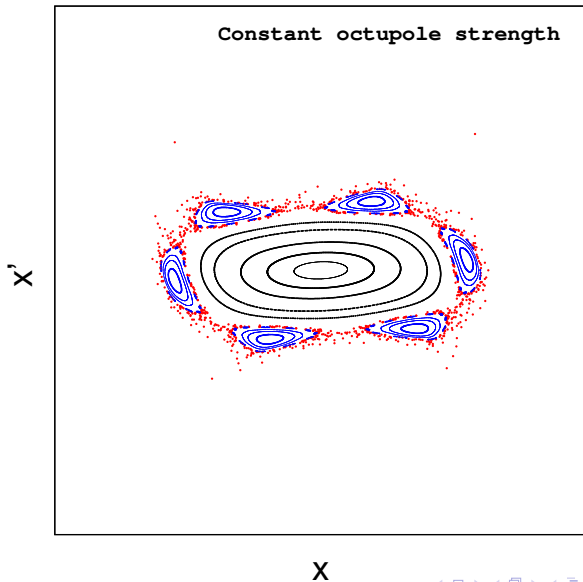


**One does not simply**

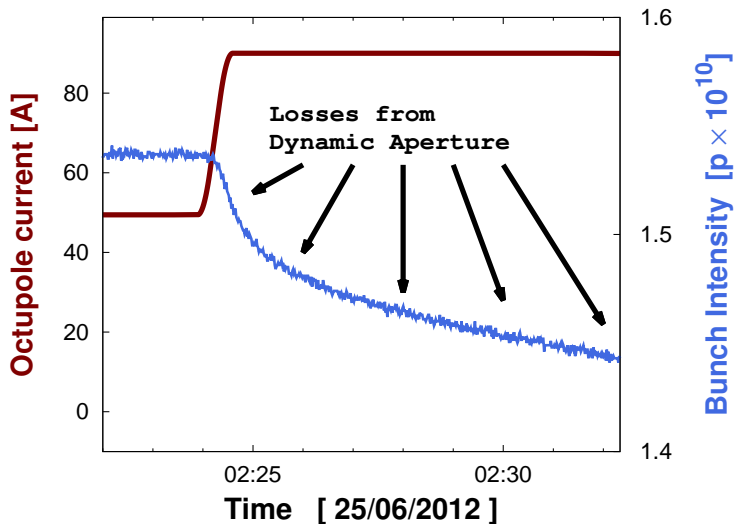
**Apply linear dynamics to  
real-world problems and  
expect everything to work**



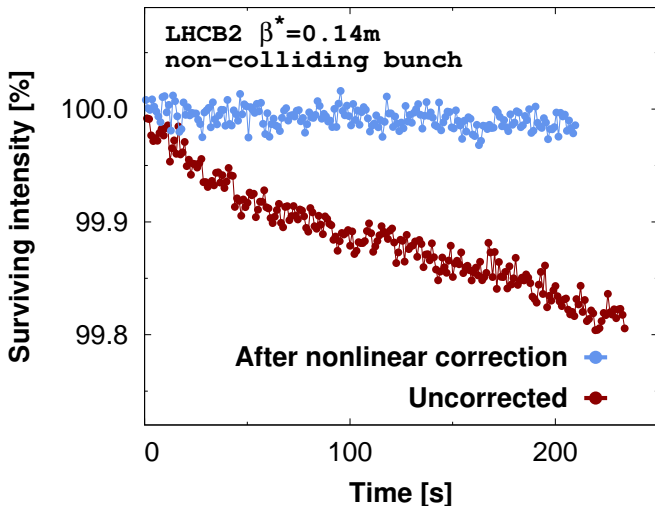
Large amplitude particles' motion can become chaotic & unstable  
→ 'Dynamic aperture'



The more nonlinear the beam dynamics becomes the smaller the dynamic aperture



## Use sextupole, octupole, decapole & dodecapole magnets to correct nonlinear dynamics in LHC & HL-LHC



$$L = \frac{(f_{\text{rev}} n_{\text{coll}}) N_1 N_2}{2\pi \sqrt{(\sigma_{x,1}^2 + \sigma_{x,2}^2)} \sqrt{(\sigma_{y,1}^2 + \sigma_{y,2}^2)}}$$

- $n_{\text{coll}}$ : Number of colliding bunches

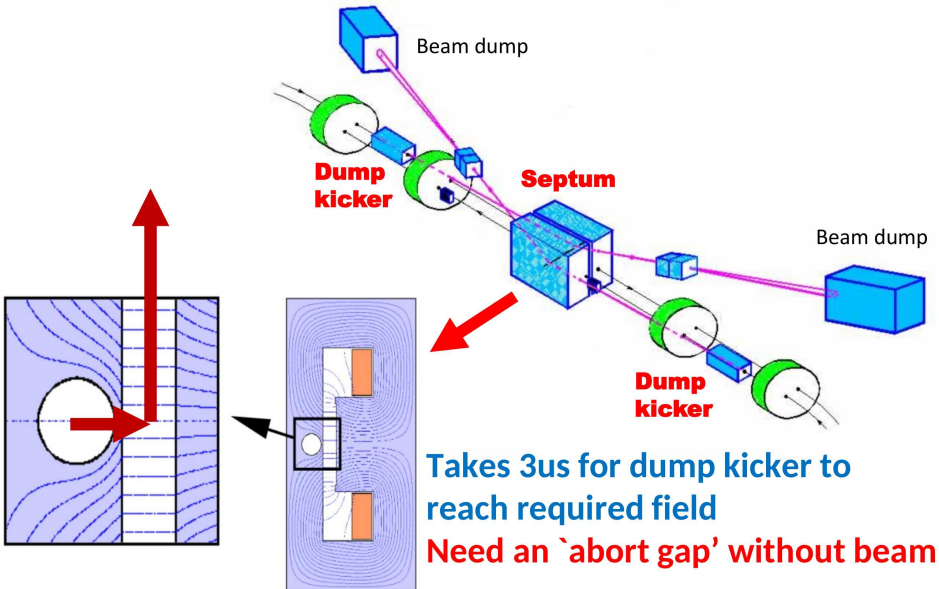
## How many bunches can we fit in the LHC?

- LHC revolution frequency  $\approx 11.245$  kHz  
→ revolution period  $\approx 89 \mu\text{s}$
- Minimum separation of bunches defined by RF system of the injector chain  
→ **25 ns** bunch spacing

soooo...  $\approx 3560$  bunches?

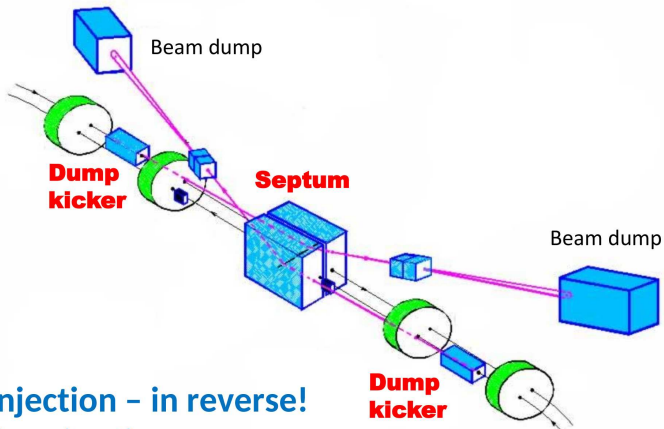
**NO!**

# Also need time to dump / inject beams





# Also need time to dump / inject beams

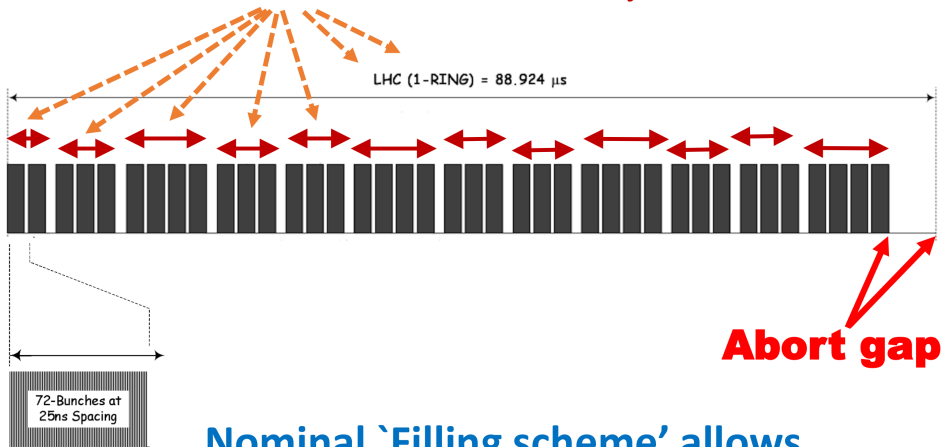


Similar issue at injection – in reverse!  
1 $\mu$ s injection kicker rise time

**Not practical to inject bunches one at a time!**

# Increase luminosity by colliding trains

Accumulate *'trains'* of bunches in SPS & inject 1 train at a time

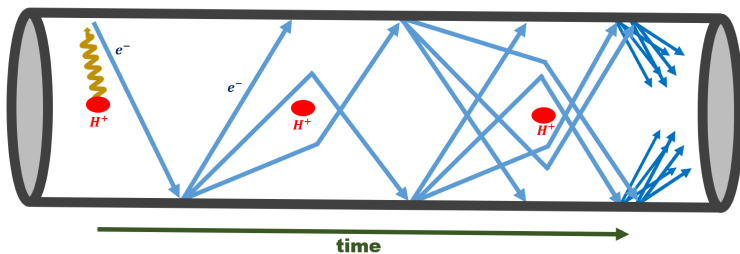


Nominal *'Filling scheme'* allows  
2808 bunches in each ring

In practice many different types of filling scheme are used in the LHC and it may not be desirable to operate with the nominal scheme

Good example of this is 'electron cloud'

- seed electron generated by e.g. photoemission / gas ionization
- electron accelerated by field of the beam hits chamber wall
- liberates more secondary electrons
- creates an avalanche of electrons in the beam pipe



Formation of electron cloud can be suppressed by leaving gaps in the bunch trains:

➡ During parts of Run2 LHC used a special '8b4e' filling scheme (micro-trains of 8 bunches followed by 4 empty slots)

For more details about electron cloud see:

G. Rumolo and G. Iadarola, *Electron Clouds*, CERN Yellow Reports: School Proceedings, Vol. 3/2017, CERN-2017-006-SP

<https://doi.org/10.23730/CYRSP-2017-003>

## Key Points

- **What is luminosity?**
- **What are its main dependencies?**
- **There are many complications which can affect the luminosity!**

## Event rate for a HEP interaction:

$$R = L \times \sigma$$

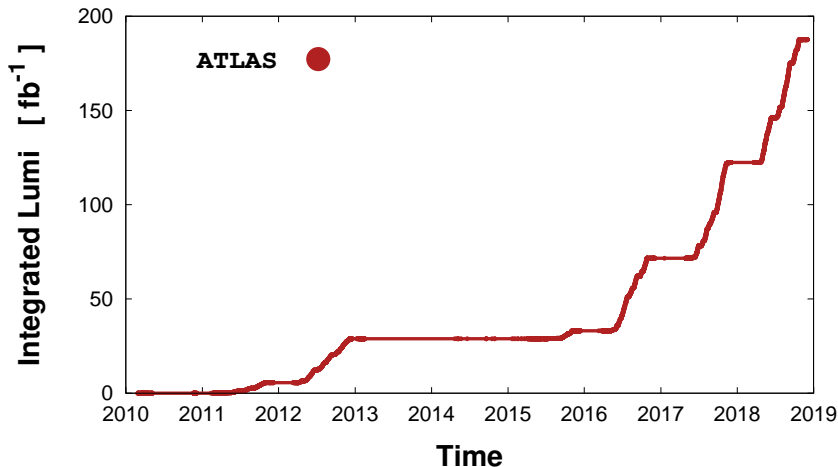
- $R$ : *Event Rate* [ $\text{s}^{-1}$ ]
- $\sigma$ : *Cross Section* [ $\text{barn} = 10^{-34} \text{cm}^2$ ]  
*property of the HEP interaction*
- $L$ : *Luminosity* [ $\text{inverse barn} / \text{s}$ ]  
*property of the collider*

Total number of interactions defined by the **Integrated Luminosity** [inverse femto-barn]

$$N = \left( \int L(t) dt \right) \times \sigma$$

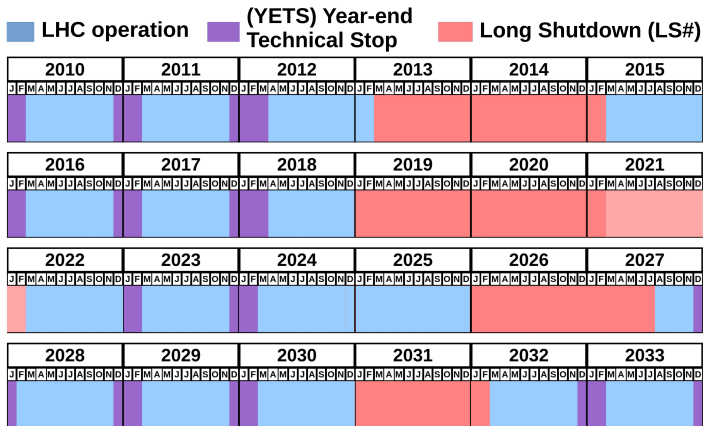
## Integrated Luminosity is key figure of merit for collider like LHC

→ significant factor is how much time spent on luminosity production



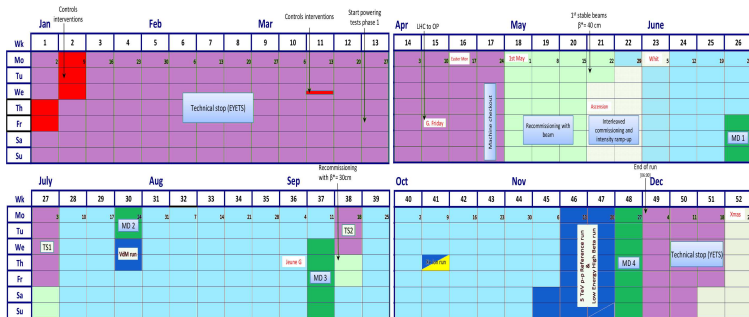
<https://lhc-statistics.web.cern.ch/LHC-Statistics/>

## Approximate schedule for LHC lifetime (accurate up to 2023)



- LHC operation is interspersed with regular **shutdown** periods for maintenance and upgrades

# LHC schedule over 1 year (2017)

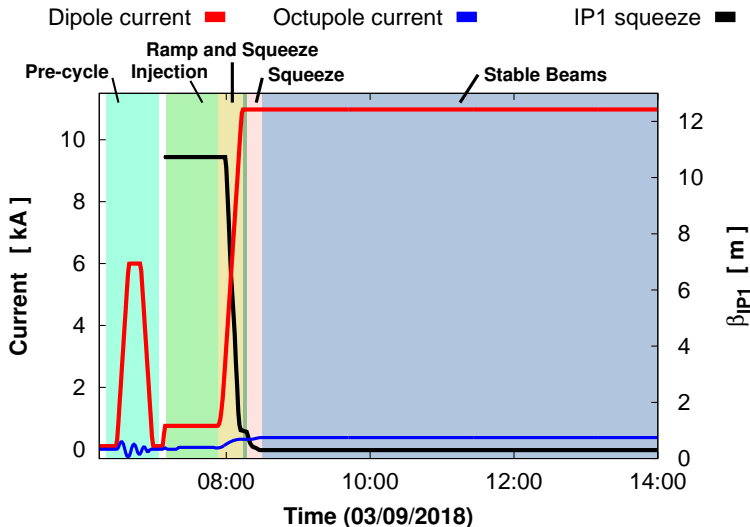


Many types of activities during 1 year of LHC operation

- **Technical Stop** (YETS + regular breaks)
- **Accelerator commissioning**
- **Accelerator physics/technology studies**
- **Luminosity production** **proton-proton** and **special runs**



## Turn-around-time between stable-beams is a key factor in achieved integrated luminosity!



## LHC and injector chain is an extremely complicated system

- Even small technical problems can add up over 1 year!

LHC Page1      Fill: 9075      E: 0 GeV      18-07-23 14:11:47

### PROTON PHYSICS: NO BEAM

	BIS status and SMP flags			B1	B2
<p style="color: yellow;">Comments (17-Jul-2023 18:57:49)</p> <p style="text-align: center;">Problem with IT.L8 leak in the insulation vacuum</p> <p style="text-align: center;">No beam until further notice (weeks)</p>	<p>Link Status of Beam Permits</p> <p>Global Beam Permit</p> <p>Setup Beam</p> <p>Beam Presence</p> <p>Moveable Devices Allowed In</p> <p>Stable Beams</p>	<p style="background-color: green; color: white;">true</p> <p style="background-color: red; color: white;">false</p> <p style="background-color: red; color: white;">false</p> <p style="background-color: red; color: white;">false</p> <p style="background-color: red; color: white;">false</p> <p style="background-color: red; color: white;">false</p> <p style="background-color: red; color: white;">false</p>	<p style="background-color: green; color: white;">true</p> <p style="background-color: red; color: white;">false</p> <p style="background-color: red; color: white;">false</p> <p style="background-color: red; color: white;">false</p> <p style="background-color: red; color: white;">false</p> <p style="background-color: red; color: white;">false</p>		
AFS: 25ns_2464b_2452_1842_1821_236bpi_12inj_hybrid	PM Status B1	ENABLED	PM Status B2	ENABLED	

## LHC and injector chain is an extremely complicated system

- Even small technical problems can add up over 1 year!



## Key Points

- **Integrated luminosity is the key figure of merit for a collider like the LHC**
- **How much time is actually spent colliding beams together?**
- **What are we doing the rest of the time?**

## The Future of laboratory based HEP?

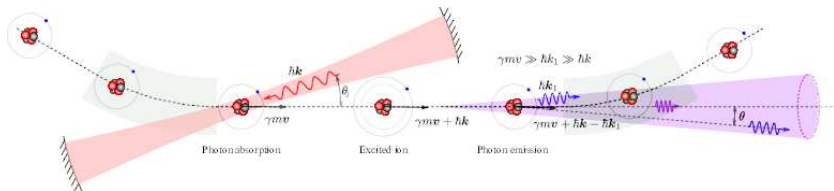
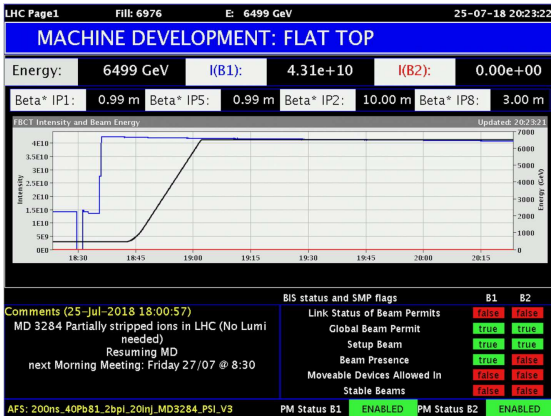
$$\Delta E/\text{turn} \propto \frac{(\beta_{\text{rel}}\gamma_{\text{rel}})^4}{\rho}$$

$$B\rho \text{ [Tm]} = \frac{10}{2.998} p \text{ [GeV/c]}$$

- linear e/e colliders (ILC/CLIC)
- 100 km e/e collider ring (FCC-ee, CEPC)
- New magnets in LHC tunnel (HE-LHC)
- 100 km hadron collider (FCC-hh, SppC)
- muon collider

# Lots of interest to accelerate/collide new types of particles!

- Collide with photons!
- In 2018 LHC accelerated  $Pb^{81+}$  to study potential future use of LHC as a  $\gamma$ -factory
- Various ideas of how to use accelerators e.g. CLIC as  $\gamma/\gamma$  colliders



# Minituration of low/intermediate energy accelerators will be one of the key developments of accelerator technology for its impact on society

- One of the most exciting topics in accelerator field today is cancer treatment via FLASH therapy with electron beams!
- Requires high-quality, high-energy electron beams on a hospital scale
- Lots of interest in applying RF technology from CLIC to FLASH!



Flash irradiation

Irradiation in a flash: Unique sparing of memory in mice after whole brain irradiation with dose rates above 100 Gy/s

Benoit Montay-Gruel<sup>1,3</sup>, Kristoffer Petersson<sup>1,3</sup>, Maud Jacard<sup>1</sup>, Gail Boivin<sup>1</sup>, Jean-François Germond<sup>1</sup>, Pierre Petit<sup>1</sup>, Raphaël Doennen<sup>1</sup>, Vincent Favard<sup>1</sup>, Jérôme Bochud<sup>1</sup>, Claude Bailat<sup>1</sup>, Jean Bourhis<sup>1,4</sup>, Marie-Catherine Vozzani<sup>1,5,6,7</sup>

<sup>1</sup>Department of Radiation Oncology, Geneva University Hospital, Switzerland; <sup>2</sup>Faculty of Life Sciences, University of Lincoln, United Kingdom; <sup>3</sup>Department of Radiation Physics, Geneva University Hospital, Switzerland; <sup>4</sup>Faculty of Life Sciences, University of Lincoln, United Kingdom; <sup>5</sup>Department of Radiation Physics, Geneva University Hospital, Switzerland; <sup>6</sup>Faculty of Life Sciences, University of Lincoln, United Kingdom; <sup>7</sup>Faculty of Life Sciences, University of Lincoln, United Kingdom

ARTICLE INFO

Article history:  
Received 27 October 2024  
Received in revised form 12 April 2025  
Accepted 4 May 2025  
Available online 22 May 2025

Keywords:  
Flash-RT  
Whole brain irradiation  
Cognitive preservation

Our recent publications have shown that irradiation at an ultra-high dose rate was able to protect normal tissue from radiation-induced injury. When compared to radiotherapy delivered at conventional dose rates (1–4 Gy/fraction), this so-called “Flash” radiotherapy (“fRCy”) Flash-RT was shown to enhance the differential effect between normal tissue and tumor in lung models [1,2] and consequently allowed for dose escalation. The biological interest of Flash-RT seems to rely essentially on a specific, yet unexplained, response occurring in normal cells and tissues. We initially hypothesized that the protective effect of Flash was related to the high-dose rate delivery, in other words related to the very short time of exposure. In order to further explore Flash-RT and to validate its protective effect on normal tissues, we decided to extend our observation from the brain to other organs. We wanted to investigate brain response to Flash-RT as it is a well-defined and robust model in radiotherapy [3–5].

When dealing with unexpected biological results, such as the ones previously described with Flash-RT, accurate dosimetry of the delivered irradiation is essential. However, dosimetry at an ultra-high dose rate in high-dose-per-fraction beams is non-trivial as current radiotherapy dosimetry protocols are not designed for such conditions and before the detectors available for online

measurements (i.e. ionization chambers, diodes, and diodeless detectors) start to saturate when the dose rate/fluence per pulse is increased beyond what is used in conventional radiotherapy [6–8]. Therefore, we needed to rely on dosimeters that had been previously validated to function accurately at more extreme irradiation conditions, i.e. mainly passive dosimeters. Among these options, we selected thermo-luminescent dosimeters (TLD) chips because of their small size (3.2 × 3.2 × 0.9 mm<sup>3</sup>) so that they could be used for measuring dose in the brain of mice. By positioning the TLD inside the skull of a sacrificed mouse, we were able to validate the dose delivered to the brain during whole brain irradiation [9,10].

Brain injuries after WB at sub-lethal doses delivered at conventional radiotherapy dose rates are well described [5,9,10]. They include functional alterations, neuronal [11,12] and myelin sheath loss [14,15]. Cognitive impairments are the most described functional deficits observed in mice and humans following WB [4,16]. They are caused by an alteration of hippocampal neurogenesis, which can occur as early as one month post WB single fraction WB [17]. These cognitive impairments can be evaluated using the “Novel Object Recognition test” [18] in mice and rodents [19]. Therefore, we used this assay to investigate the functional effect of Flash-RT on the normal brain of adult mice.

Using a combination of accurate dosimetry measurements and robust biological tests, we first aimed to investigate the potential neuroprotective effect of Flash-RT and indeed found memory preservation in mice after 10-Gy WB with Flash-RT (delivered in

RESEARCH ARTICLE

RESULTS

## FLASH irradiation protects lungs from radiation-induced fibrosis

Two hundred forty mice were divided into groups ( $n = 3$  to 14), sham-irradiated or exposed to single-dose 15- or 17-Gy CONV (1<sup>st</sup> Ca<sup>2+</sup>) or 17-Gy FLASH (4.5-MeV electron beam) with three different irradiation rates, and then sampled at 8, 16, 24, and 30 weeks post-irradiation (Fig. 1) for evaluation of complications and histopathological analysis of lung fibrosis.

The initiation and development of pulmonary fibrosis was compared in mice exposed to 17 Gy in either the CONV or FLASH mode (Fig. 1A). Fibrogenesis in the CONV group started early and was progressive and progressive, resulting in dose-dependent fibrotic foci at the CONV dose rate were as efficient as 17<sup>th</sup> Ca<sup>2+</sup> rays with regard to the production of fibrotic patterns in the lung (Fig. 1A). Pulmonary lesions consisted of consolidated foci, localized mostly in subpleural areas and sometimes at the extremity of pulmonary lobes or in peribronchovascular areas (Fig. 1A, HES panels, and Fig. S9). These foci were dense and associated with Masson's trichrome staining (Fig. 1A, MT panels), with thickening and reorganization of alveolar septa, intense collagen deposition, and activation of the transforming growth factor- $\beta$  (TGF- $\beta$ 1/SMAD cascade) (Fig. S10) but with low signs of vascular healing, scarring or retraction. Major signs of inflammatory lesion were seen 24 weeks post-irradiation (Fig. S11), with infiltration of alveolar septa by eosinophils, by fewer macrophages, occasional uncontracted giant cells associated with lymphocytes, and plasma cells or occasional neutrophils (frequently elaborating eosinophil deodorant granules). 15-Gy CONV was sufficient to initiate lung fibrosis, as expected [7–10]. In contrast, no histological signs of pulmonary fibrosis (Fig. 1A, A to C) and no activation of the TGF- $\beta$ 1/SMAD cascade (Fig. S10) were observed in the 17-Gy FLASH group.

A dose escalation study of 16- to 20-Gy FLASH was then performed ( $n = 3$  to 12). Mice had received 20-Gy FLASH did not develop fibrosis (Fig. 1C). No macroscopic signs of airway lesions were observed either, although we observed well-defined hair degeneration observed in the irradiated area (Fig. 1D and Fig. S21), consistent with the fact that the dose delivered to animals was >15-Gy (20). In contrast, animals exposed to 17-Gy CONV developed severe cutaneous lesions (Fig. 1E) and the irradiated skin (Fig. S21). Mice exposed to <25-Gy FLASH experienced cachexia within 32 weeks. After 24 weeks post-17-Gy CONV resulted in massive pulmonary edema and fibrotic intrapulmonary patches with inflammatory lesions and macrophage infiltration in thickened alveolar lamina (Fig. 1A). In conclusion, FLASH was shown to be less fibrogenic than CONV irradiation (Fig. 1A to C).

## FLASH protects blood vessels and bronchi from radiation-induced acute apoptosis

Early (1 hour post) and late (24 hours post) markers of apoptosis were probed in histological sections of irradiated lungs by the determination of caspase-3 cleavage and terminal deoxynucleotidyl transferase (TdT)-mediated dUTP nick end labeling (TUNEL) and caspase-3 immunohistochemical labeling, respectively. 7.5-Gy CONV was sufficient to induce massive cleavage of caspase-3 at 1 hour post in mice from vascular and bronchial structural cells, whereas in contrast, no major signs were observed in animals exposed to 17-Gy FLASH (Fig. 2A). In animals exposed to

7.5-Gy CONV, TUNEL-positive nuclei were observed 24 hours after in epithelial cells of the bronchi, inflammatory cells embedded into the stroma, and smooth muscle cells surrounding the bronchi (Fig. 2B). No TUNEL staining was observed in pulmonary cells of the rat in mice exposed to 17-Gy FLASH, but rare inflammatory cells invading the tissue proved to be TUNEL-positive (28). 30-Gy FLASH was required to induce caspase-3 and TUNEL responses in an organ similar to that of 7.5-Gy CONV.

These observations suggest that vascular apoptosis in the lung could be the primary signal that would trigger lung-stromal complications, including fibrosis, as already suggested in the gut [13]. To test this model, 24 hours before irradiation, mice were treated with neurotrophin factor-4 (NTF), a key cytokine known to be involved in endothelial cell survival, inflammation, myofibroblast transdifferentiation, and the pathogenesis of radiation pneumonitis [14,15]. Apoptosis was monitored 2 hours post-irradiation by the IIS Spectrum system (PerkinElmer) and a fluorescent antibody V probe for *in vivo* imaging. In the absence of TNF, the total signal of annexin V fluorescence after 30-Gy FLASH was twofold lower than that after 15-Gy CONV (Fig. 2C), thus confirming the low pro-apoptotic potential of FLASH irradiation. TNF- $\alpha$  also increased the annexin V signal by 26-fold over non-treated controls. It also increased to 15-Gy CONV or 36-Gy FLASH, complementation by TNF- $\alpha$  increased the amount of fluorescence by two- and fourfold, respectively (Fig. 2C). These observations thus, thus allowing follow-up until 15 weeks after irradiation. Major signs of inflammation and fluid extravasation (Fig. 2A, asterisks) which are signs of persistent vascular lesions, were present in the TNF- $\alpha$  treated groups. Patches of subpleural fibrosis (Fig. 2C, black arrows) were observed only in the group treated with 15-Gy CONV.

In conclusion, TNF- $\alpha$  promoted acute apoptosis in the lungs of FLASH-irradiated animals and triggered dramatic pulmonary edema, consistent with enhanced vascular permeability. However, TNF- $\alpha$  did not induce a higher level of acute apoptosis in animals treated with FLASH irradiation. This observation suggests that protection against vascular apoptosis is only a part of the neurotrophic character of FLASH.

## FLASH is as efficient as CONV in controlling nasopharyngeal tumor growth

Human breast cancer HBC-12A tumor xenografts (Fig. S22) were treated by 17-Gy FLASH or CONV in two fractional courses at a 24-hour interval (Fig. 1C). FLASH was as efficient as CONV in regressing tumor growth (Fig. 3).

Human head and neck carcinoma HNS-2 xenografts (Fig. S22) were not established and exposed to 15-, 20-, or 25-Gy FLASH or 19.5-Gy CONV in a single fraction. After 48 days post-irradiation, the development of tumor growth was observed in all irradiated groups regardless of the radiation source and dose rate used. Remarkably, 25-Gy FLASH allowed a complete tumor growth arrest after 40 days (Fig. 3), without any skin damage in the irradiated area.

## FLASH is as efficient as CONV in controlling myeloid, fibrotic lung tumors

We used a murine model of irradiated lung by the determination of caspase-3 cleavage and terminal deoxynucleotidyl transferase (TdT)-mediated dUTP nick end labeling (TUNEL) and caspase-3 immunohistochemical labeling, respectively. 7.5-Gy CONV was sufficient to induce massive cleavage of caspase-3 at 1 hour post in mice from vascular and bronchial structural cells, whereas in contrast, no major signs were observed in animals exposed to 17-Gy FLASH (Fig. 2A). In animals exposed to

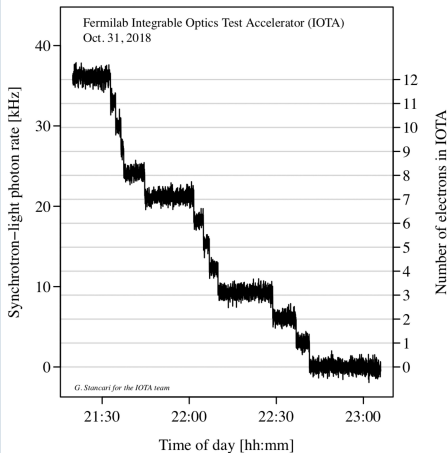
\* Corresponding author at: Laboratoire de Radio-Oncologie, Centre Hospitalier Universitaire Vaudois, Hôpital de la Croix-Rouge, 40, 1011 Leysin, Switzerland.  
E-mail address: marc.vozzani@unige.ch (M.-C. Vozzani).  
✉ Equid authors.

https://doi.org/10.1016/j.radonc.2025.07.009  
0958-8486/2025 Elsevier B.V. All rights reserved.



# Very interesting work storing single particles at IOTA accelerator in US!

## Accelerator research



<https://news.fnal.gov/2018/11/single-electron-beam-observed-in-iota-for-the-first-time/>

IPAC'19, Particle Accelerator Conf.  
ISBN: 978-3-95450-288-8

IPAC'19, Melbourne, Australia  
doi:10.18429/JACoW-IPAC2019-MOP0089

### EXPERIMENTAL STUDY OF A SINGLE ELECTRON IN A STORAGE RING VIA UNDULATOR RADIATION

S. Nagaitsev<sup>1,\*</sup>, G. Stancari, A. Romanov, Fermilab, Batavia, USA  
A. Arodzhan, M. Murokh, M. Ruelas, RadiaBeam Technologies, Santa Monica, USA  
I. Lobach, The University of Chicago, Chicago, USA  
T. Shafiq, BNL, Upton, USA  
<sup>1</sup>also at the University of Chicago, Chicago, USA

#### Abstract

A single electron orbiting around a ring and emitting single photons at the rate of about one event per hundred turns could produce a wealth of information about physical processes in large traps (i.e. storage rings) for charged particles. It should be noted that Paul and Perring traps in the 1980s led to the Nobel prize for studying state and motion of single quantum particles, and just recently the Perring trap ion-trap has enabled the measurement of a single proton magnetic moment with an unprecedented precision of 10 decimal places. The information from the storage ring traps could also be used for characterization of a quantum system as well as the “trap” itself, i.e. measuring properties of the storage ring lattice and electron interaction with the laser fields. Although, the interest in single-electron quantum processes today is mostly academic in nature, the diagnostics and methodology developed for single electron radiation studies could find subsequent applications in a variety of applied disciplines in quantum technology, including quantum communications and quantum computing.

#### INTRODUCTION

PHYSICAL REVIEW ACCELERATORS AND BEAMS 23, 054701 (2020)

#### Towards storage rings as quantum computers

K. A. Browne<sup>1</sup> and T. Rasser<sup>2</sup>  
<sup>1</sup>Brockhaus National Laboratory, Gießen, New York 13673-5000, USA

(Received 28 February 2020; accepted 4 May 2020; published 13 May 2020)

We explore the possible use of particle-beam storage rings as quantum computers. More precisely, we consider creating an ion trap system, in which the same computational basis states can be defined as in a neutral ion trap system, but in which the ions have a constant velocity and are rotating in a circular trap. The basic structures that we explore are classical and ultracold crystalline chains. What we propose is a novel method that uses the ion trap quantum concept, but puts the ions into a rotating frame of reference. The benefits of this approach are discussed.

DOI: 10.1103/PhysRevAccelBeams.23.054701

#### 1. INTRODUCTION

A particle accelerator storage ring is an apparatus that stores charged particle beams. The beams, if not cooled, can have very high temperatures and can be treated as classical thermodynamic ensembles of particles confined to some volume. When cooled, either in bunches of particles or debunched into a uniform longitudinal (temporal) distribution, the ensemble is in steady state and has constant entropy. In general, such a beam has no specific structure and should act like an ideal gas. However, the particles are necessarily charged and can interact with each other through interbeam collisions and other phenomena. These processes can cause beam heating, increasing the entropy. In addition, these particle distributions do contain information encoded into the behavior of the beams as they traverse the electromagnetic optics that keep them confined within the storage ring [1–4].

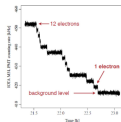


Figure 2: A measured photo-multiplier signal from a synchrotron radiation monitor after the bend magnet. One can clearly see little jumps in the average photon count rate as the number of trapped electrons becomes small, until a single electron is left in the IOTA storage ring.

$$e_n = 4\pi[(\Delta x)^2/(\Delta t)^2 - (\Delta y)^2], \quad (1)$$

where  $e_n$  is the horizontal or vertical beam emittance. We will call the transverse-beam temperature the temperature associated with the transverse emittance. Longitudinally, the temperature,  $T$ , is a function of the momentum spread [8],

$$\frac{1}{2}k_B T = \frac{1}{2}m_0(\Delta v)^2, \quad (2)$$

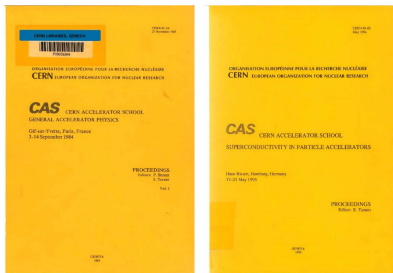
where  $\Delta v$  is the spread in velocity of the ions in the beam.  $k_B$  is Boltzmann's constant. In more practical units, temperatures for ion beams can be expressed as,

$$T_e[\text{K}] = \frac{2}{k_B} \left( \frac{\Delta p}{p_0} \right)^2 m_0 c^2 V \quad (3)$$



## Some useful resources for further study!

### Proceedings of the CERN Accelerator School

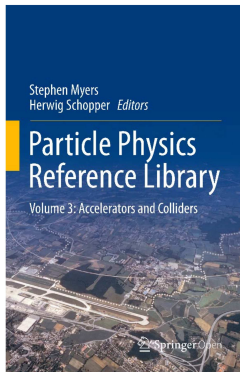


*Wide range of general & specialized courses ranging from introductory to advanced from schools going back to 1983*

**Proceedings available at:**

<https://cas.web.cern.ch/previous-schools>

### Particle Physics Reference Library, Vol. 3, Accelerators and Colliders



*3 volume textbook on Accelerators, Detectors & HEP jointly produced by CERN & Springer*

**Available free as open-access ebook at:**

<https://www.springer.com/gp/book/9783030342449#aboutBook>  
<https://cds.cern.ch/record/2702370>

# Many thanks for your attention!



# Reserve

LHC Page1

Fill: 2174

E: 59 GeV

30-09-2011 21:29:33

# PROTON PHYSICS: RAMP DOWN

Energy:

59 GeV

## Post Mortem Information

PM event ID: Fri Sep 30 20:48:21 CEST 2011  
 PM event category: PROTECTION\_DUMP  
 PM event classification: MULTIPLE\_SYSTEM\_DUMP  
 PM BIS Analysis result: First USR\_PERMIT change: Ch 4-Operator Buttons: A T -> F on CIB.CCR.LHC.B1  
 PM comment:

Comments 30-09-2011 21:04:44 :

So long Tevatron. We'll miss you.  
 Thanks for everything.

BIS status and SMP flags

B1

B2

Link Status of Beam Permits	false	false
Global Beam Permit	false	false
Setup Beam	true	true
Beam Presence	false	false
Moveable Devices Allowed In	false	false
Stable Beams	false	false

AFS: Single\_2b+12small\_13\_1\_1\_1bpi14inj

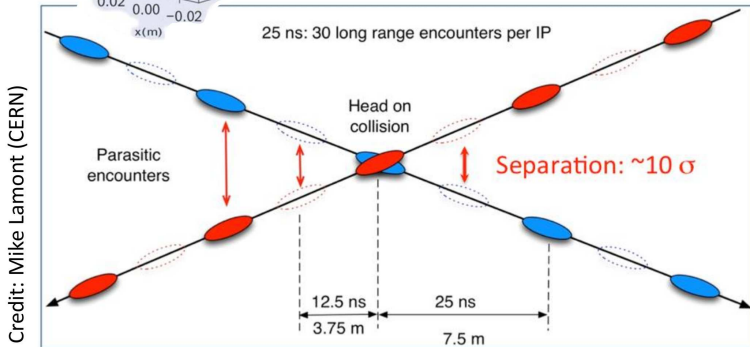
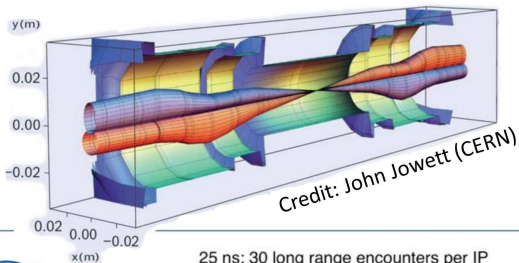
PM Status B1

ENABLED

PM Status B2

ENABLED

# Introduce 'crossing angle' to prevent parasitic collisions either side of the IP

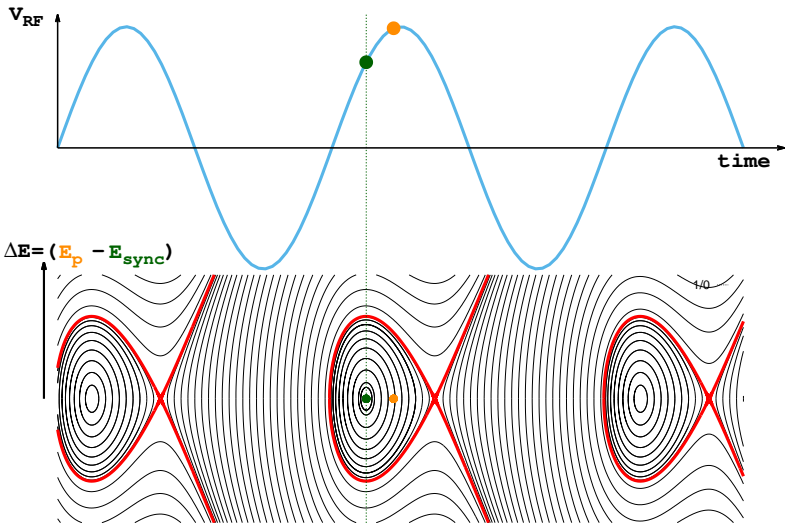


## Crossing angles reduce the luminosity

$$L = \frac{(f_{rev} n_{coll}) N_1 N_2}{2\pi \sqrt{(\sigma_{x,1}^2 + \sigma_{x,2}^2)} \sqrt{(\sigma_{y,1}^2 + \sigma_{y,2}^2)}} \times S$$

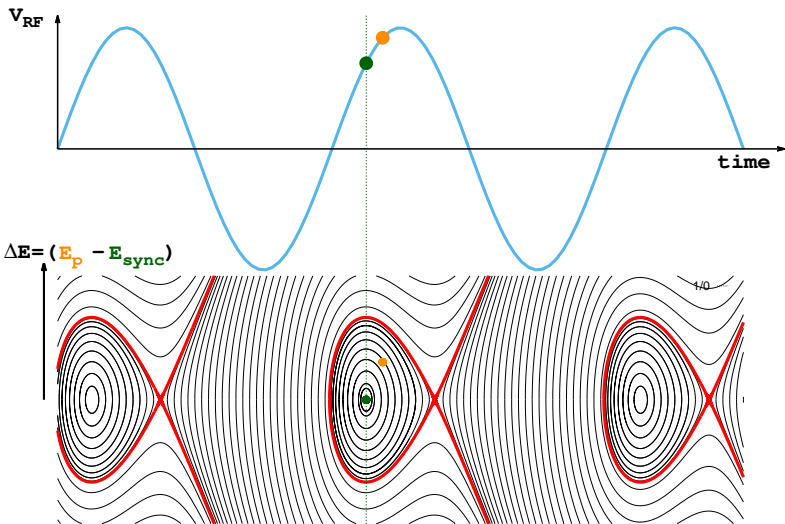
- Exact value of  $S$  depends on operating conditions
- Very approximately  $S \approx 0.8$

## Particles come in bunches!



*Picture valid for low-energy particles (below transition energy). For high energy particles (above transition) picture can be reversed if higher-energy particles take longer to travel around the ring due to relativistic saturation of particle velocity and dependence of path length on particle momentum.*

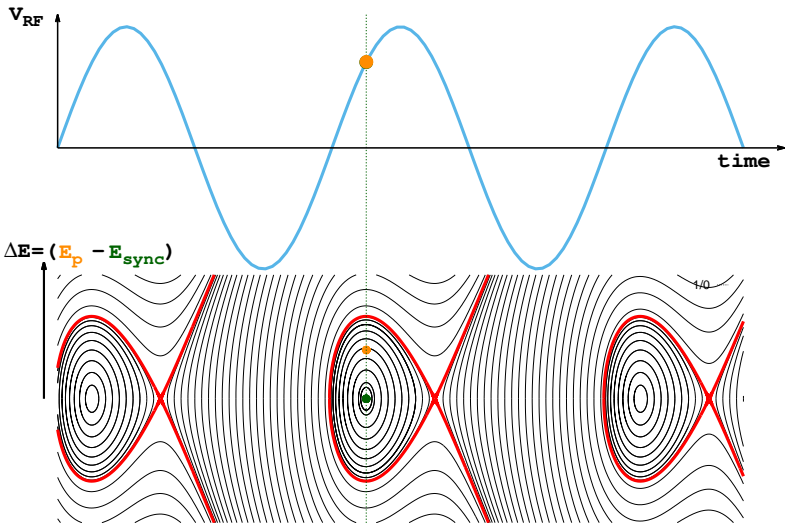
## Particles come in bunches!



*Picture valid for low-energy particles (below transition energy). For high energy particles (above transition) picture can be reversed if higher-energy particles take longer to travel around the ring due to relativistic saturation of particle velocity and dependence of path length on particle momentum.*

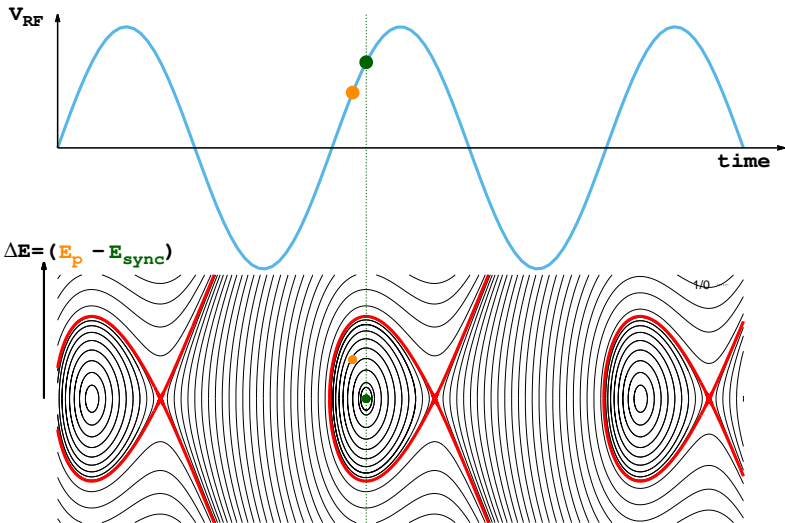


## Particles come in bunches!



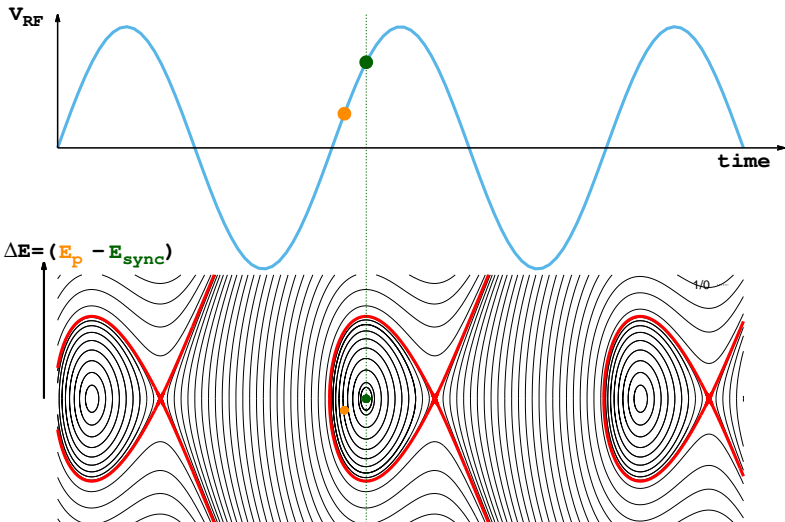
*Picture valid for low-energy particles (below transition energy). For high energy particles (above transition) picture can be reversed if higher-energy particles take longer to travel around the ring due to relativistic saturation of particle velocity and dependence of path length on particle momentum.*

## Particles come in bunches!



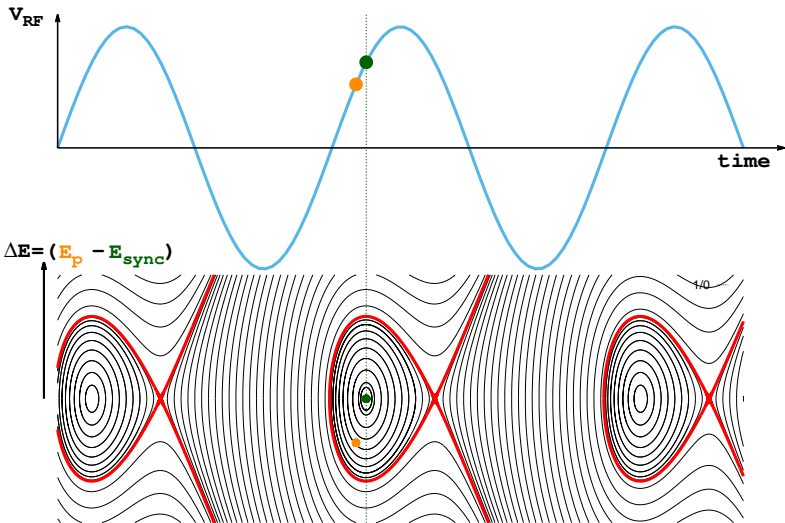
*Picture valid for low-energy particles (below transition energy). For high energy particles (above transition) picture can be reversed if higher-energy particles take longer to travel around the ring due to relativistic saturation of particle velocity and dependence of path length on particle momentum.*

## Particles come in bunches!



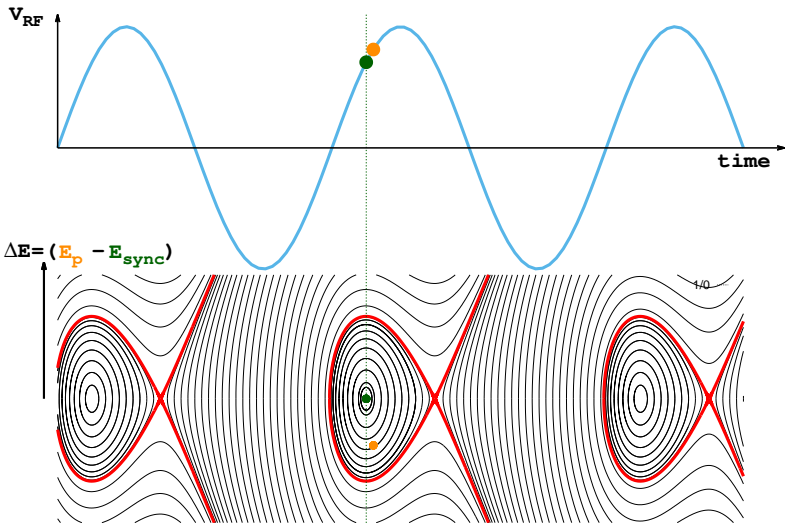
*Picture valid for low-energy particles (below transition energy). For high energy particles (above transition) picture can be reversed if higher-energy particles take longer to travel around the ring due to relativistic saturation of particle velocity and dependence of path length on particle momentum.*

## Particles come in bunches!



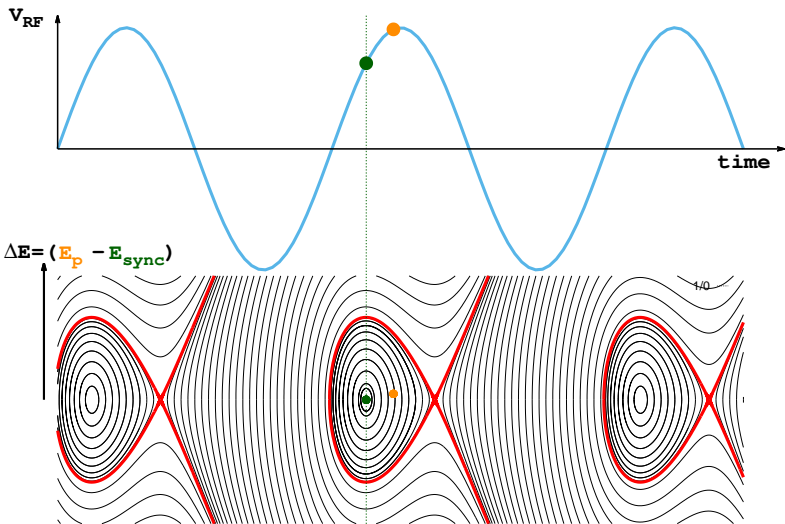
*Picture valid for low-energy particles (below transition energy). For high energy particles (above transition) picture can be reversed if higher-energy particles take longer to travel around the ring due to relativistic saturation of particle velocity and dependence of path length on particle momentum.*

## Particles come in bunches!



*Picture valid for low-energy particles (below transition energy). For high energy particles (above transition) picture can be reversed if higher-energy particles take longer to travel around the ring due to relativistic saturation of particle velocity and dependence of path length on particle momentum.*

## Particles come in bunches!



*Picture valid for low-energy particles (below transition energy). For high energy particles (above transition) picture can be reversed if higher-energy particles take longer to travel around the ring due to relativistic saturation of particle velocity and dependence of path length on particle momentum.*

# But what about the moon?



Credit: NASA/Goddard Space Flight Center/Arizona State University

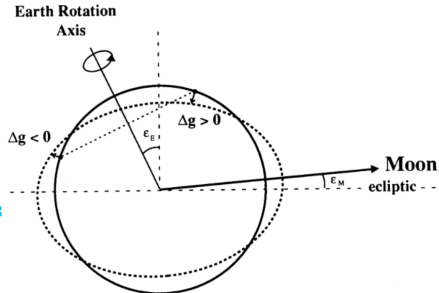
## Tidal deformation of earths crust changes the LHC circumference



If uncorrected this causes a drift in the beam energy

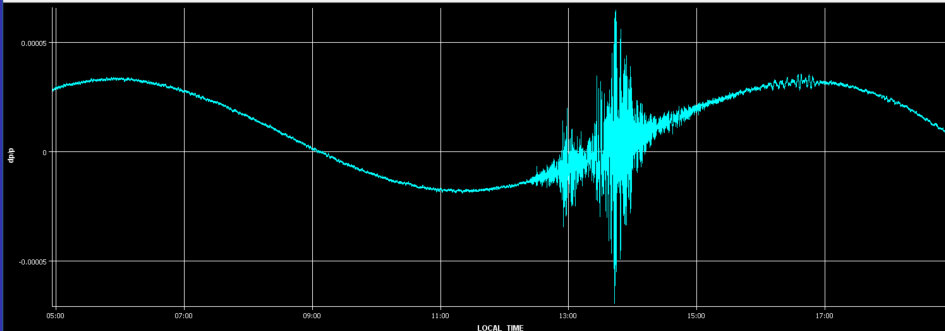
Effect of terrestrial tides on the LEP beam energy

L. Arnaudon et al. CERN SL/94-07 <http://cds.cern.ch/record/260368>



Timeseries Chart between 2016-11-13 04:55:51.338 and 2016-11-13 18:55:51.338 (LOCAL\_TIME)

→ LHC BOFSU\_RADIAL\_LOOP\_ERROR\_B1





# Medicine



Sign in

News

Sport

Weather

Shop

Reel

Travel

## NEWS

Home

Video

World

UK

Business

Tech

Science

Stories

Entertainment & Arts

Wales

Wales Politics

Wales Business

North West

North East

Mid

South West

physicsworld



Magazine | Latest | People | Impact

## Wales cancer patients to get proton beam therapy on NHS

particle therapy

PARTICLE THERAPY / ANALYSIS

Proton therapy on an upswing

Gantry 1

COMET

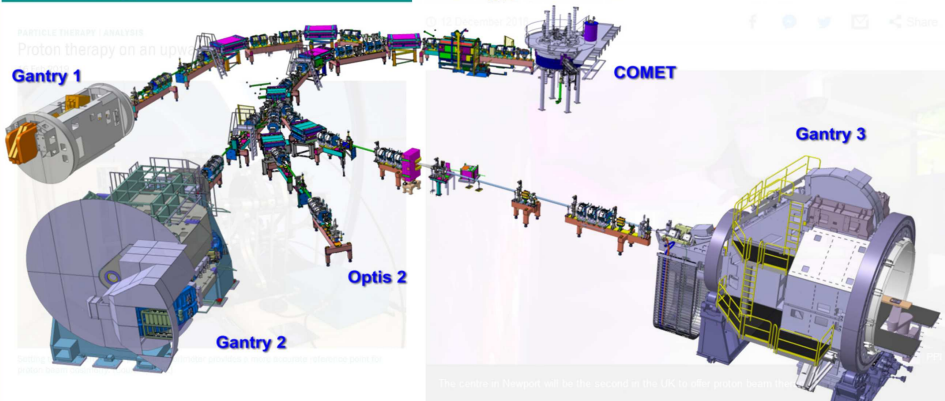
Gantry 3

Optis 2

Gantry 2

The centre in Newport will be the second in the UK to offer proton beam therapy.

Center for proton therapy, Paul Scherrer Institute, Villigen, Switzerland

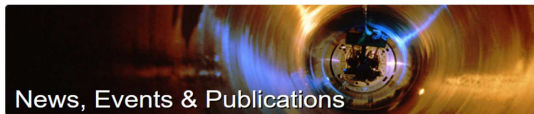


# INDUSTRY



UK Research and Innovation

- Funding
- Research
- Innovation
- Skills
- Public engagement
- News, events and publications
- About us



## News, Events & Publications

Home / News / STFC launches VELA – bringing a new imaging capability for UK industry

## STFC launches VELA – bringing a new imaging capability for UK industry

13 March 2015



Sign in

News

Sport

Weather

Shop

Reel

Travel

M

## NEWS

- Home
- Video
- World
- UK
- Business
- Tech
- Science
- Stories
- Entertainment & Arts

- World
- Africa
- Asia
- Australia
- Europe
- Latin America
- Middle East
- US & Canada

## World's only particle accelerator for art is back at the Louvre

© 23 November 2017

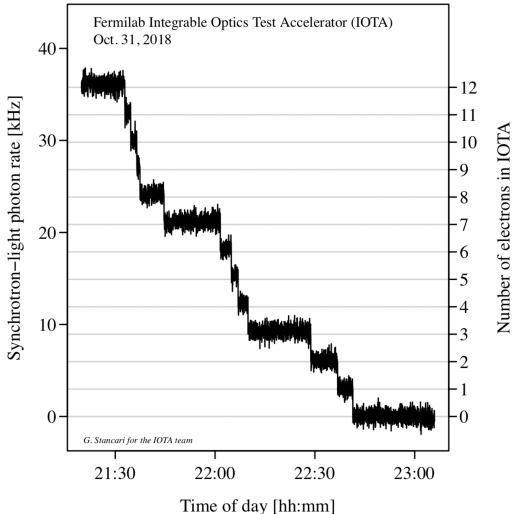
- f
- 📧
- 🐦
- ✉
- Share



The machine bombards sculptures with helium and hydrogen atoms

AFP

# Accelerator research



<https://news.fnal.gov/2018/11/single-electron-beam-observed-in-iota-for-the-first-time/>

10th Int. Particle Accelerator Conf.  
ISBN: 978-3-95459-288-8

IPAC2019, Melbourne, Australia  
doi:10.18422/JACoW-IPAC2019-MOP98888

JACoW Publishing  
doi:10.18422/JACoW-IPAC2019-MOP98888

## EXPERIMENTAL STUDY OF A SINGLE ELECTRON IN A STORAGE RING VIA UNDULATOR RADIATION

S. Nagaitsev<sup>\*1</sup>, G. Stancari, A. Romanov, Fermilab, Batavia, USA  
A. Arndt, A. Murokh, M. Ruelas, RadiaBeam Technologies, Santa Monica, USA  
I. Lobach, The University of Chicago, Chicago, USA  
T. Shafiq, BNL, Upton, USA  
<sup>1</sup>also at the University of Chicago, Chicago, USA

### Abstract

A single electron orbiting around a ring and emitting single photon quanta at the rate of about one event per hundred turns could produce a wealth of information about physical processes in large traps (i.e. storage rings) for charged particles. It should be noted that Paul and Penning traps in the 1980s led to the Nobel prize for studying state and motion of single quantum particles, and just recently the Penning trap technique has enabled the measurement of a single proton magnetic moment with an unprecedented precision of 10 decimal places. The information from the storage ring trap could also be used for characterization of a quantum system as well as the “trap” itself, i.e. measuring properties of the storage ring lattice and electron interaction with the laser fields. Although, the interest in single electron quantum processes today is mostly academic in nature, the diagnostics and methodology developed for single electron radiation studies could find subsequent applications in a variety of applied disciplines in quantum technology, including quantum communications and quantum computing.

### INTRODUCTION

PHYSICAL REVIEW ACCELERATORS AND BEAMS 23, 054701 (2020)

### Towards storage rings as quantum computers

K. A. Brown<sup>✉</sup> and T. Roser<sup>✉</sup>  
Brookhaven National Laboratory, Upton, New York 11973-5000, USA

✉ (Received 28 February 2020; accepted 4 May 2020; published 13 May 2020)

We explore the possible use of particle beam storage rings as quantum computers. More precisely, we consider creating an ion trap system, in which the same computational basis states can be defined as in a modern ion trap system, but in which the ions have a constant velocity and are rotating in a circular trap. The basic structures that we explore are classical and ultracold crystalline beams. What we propose is a novel method that uses the ion trap quantum computer concept, but puts the ions into a rotating frame of reference. The benefits of this approach are discussed.

DOI: 10.1103/PhysRevAccelBeams.23.054701

### I. INTRODUCTION

A particle accelerator storage ring is an apparatus that stores charged particle beams. The beams, if not cooled, can have very high temperatures and can be treated as classical thermodynamic ensembles of particles confined to some volume. When stored, either as bunches of particles or debunched into a uniform longitudinal (temporal) distribution, the ensemble is in steady state and has constant entropy. In general, such a beam has no specific structure and should act like an ideal gas. However, the particles are necessarily charged and can interact with each other through intrabeam collisions and other phenomena. These processes can cause beam heating, increasing the entropy. In addition, these particle distributions do contain information encoded into the behavior of the beams as they traverse the electromagnetic optics that keep them confined within the storage ring [1–4].

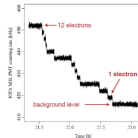


Figure 2: A measured photo-multiplier signal from a synchrotron radiation monitor after the bend magnet. One can clearly see little jumps in the average proton count rate level as the number of trapped electrons becomes small, until a single electron is left in the IOTA storage ring.

$$\epsilon_c = 4\pi(\langle u^2 \rangle \langle v^2 \rangle - \langle uv \rangle^2), \quad (1)$$

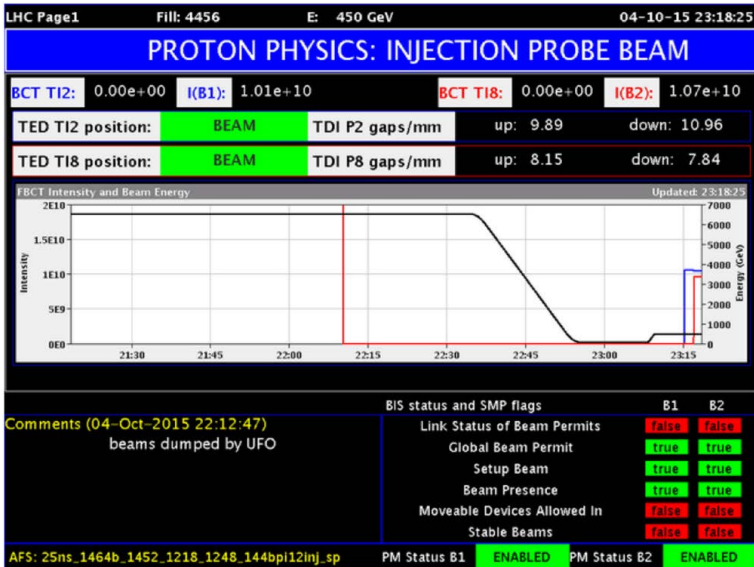
where  $\epsilon_c$  is the horizontal or vertical beam emittance. We will call the transverse beam temperature the temperature associated with the transverse emittance. Longitudinally, the temperature,  $T_c$ , is a function of the momentum spread [8],

$$\frac{1}{2}k_B T_c^2 = \frac{1}{2}m(\delta v)^2, \quad (2)$$

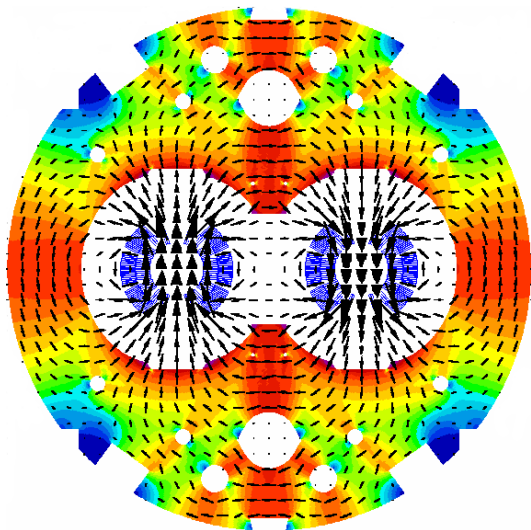
where  $\delta v$  is the spread in velocity of the ions in the beam,  $k_B$  is Boltzmann's constant. In more practical units, temperatures for ion beams can be expressed as,

$$T_c[\text{K}] = \frac{2}{k_B} \left( \frac{\Delta p}{p_0} \right)^2 k_B eV \quad (3)$$

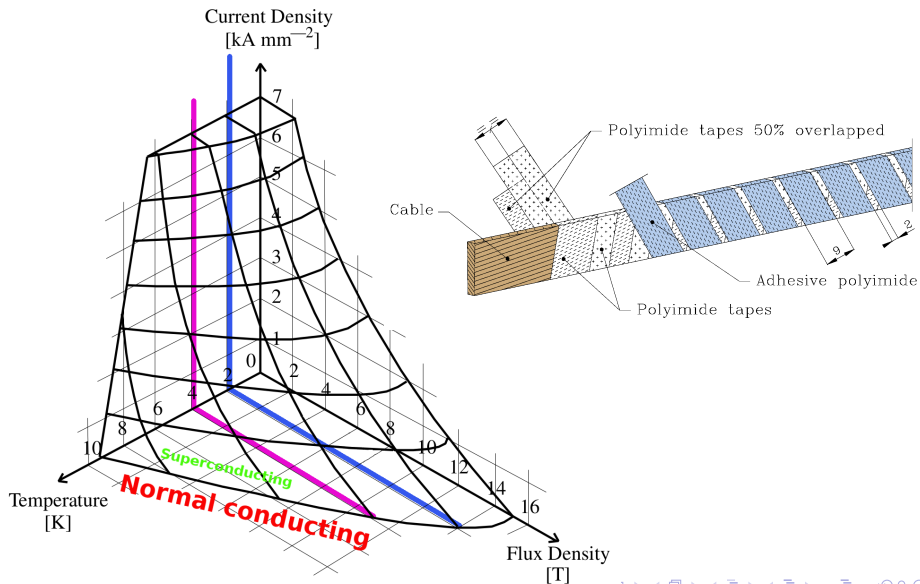
## 8b4e filling scheme was a significant factor in limiting the impact of UFO's on LHC Run2!

**UFO = Unidentified Falling Object**J.M. Jiménez et. al, *Observations, analysis and mitigation of recurrent LHC beam dumps caused by fast losses in arc half-cell 16L2, MOPMF053, IPAC2018*, <https://doi.org/10.18429/JACoW-IPAC2018-MOPMF053>

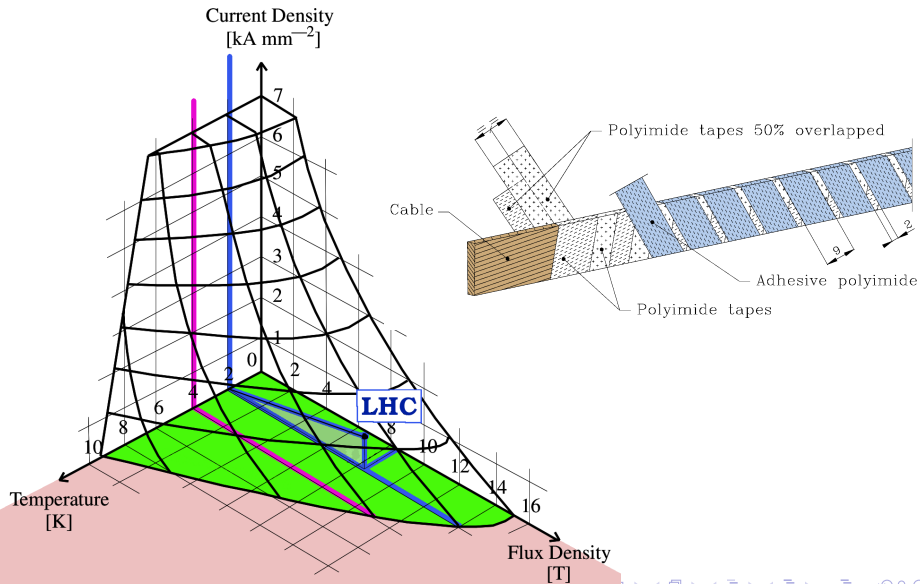
## Arcs utilize superconducting 8.3 T dual bore dipoles



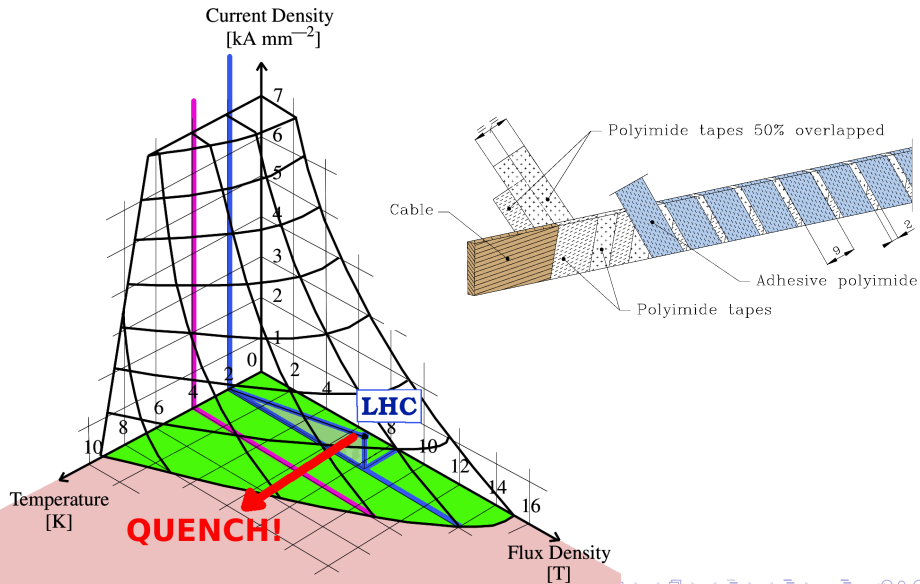
# NbTi coils cooled to 1.9 K with superfluid helium



# NbTi coils cooled to 1.9 K with superfluid helium



# NbTi coils cooled to 1.9 K with superfluid helium



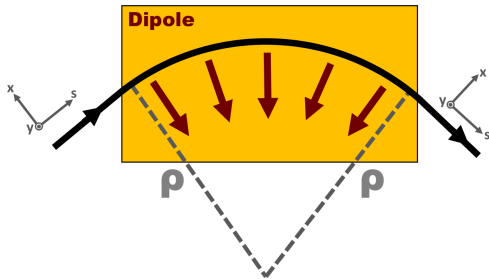


## Limiting factor for circular hadron collider:

- need sufficient dipole field strength to bend beams around the ring
- **High Energy = high magnetic rigidity**

$$F_{Lorentz} = F_{centrip}$$

- consider pure dipole fields
- $(p_x, p_y) \ll p_s$



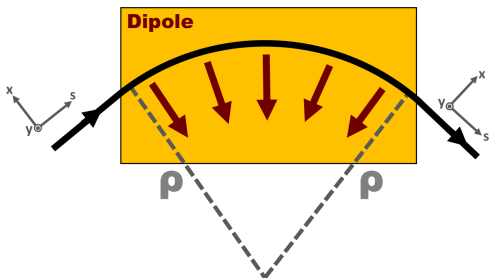
## Limiting factor for circular hadron collider:

→ **High Energy = high magnetic rigidity**

$$F_{Lorentz} = F_{centrip}$$

$$F_{Lorentz} = q(\vec{E} + \vec{v} \times \vec{B})$$

- consider proton ( $q/A = 1$ )
- assume pure dipole fields
- $(p_x, p_y) \ll p_s$



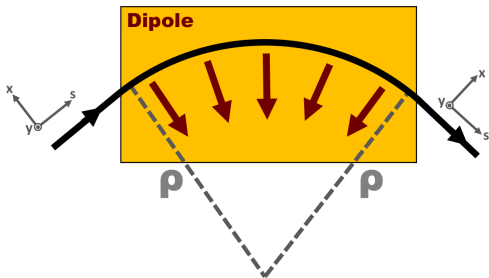
Limiting factor for circular hadron collider:

→ **High Energy = high magnetic rigidity**

$$F_{\text{Lorentz}} = F_{\text{centrip}}$$

$$F_{\text{Lorentz}} = q(\vec{E} + \vec{v} \times \vec{B})$$

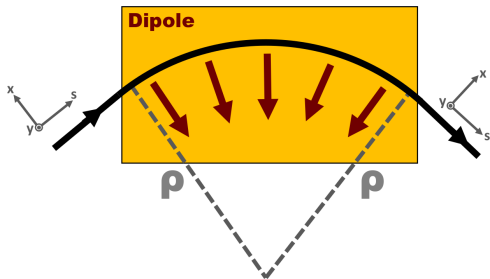
$$= evB_{\text{dipole}}$$



Limiting factor for circular hadron collider:

→ **High Energy = high magnetic rigidity**

$$F_{centrip} = \frac{dp}{dt}$$



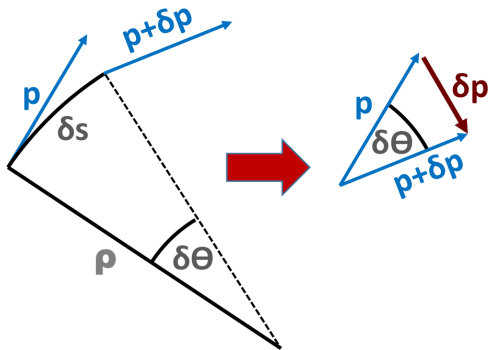
## Limiting factor for circular hadron collider:

→ **High Energy = high magnetic rigidity**

$$dp = p d\theta$$

$$ds = \rho d\theta$$

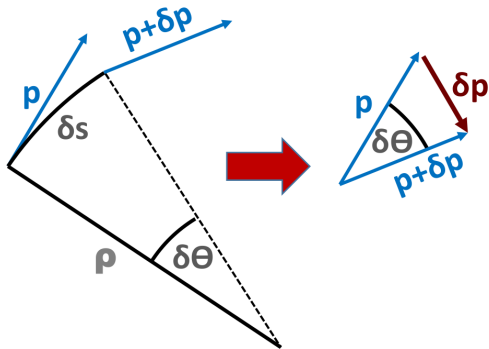
$$p = \gamma_{rel} m_{rest} v$$



## Limiting factor for circular hadron collider:

→ **High Energy = high magnetic rigidity**

$$\begin{aligned}
 F_{centrip} &= \frac{dp}{dt} \\
 &= p \frac{d\theta}{dt} = \frac{p ds}{\rho dt} \\
 &= \frac{pv}{\rho} = \frac{\gamma m_0 v^2}{\rho}
 \end{aligned}$$



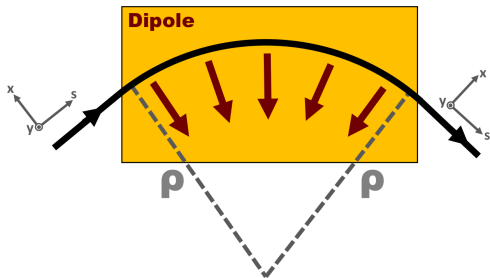
Limiting factor for circular hadron collider:

→ **High Energy = high magnetic rigidity**

$$F_{\text{Lorentz}} = F_{\text{centrip}}$$

$$evB = \frac{\gamma m_0 v^2}{\rho} = \frac{pv}{\rho}$$

$$B\rho = \frac{p}{e}$$

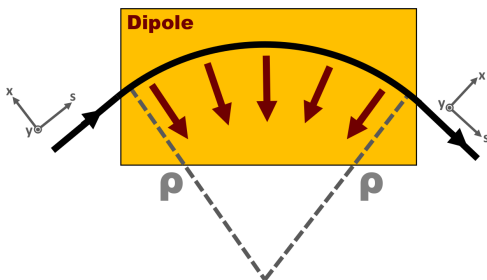


Limiting factor for circular hadron collider:

→ **High Energy = high magnetic rigidity**

$B\rho$  is '*Magnetic Rigidity*'

$$B\rho \text{ [Tm]} = \frac{p \text{ [kgms}^{-1}\text{]}}{e \text{ [C]}}$$



- Not so convenient units

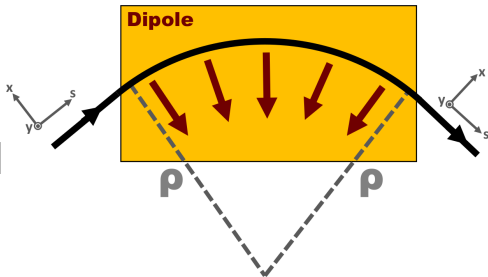


Limiting factor for circular hadron collider:

→ **High Energy = high magnetic rigidity**

$B\rho$  is '*Magnetic Rigidity*'

$$B\rho \text{ [Tm]} = \frac{10}{2.998} p \text{ [GeV}/c\text{]}$$



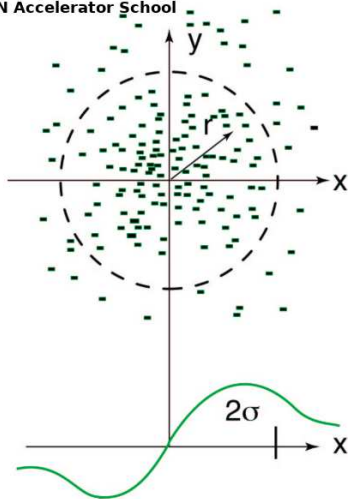
**Magnetic rigidity** defines the maximum energy you can reach for a given dipole field in a given tunnel geometry

Beams themselves can introduce large nonlinearities into the dynamics e.g.

### Direct Space Charge

- Repulsive (defocusing) force on a particle due to the field of all other particles in the bunch
- **A big challenge at low energy in injector chain**

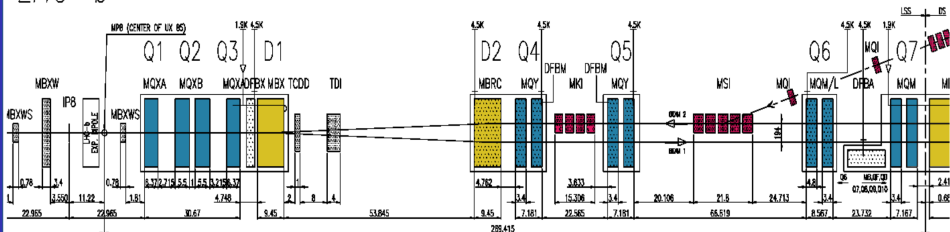
K.Schind, 'Space Charge'  
CERN Accelerator School



# Similar problem at injection

IR8 (LHCb / beam2 injection)  
Right side viewed from above

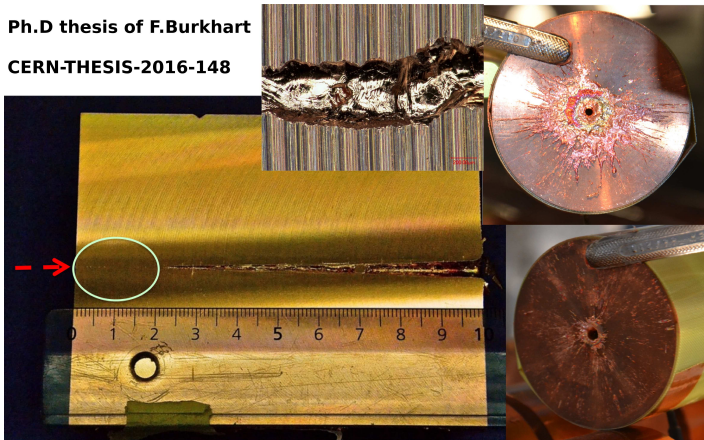
LHC-b



Injection kickers have rise time of  $\sim 1\mu\text{s}$

- Optics errors can reduce data delivered to HEP experiments
- Create Luminosity imbalance between HEP experiments  
→ Aim for  $\beta^*$ -beat  $\leq 1\%$
- **MACHINE PROTECTION** → require beta-beat  $\leq 18\%$

Ph.D thesis of F.Burkhart  
CERN-THESIS-2016-148



## Emittance conserved provided particle's energy is constant

### Acceleration

Define '*normalized emittance*' which is invariant with the beam energy

$$\epsilon^* = \beta_{rel} \gamma_{rel} \epsilon$$

In practice many effects can change or dilute emittance

- Injection errors
- Synchrotron radiation
- IntraBeam Scattering
- **Emittance evolution in LHC still not fully understood!**